UNIVERSIDAD COMPLUTENSE
FACULTAD DE CIENCIAS MATEMATICAS

CONSEJO SUPERIOR
DE INVESTIGACIONES CIENTIFICAS

INSTITUTO DE ASTRONOMIA Y GEODESIA
(Centro Mixto C.S.I.C. - U.C.M.). MADRID

Publicación núm. 184

MARE NOSTRUM

GEOMED Report - 2

Edited by

M. J. SEVILLA

MADRID
1992

FOREWORD

GEOMED is a project for the determination of the geoid and of the Sea Surface Topography in the Mediterranean Sea. The existing set of data available on the Mediterranean in already quite significant and it is going to be improved in these years because of the new altimetric data coming from ERS1 and the TOPEX-POSEIDON missions. In the execution of the project we use, mainly, radar altimetric data (from SEASAT, GEOSAT and ESR1 missions) gravimetric data, bathymetric models, as well as land gravity data set and DTMs of surrounding regions: these data sets are generally poor on the southern side of the Mediterranean. More geophysical data, like tidal and Moho depth models, will be user too. The particularity of this project is in that the dynamics of the Mediterranean, as a closed sea, cannot be easily modelled, so that the time dependent part of the altimetric signal has to be modelled empirically together with the radial orbit error; on the other hand, since the satellite arcs are very short, this choice is well justified. The separation between the stationary Sea Surface Topography and the geoid can be done in such an area using both data sets, the altimetric and the gravimetric one, which is available contrary to the situation in open oceanic areas.

The groups that are working on this project are:

Dept. of Environmental Engineering, Milan, Italy. (Coordinator);
Dept. of Geodesy and Surveying. Thessaloniki, Greece;
Inst. of Astronomy and Geodesy, Madrid, Spain;
Inst. of Mathematical Geodesy, Graz, Austria;
Dept. of Geophysics, Copenhagen, Denmark;
National Survey and Cadastre, Copenhagen, Denmark;
Finnish Geodetic Institute, Helsinki, Finland.

This project in supported by a contract within the Program Science of the European Economic Community.

This volume, the second of the MARE NOSTRUM Series, collect the works done by many groups involved in the GEOMED organization, in the last year, as informed in the GEOMED Meeting held in Madrid at october 1992, and will be followed by others with new contributions.

INDEX

The Geomed Project: the state of the art

M.A. Brovelli*, F. Sansó**

* I.Ge.S. - Istituto Nazionale di Geofisica (Milano)

** D.I.I.A.R. - Politecnico di Milano

1. Introduction

It was more than one year ago that 7 scientific groups from 6 nations (Spain, Italy, Austria, Greece, Denmark and Finland) met with the purpose of setting up an international cooperative effort to determine the geoid and the Sea Surface Topography (SST) on the Mediterranean Sea. The Geoid, or better some equipotential surface of the gravity field suitably fitting the physical surface of the Mediterranean, is determined as the basic surface in Geodesy to which orthometric heights are referred; a good knowledge of the geoid could for instance allow for a much better reattachment of the different national height systems usually conventionally referred to some tide gauges as zero points.

The SST, i.e. the stationary height of the sea above the ellipsoid, is a fundamental parameter of physical oceanography strongly related to the steady circulation pattern involving surface as well as deep water streams (geostrophic flow) (cfr. e.g. C. Wunsch, [1992]).

These two surface can nowadays be separated because the geoid can be determined by measurements related to the gravity field only, while the physical surface of the ocean can be achieved by the radaraltimetric measurements performed by dedicated satellite missions (like the now flying ERS1 and Topex Poseidon satellites) after several corrections (firstly the radial orbital correction) and time averaging are applied (cfr. G. Balmino, [1992] and V. Zlotnicki, [1992]).

In the most advanced approaches the global analysis of the available data sets (gravimetric, altimetric, satellite tracking, etc.) proceeds as follows (cfr. R. H. Rapp, [1989b]):

1) let us call Δg the field of mean block values of gravity anomalies usually known on land areas (e.g. over $1° \times 1°$ blocks), T the anomalous gravity potential, t the stationary sea surface topography, h the measured heights of the sea above the ellipsoid (already corrected by the time varying components), T_P a reference (prior) model of the anomalous potential developped in spherical harmonics up to some degree N_{max} (e.g. $N_{max} = 50$) and derived from the adjustment of pure satellite tracking data, ξ_r the radial orbital error of the orbit computed for the flying altimetric satellite from T_P (this error is due to both imperfect knowledge of the initial state and errors contained in T_P propagated to the orbit); then we can write observation equations of the form:

$$\Delta g = -\frac{\partial T}{\partial r} - \frac{2}{r}T + \nu_g \tag{1.1}$$

$$h = \frac{T}{\gamma} + t + \xi_r + \nu_n \tag{1.2}$$

$$T_P = T + \nu_T, \tag{1.3}$$

where γ is the normal gravity and ν_g, ν_n, ν_T are independent noises; (1.1) holds on continental areas, while (1.2) holds on oceanic areas.

2) in the above equations usually T is modelled as a sum of spherical harmonics up to the same degree N_{max} as T_P, t is also represented by some truncated development, e.g. again by spherical harmonics up to some degree which in principle can be as high as N_{max} but usually is much lower (e.g. degree 12 or 20), ξ_r is also parametrized by a small number of parameters (e.g. $5 \sim 6$) over some time span (e.g. 1 day) in consideration of the fact that most of the power of this perturbation is known to be concentrated at the frequencies of once per rev and twice per rev (cfr. C. Wagner, [1989]); all these unknowns are then estimated by applying a big least squares process to (1.1), (1.2) and (1.3) where, as one can easily recognize, ξ_r is separated from T and t as it is the only time varying unknown, while T is separated from t mainly by virtue of the equations (1.1) and (1.3); all this happens at the degree of resolution given by N_{max} which is supposed to be enough to get a good estimate of t and ξ_r.

3) Once t and ξ_r are known, track by track, they are subtracted from h at block averaged to obtain estimates of mean values of T with a much higher resolution; from the mean values of Δg on land and of T on sea one can derive high degree global models (e.g. up to $N_{max} = 360$) of T by applying one of several known techniques (see for instance R.H. Rapp, [1992] or M. A.Brovelli and F.Migliaccio, [1992] and F. Sansó , [1992]). This approach, although criticizable in some point, has certainly contributed an enormous improvement in the knowledge of global gravity field models. Unfortunately however it cannot contribute as much in an area like the Mediterranean for two reasons:

a) the time dependent pattern of the sea surface is generally more complicated in closed seas than in open ocean where simpler tidal corrections hold;

b) the orbital corrections ξ_r are more difficult to be estimated because of the shortness of the arcs which cannot last longer than few minutes before hitting continental areas; moreover the bad performance of global models on Eastern European countries (due to the non availability of gravity material there) makes the radial orbital error to display systematic effects and larger values (cfr. P. Knudsen and M.A. Brovelli, [1991]). On such a sea however there are available many gravity measurements derived from marine gravimetry; this allows for an independent computation of the gravimetric geoid which compared with the stationary surface rising from altimetric measurements can supply the sought SST. Very similar reasons and reasonings apply to the case of Baltic sea and this, beyond the

scientific and personal closeness of the groups, is another justification for their cooperation. We conclude this paragraph by mentioning that also other groups have decleared their interest for the project and cooperate directly or indirectly in it like: CERGA- France (Dr. F. Barlier), University of Barcellona (Dr. M.A. Andreu), Institut of Cataluña (Dr. I. Colomina), General Command of Mapping, Geodetic Computing - Ankara (Dr. A. Ayhan)

2. Data

We try to summarize in this paragraph the type of data we have been able to collect till now focussing on their validation and on the need of new data to solve some ambiguous case.

The main data files used for the purpose of Geomed concern:

- **Marine Gravity Data**: these are F.A. anomalies given on the sea surface (Fig. 1), mainly derived by digitizing the famous maps by Morelli (cfr. C. Morelli, [1970]; T.D. Allan and C. Morelli, [1971]; C. Morelli et al., [1975a], C. Morelli et al., [1975b]; C. Morelli et al. [1975c]; D. Arabelos, [1980]; D. Arabelos, [1987]; D. Arabelos and C.C. Tscherning, [1988]; D. Arabelos and I.N. Tziavos, [1989]), although other gravity files are now available and in future they will be compared with the above for the scope of validation. By the way the actual data have all been scrutinized and essentially submitted to internal validation, so that doubious or possibly spourious data are now properly flagged in our files.
- **Land Gravity Data**: we have (available) the national archives of Spain, Portugal and Italy; the Greek gravity data are not open, however they can be used by the Thessaloniki University in computations of the geoid in the Eastern Mediterranean. To these a few more data must be added, mainly provided by the Bureau Gravimetrique International which is considering to deliver a set of low resolution gravity for France. Moreover there is a possibility to get similar data for northern Africa from the University of Leeds. (see Fig. 2)
- **Digital Terrain Models**: these include both topographic heights on land and the bathymetry of Mediterranean (Fig. 3). As for land data only a small part of what would be needed with the proper resolution, is available. On the other hand on the whole region, including bathymetry, we have two global models, namely TUG87 and ETOPO5U both with a resolution of $5' \times 5'$.

  Moreover the bathymetric maps of Morelli (resolution $5' \times 7.5'$, equidistance 200 m) are also available in a digitized form thanks to the work of the Thessaloniki group.

  Some work has been already done by using the TUG87 Model, however there are several doubts about its effectiveness due to a recent experience in the computation of the geoid in Italy where it was shown that there are large discrepancies with the national DTM particularly in Southern Italy. Furthermore looking at any

contour map, it seems quite obvious that it is unrealistically too flat in the whole central Mediterranean; the good point on the other hand is that there seems to be a fair agreement with the shore line and with the islands locations, proving that in applying a remove-restore technique the highest frequency contribution to the geoid should be possibly guessed. Some work will be done in the next future in order to obtain an improved bathymetry by merging the existing data.

- **Altimetric Data**: we have collected the available altimetric data for Mediterranean concerning the Seasat mission (Fig. 4) as well as the Geosat mission (Fig. 5), the last restricted to the (ERM) Exact Repeat Mission (of periof 17 days) for the first 22 repetitions. These data have already been cleaned and processed in global adjustments by the OSU University and in particular for Geosat the radial orbital error has been corrected for (Y.M.Wang and R.H. Rapp, [1990]). Naturally the correction for the radial orbital error in a global treatment suffers of the drawbacks we have already discussed in §1, as a local postprocessing has made clear.

  A new altimetric data set is now in the process of being collected and validated, namely that produced by the ERS1 mission; for the moment our files include the ERM(1-4) with a 35 days period (Fig. 6) and the ERM(1-4) with a 3 days period (Fig. 7).

- **Global Geopotential Models**: many global models are availbale in the Geomed Files, including IfE 88, OSU78, GPM2, OSU81, OSU86E, OSU86F, OSU89A, OSU89B, OSU91A, DGFI92A, GEM10C . All these models have been tested statistically in the area of interest against gravity or altimetric data to decide which one could conveniently represent the data locally. At the end the choice has been for OSU91A (cfr. Fig. 8) as, although its performance was comparable to that of IfE88, it is credited to have superior global representativity.

  Beyond these data which are essential either in computing the gravimetric geoid or the stationary sea surface, other two data sets are currently collected in the Geomed Project as, so to say, subsidiary data, namely:

- **Tide Gauge Data**: these are currently corrected by the Madrid and the Thessaloniki groups and attempts are now made to set up an empirical tidal model for the Mediterranean, split into 3 basins (Western, Central, Eastern);
- **Geophysical Data**: in particular we have collected information on the Moho depth in order to be able to smooth as much as possible the gravity field and to be able to predict it as accurately as possible. The Graz group has already performed some experiments in this direction.

3. Methods and first results

In this paragraph we try to summarize the different methods proposed to solve our problem as well as the first results obtained, trying to make it clear which are

the problems still open.

A) For altimetry only

This treatment is essentially an adjustment of cross-over values based on the observation equations

$$h = (N + t) + (\xi_r + \tau) + \nu, \tag{3.1}$$

where $N = T/\gamma, t, \xi_r$ have the same meaning as in (1.2), while τ is a time varying component. Let's assume that ξ_r and τ are so smooth that on a time span of a few minutes (so long can last at the maximum a track on the Mediterranean before hitting a land) they can be well approximated by a linear function of time

$$\xi_r + \tau = aT + b; \tag{3.2}$$

this is certainly true for ξ_r (cfr. E.J.O. Schrama, [1989]) and probably true, at least roughly, for τ at least when the subsatellite point is not too close to a coast.

Due to the very regular shape of the satellite orbit which is close to a circle, in (3.2) the variable time T can be substituted by λ.

Now assume also that the observation (3.1) refers exactly to a point where two tracks cross each other (if this is not the case one can always perform an interpolation along the track), then since $(N + t)$ is the same in both tracks i and j we can write

$$h_i - h_j = (a_i\lambda + b_i) - (a_j\lambda + b_j) + \nu_{ij} \tag{3.3}$$

A system of equations of the type (3.3) can be adjusted by a least squares approach once the relevant rank deficiency problem is solved; in practice one can show that a bilinear surface ($z = Axy + Bx + Cy + D$ in planar coordinates) cannot be determined by this system of equations (cfr. R. Barzaghi et al., [1990]) so that some constraint has to be imposed. The most convenient of such constraints is to minimize the sum of the squares of the differences:

$$h_i - N_{Mod} - (a_i\lambda + b_i) = \Delta_i \tag{3.4}$$

on condition that realistic weights be chosen for (3.4) (on this subject cfr. R. Barzaghi et al., [1992]).

It is interesting to observe that to strengthen the solution also different data sets can be adjusted, while "almost" separated tracks can be stacked together (collinear analysis) to obtain stronger profiles.

In this way for instance an altimetric geoid for the Mediterranean has been computed by the Copenhagen and the Milan groups jointly from the available Seasat and Geosat data.

To perceive the effectiveness of the adjustment we can say that (cfr. P.Knudsen and M.A. Brovelli ,[1991]) from row data to adjusted we have discrepancies Δ with the model (see (3.4)) with s.d. going from 60 cm down to 36 cm and, even more important, crossover residuals ν (see (3.3)) with s.d. decreasing from 30 cm down to 5 cm.

B) The gravimetric geoid

This can be computed in several different ways following the classical approach of the collocation method; in either cases it is convenient first of all to modify the gravity data set by a process, called remove-restore, which has the effect to smooth and regionalize the gravity field.

Essentially first of all the free air anomalies Δg_F are filtered at the long wavelengths by subtracting the anomalies computed by a global model Δg_M; with this manipulation the data set is regionalized in the sense that in principle it becomes devoid of signals at wavelengths larger or even comparable with the sides of the window where the data are given.

The remaining signal is therefore well estimable with the available data and we can neglet the data outside the window, which are not available.

Second we reduce considerably the power of the signal by further subtracting the effect of the Residual Terrain Modelling, Δg_t, (cfr. R. Forsberg, [1985]) i.e. the high frequency part of the Terrain correction; therefore we are left with a residual field

$$\Delta g_r = \Delta g_F - \Delta g_M - \Delta g_t \tag{3.5}$$

which is both smooth and regionalized and it is generally this field to which we apply a proper operator transforming it into an estimate of the anomalus potential T_r. As a final step we add back to T_r the contribution of the global model, T_M, that of the RTM, T_t, to obtain a final estimate of the geoid through

$$N = \frac{1}{\gamma}(T_r + T_M + T_t). \tag{3.6}$$

Just to give an idea the model undulation N_M is of the order of $45m \pm 3m$ in the Western Mediterranean (but it goes down to $10m \pm 5m$ in the Eastern part) while the topographic correction N_t and the residual part N_r are in the order of 1 m.

B1) Stokes formula by FFT

Two test computations have been performed by this method which is nothing but the application of the Stokes formula, to the window where we have data, computed by the FFT techniques exploiting its shape of a quasi-convolution (cfr. M.G. Sideris ,[1987], G. Strang van Hees, [1991]).

The two geoids refer one to the Western Mediterranean ($0° \leq \lambda \leq 10°; 37° \leq \phi \leq 50°$), and it has been computed by the Milan group, the other is in the Eastern Mediterranean ($14° \leq \lambda \leq 25°; 34° \leq \phi \leq 40°$) and it has been computed by the Thessaloniki group, both for the purpose of comparison with the results obtained by other techniques.

The result of the experiment in the Eastern Mediterranean is displayed in Fig 9.

B2) Collocation

One of the drawbacks of this approach was till a few time ago its limited capacity of treating a number of points together ($\sim$ 3000 points) since the method implies the solution of a system of as many equations as points, with a completely filled in normal matrix. Fortunately enough we have now a technique (cfr. G.P. Bottoni and R. Barzaghi, [1992]) which allows a very fast solution even for very large systems of this kind on condition that the data be regoularly gridded, so that a suitable combination of Toeplitz and FFT methods can be applied.

A large experiment with 17557 points has been performed in the Western Mediterranean by the Copenhagen and Milan groups (cfr. Fig. 10), comparing the results with those obtained with the Stokes/FFT approach; the comparison is satisfactory, since the mean square difference between the two geoids is 13 cm as compared to 66 cm of signal. These numbers ignore the 45 cm of bias which is due to the fact the FFT techniques works with data referred to their average.

B3) Pure collocation

Since in open sea the topographic correction is not so strong and rough, in this case it is conceivable to perform a geoid computation by pure collocation, i.e. with no remove and restore of the topographic effects, with the main concern that the estimate will not be very accurate in coastal regions.

When the data are treated in their original locations no fast algorithm is available, so the computational burden has to be controlled by limiting the area of computation; the Madrid group has estimated a geoid in this way on the Mediterranean by splitting it into 330 ($1° \times 1°$) zones on each of which the prediction was performed from a ($2° \times 2°$) block covering the estimation area. The computed geoid is displayed in Fig.11. The prediction error is in most cases around 5 cm, apart from some coastal regions where it grows to tens of centimeters.

C) An integrated approach

This approach, pussed by the Thessaloniki group, is essentially a full collocation procedure, with adjustment of parameters, applied to the set of equations

$$\begin{cases} h & = \frac{1}{\gamma}T + (a\lambda + b) + \varepsilon \\ \Delta g & = -(\frac{\partial T}{\partial r} + \frac{2}{r}T) + \eta \ . \end{cases} \tag{3.7}$$

The interesting point in (3.7) is specially that the density of data referring to the anomalous potential, is extremely increased by the altimetric observations, thus filling the gaps of marine geodesy. Whence the accuracy of the estimate of the geoid should be better. On the other hand in (3.7) the sea surface topography is disappeared, which means that in part it will enter naturally in $(a\lambda + b)$, giving rise to a bilinear surface and in part it can deform T, i.e. the geoid. The first

part is certainly the biggest and probably a bilinear model for a window like $26° \leq \lambda \leq 36°, 31° \leq \phi \leq 37°$, is good for it, as one would infer from a global model of SST like the one by R. Rapp (cfr. R.Rapp, [1989a]); the second part, though smaller, is of interest but not available in this approach.

In any way the internal consistency of the results is certainly very good as it has been tested by living 73 altimetric heights h out of the treatment and then comparing them with quantities predicted in the processing; the differences between the two turned out to be zero in the average (as it ought) and have a s.d. of 4 cm.

D) The sea surface topography

One of the crucial questions of this project is: do we really believe that the accuracy of our data and the riliability of our models is sufficient to produce a significant estimate of the SST?

In western Mediterranean we have computed a SST by subtracting the gravimetric geoid from the altimetric one; the result is shown in Fig. 12. As one can see we have a surface waving from -0.80 m along the African coast to -0.20 m along France and 0.20 m in Cataluña. These variations seem to be certainly higher than the noise we expect in each geoid, which is of the order of 5 cm for both of them. However, whether there are undetected systematic effects distorting our solutions we are not yet able to say.

4. Comparisons

There are two prossibilities of making external checks of our data; namely either we compare them with independent data of the same kind but coming from different sources, or we try to compare with other geophysical fields exploiting some mutual relation with the gravity field.

Only little work has been done till now in this field, yet we like to mention:

a) **geoids comparisons**: an external comparison has been performed between the Geomed geoid in the Western Mediterranean and another gravimetric geoid supplied by the Bureau Gravimetrique International. This last has been computed (J.P.Barriot, [1987]) over a large window ($-15° \leq \lambda \leq 28°, 25° \leq \phi \leq 55°$) by applying a truncated Stokes formula, with a 6° cap; terrain effects have not been considered (cfr. Fig 13).

The difference, on 17557 points, shows that there is a bias of 0.49 m and an r.m.s. of 0.81 m. This suggest rather pessimistic conclusions; however by looking at the contour plot of these differences (cfr. Fig 14) we find they are quite flat in the marine area and they become very high and systematic (only positive signs) on land; this could be attributed to the different treatment of the contribution of topography.

In particular we believe that in Corse, where we have the maximum differences, there might be a problem with the gravity material;

b) **isostatic topographic corrections**: some work has been done by applying different isostatic-topographic corrections to the field of free air gravity anomalies, to verify which one would produce the best smoothing and homogeneization of the gravity field.

The Moho depths used in the computation have been derived from the Airy-Heiskanen theory or an improved version of it; another Moho model was derived from the analysis of seismic data. By using the central Mediterranean as a test area, it has been proved by the Graz group that the Airy-Heiskanen corrections have a much higher performance, while the seismic Moho produced very large descrepancies in the southern Sicily and along the Calabrian arc.

5. Discussion

The following points represent the goals defined by the Geomed groups for the next period:

a) **new data**: in particular it seems essential to acquire new gravity data, may be not at a high resolution, in north Africa and in France, Croatia, Turkey, etc. It also been decided to collect GPS, levelling data and deflections of the vertical, particularly along the coasts;

b) **validation**: a project has been established to validate our marine gravity data sets with gravimetric profiles owned by DMA; very essential is the validation of ETOPO5U by comparing it with Morelli's bathymetry as well as with national DTM's; mean-while the new ERS1 data will be validated and included in the altimetric adjustments;

c) **new computations**: the computation of the geoid and SST in the Central Mediterranen, will be completed in one year.

After these intermediary goals will be reached we will have at least a geoid and a SST over the whole Mediterranean.

The problems at that point will be to homogenize the solutions and to proceed to their interpretation at least in terms of geostrophic circulation.

Figure captions:

Fig. 1a - Distribution of the free air anomalies in the Eastern Mediterranean.

Fig. 1b - Distribution of the free air anomalies in the Central Mediterranean.

Fig. 1c - Distribution of the free air anomalies in the Western Mediterranean.

Fig. 2 - Available land gravity data.

Fig. 3a - Bathymetry (on the left) and ETOPO5U Model (on the right) in the Eastern Mediterranean.

Fig. 3b - Bathymetry (on the left) and ETOPO5U Model (on the right) in the Central Mediterranean.

Fig. 3c - Bathymetry (on the left) and ETOPO5U Model (on the right) in the Western Mediterranean.

Fig. 4 - Seasat observations.

Fig. 5 - Geosat observations.

Fig. 6 - ERS1 35 days period observations.

Fig. 7 - ERS1 3 days period observations.

Fig. 8a - OSU91A model in the Eastern Mediterranean: geoid (on the left) and free air anomalies (on the right).

Fig. 8b - OSU91A model in the Central Mediterranean: geoid (on the left) and free air anomalies (on the right).

Fig. 8c - OSU91A model in the Western Mediterranean: geoid (on the left) and free air anomalies (on the right).

Fig. 9 - Geoid computed by FFT techniques in the Eastern Mediterranean.

Fig. 10 - Geoid computed by fast collocation in the Western Mediterranean.

Fig. 11 - Geoid computed by pure collocation in the Mediterranean sea.

Fig. 12 - Sea surface topography in the Western Mediterranean sea.

Fig. 13 - Gravimetric geoid in the Western Mediterranean (J.P. Barriot, [1987]).

Fig. 14 - Differences between Geomed geoid and the geoid supplied by the BGI in the Western Mediterranean.

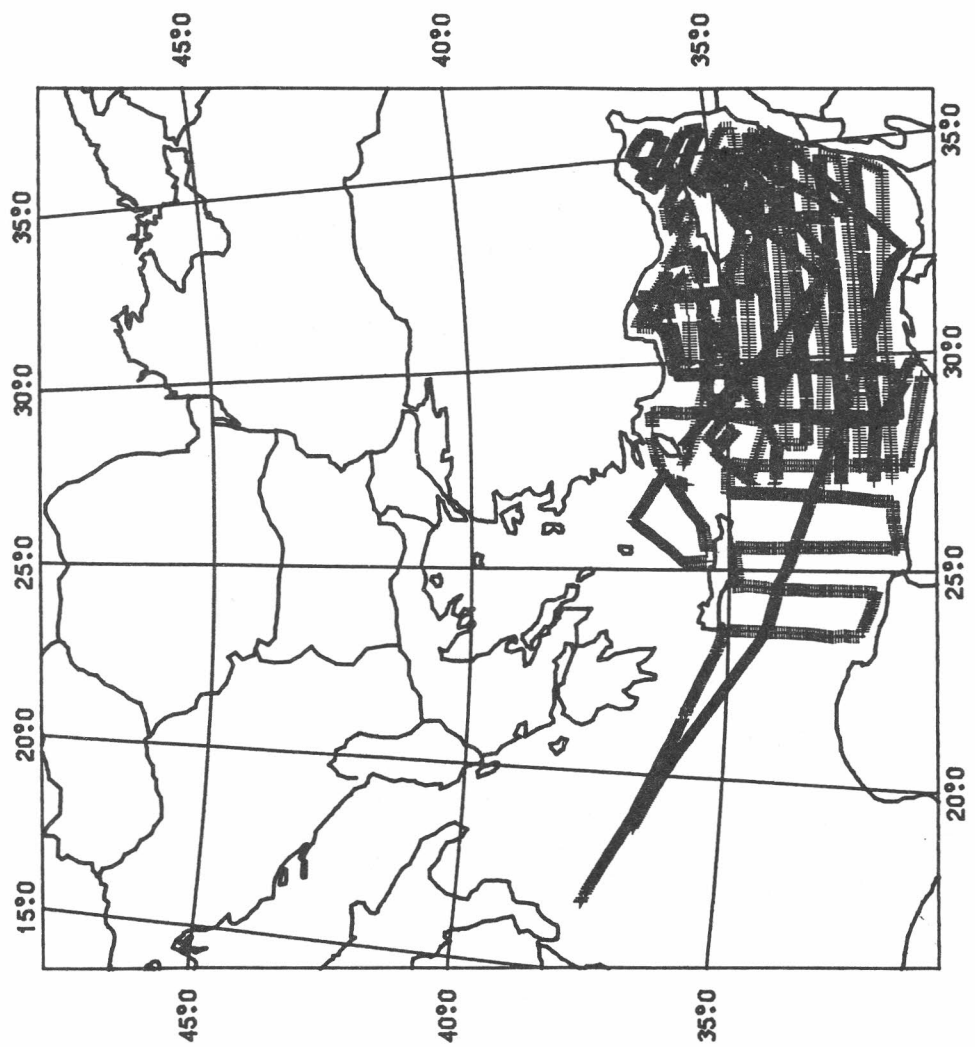

Fig. 1a

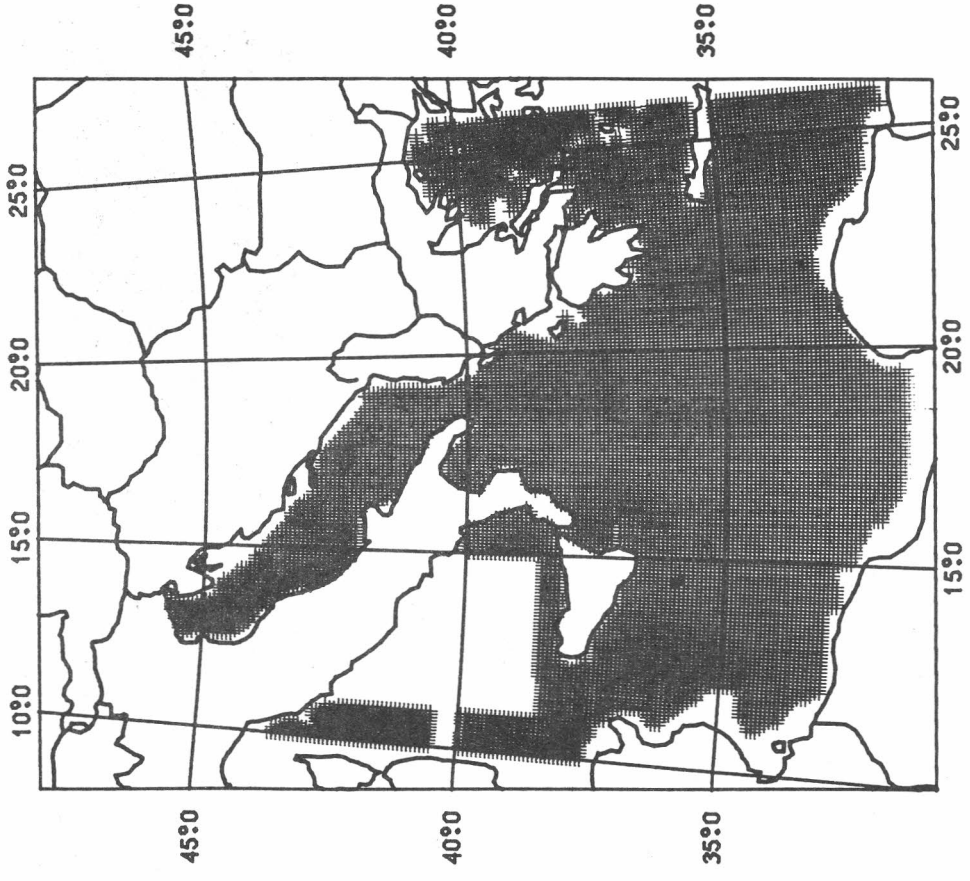

Fig. 1b

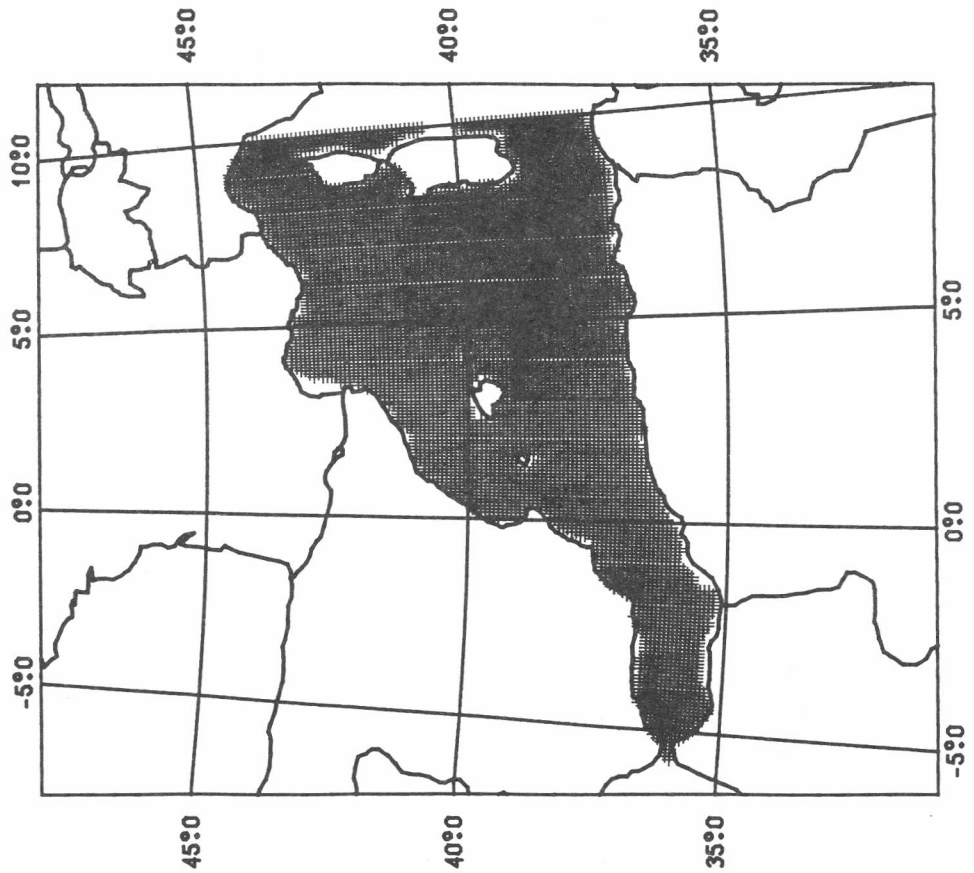

Fig. 1c

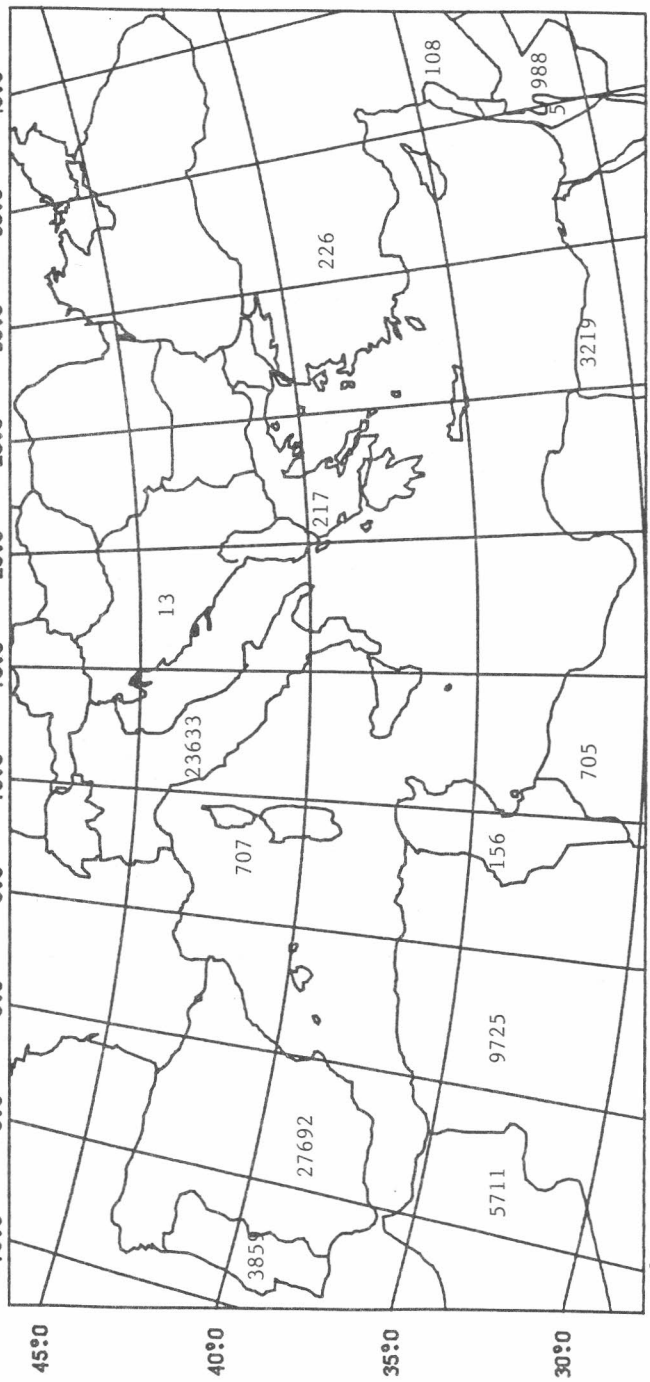
40°0
35°0
30°0
25°0
20°0
15°0
10°0
5°0
0°0
-5°0
-10°0
45°0
40°0
35°0
30°0
-5°0
0°0
5°0
10°0
15°0
20°0
25°0
30°0
35°0
108
988
226
3219
217
13
23633
707
705
156
9725
27692
5711
3859

Fig. 2

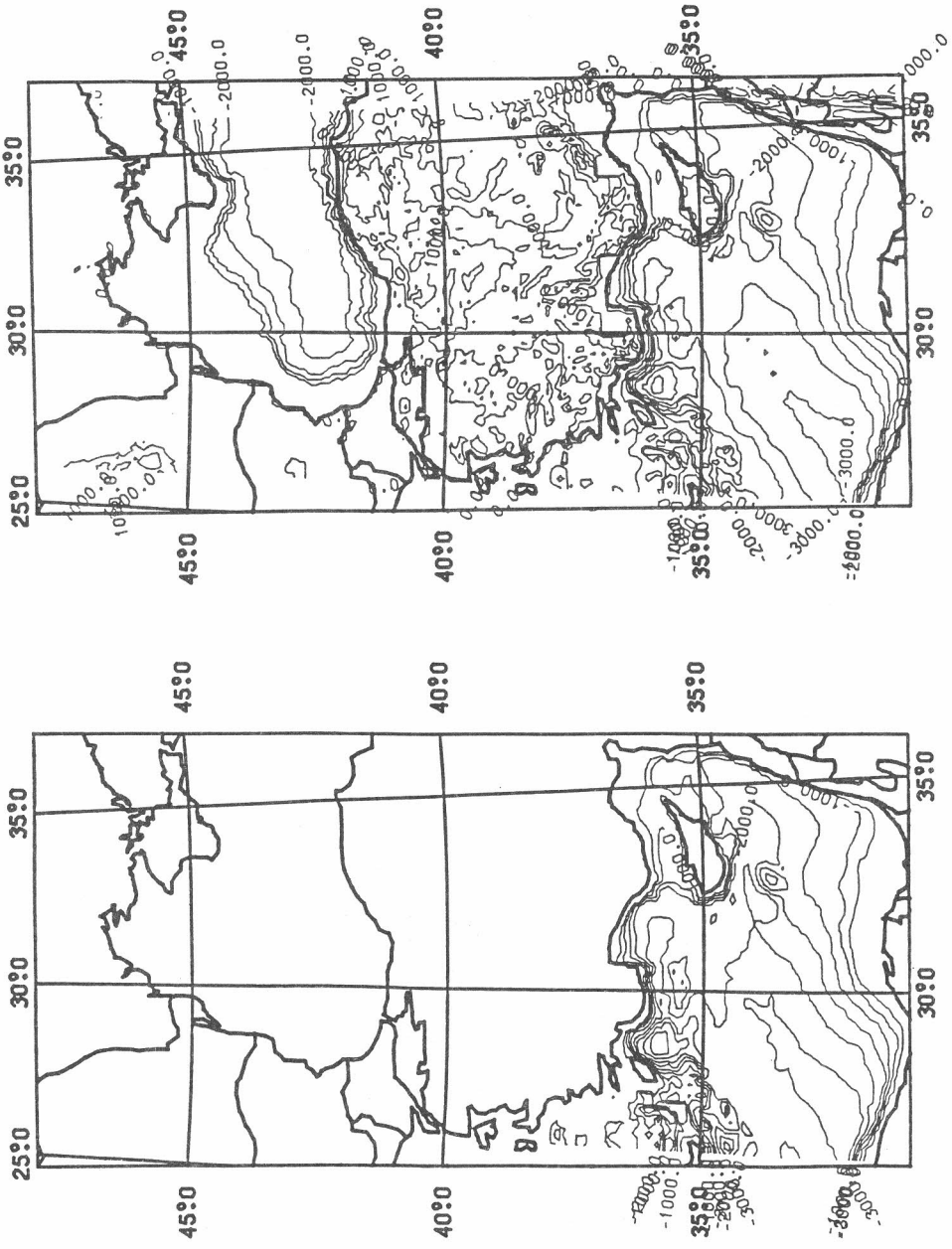

Fig. 3a

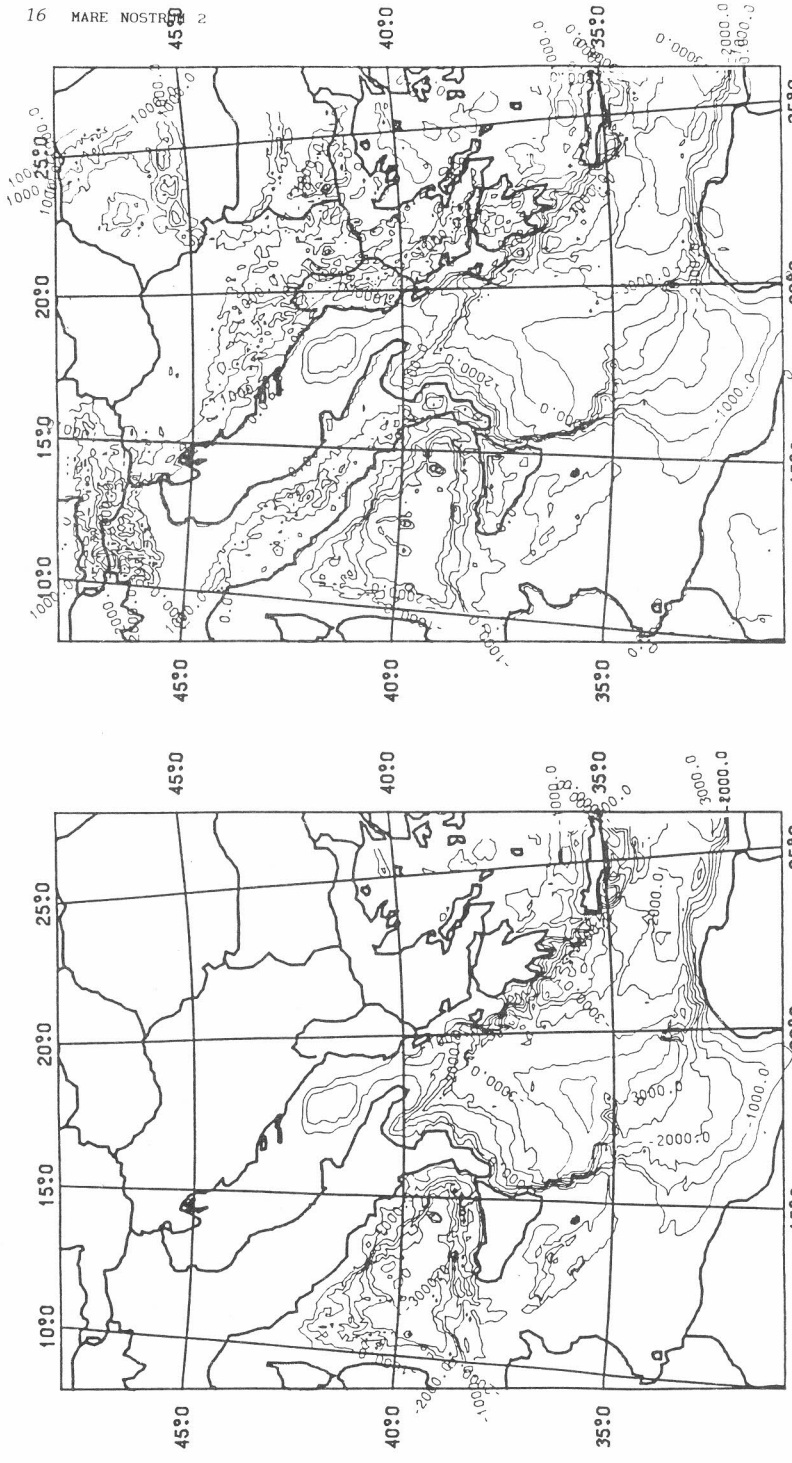

Fig. 3b

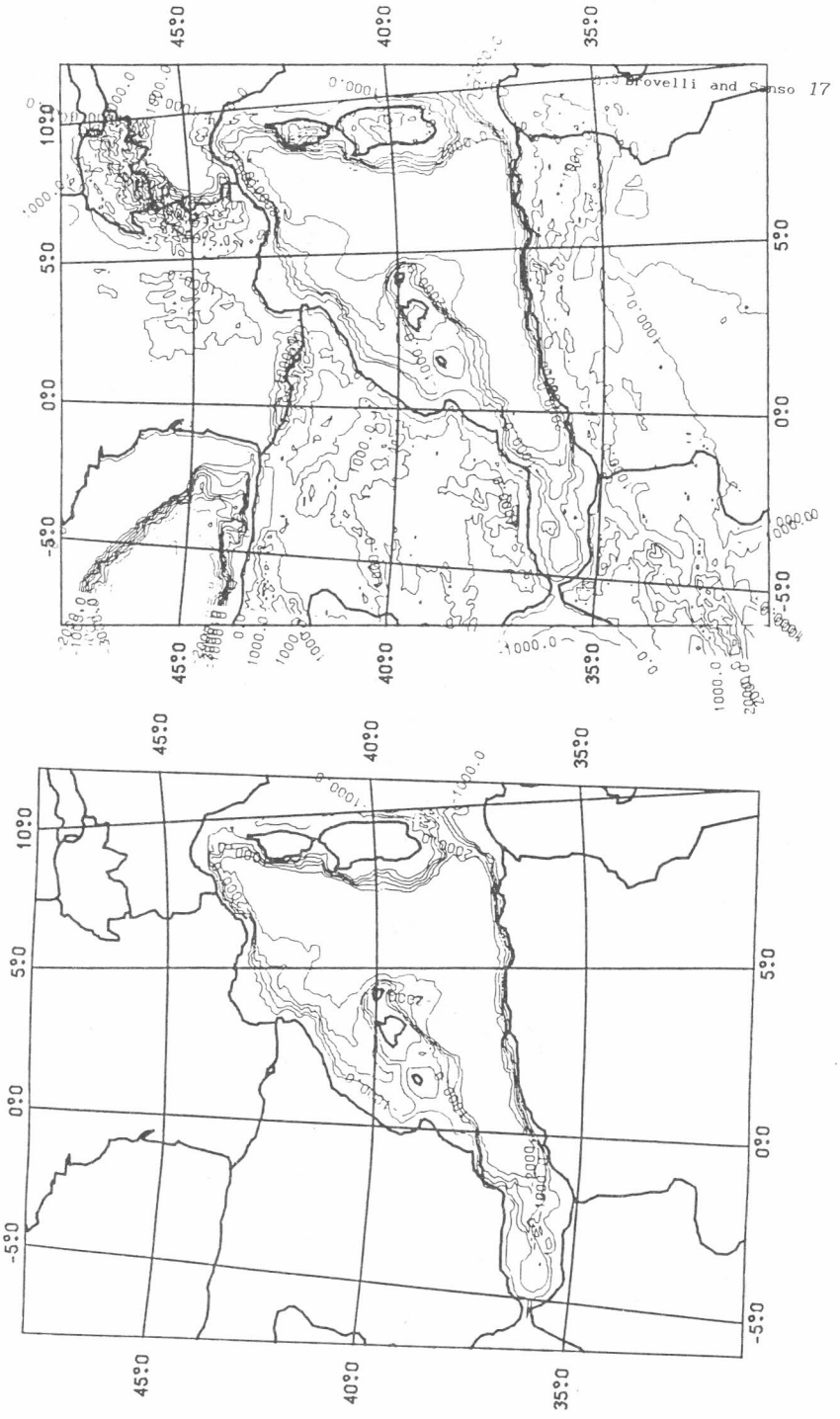

Fig. 3c

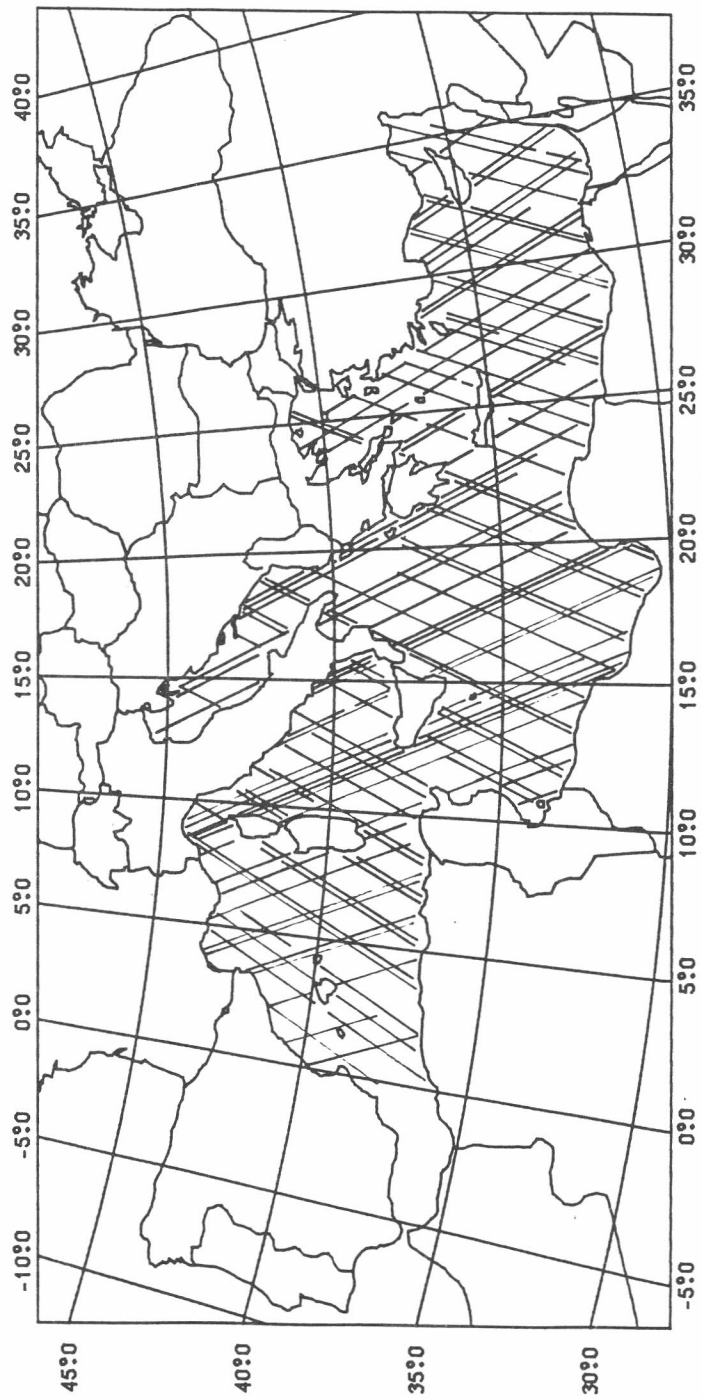
40°0
35°0
30°0
25°0
20°0
15°0
10°0
5°0
0°0
-5°0
-10°0
45°0
40°0
35°0
30°0
35°0
30°0
25°0
20°0
15°0
10°0
5°0
0°0
-5°0

Fig. 4

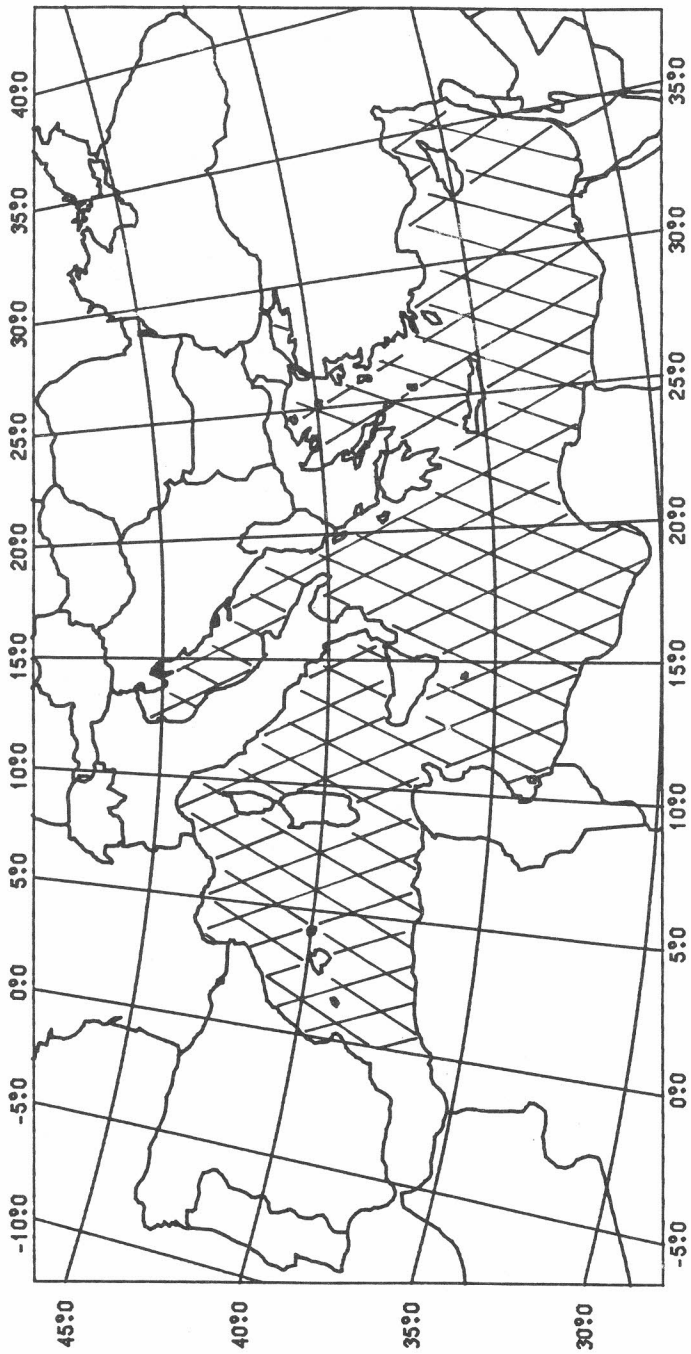
40°0
35°0
30°0
25°0
20°0
15°0
10°0
5°0
0°0
-5°0
-10°0
45°0
40°0
35°0
30°0
35°0
30°0
25°0
20°0
15°0
10°0
5°0
0°0
-5°0

Fig. 5

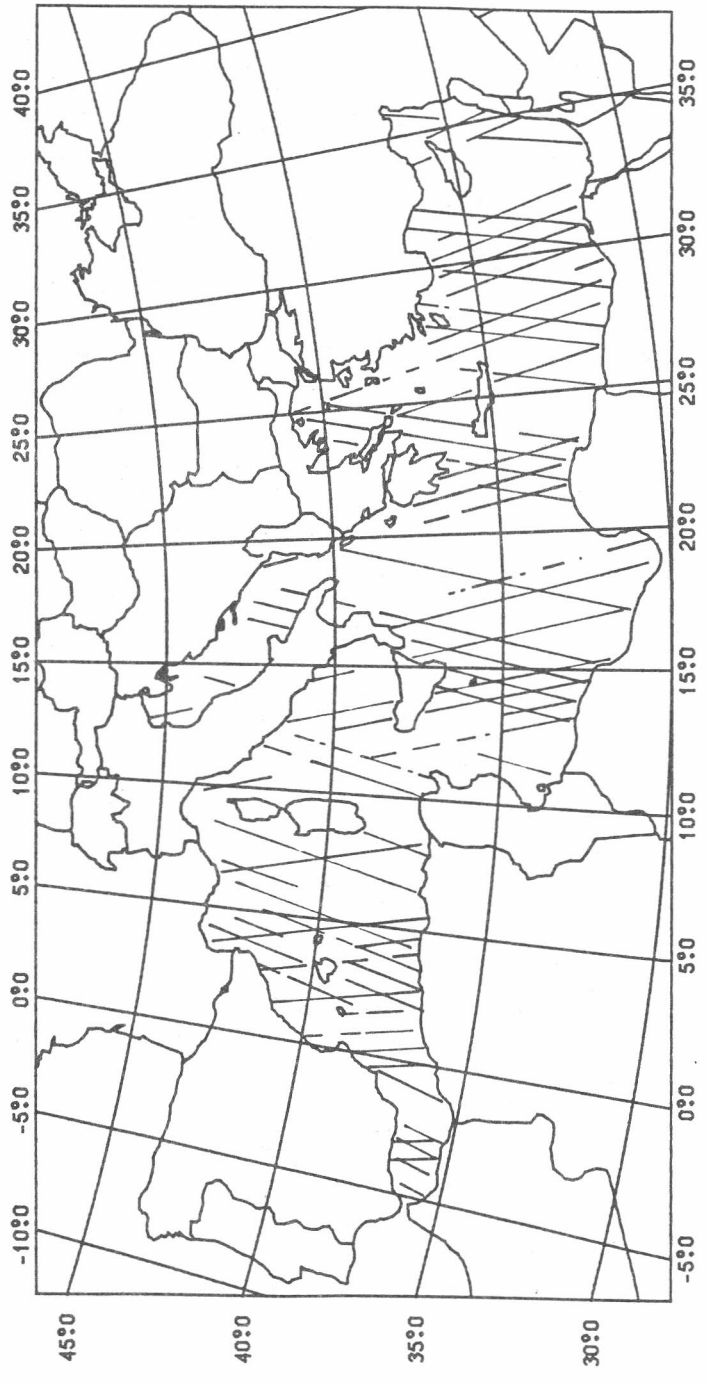
40°0
35°0
30°0
25°0
20°0
15°0
10°0
5°0
0°0
-5°0
-10°0
45°0
40°0
35°0
30°0
35°0
30°0
25°0
20°0
15°0
10°0
5°0
0°0
-5°0

Fig. 6

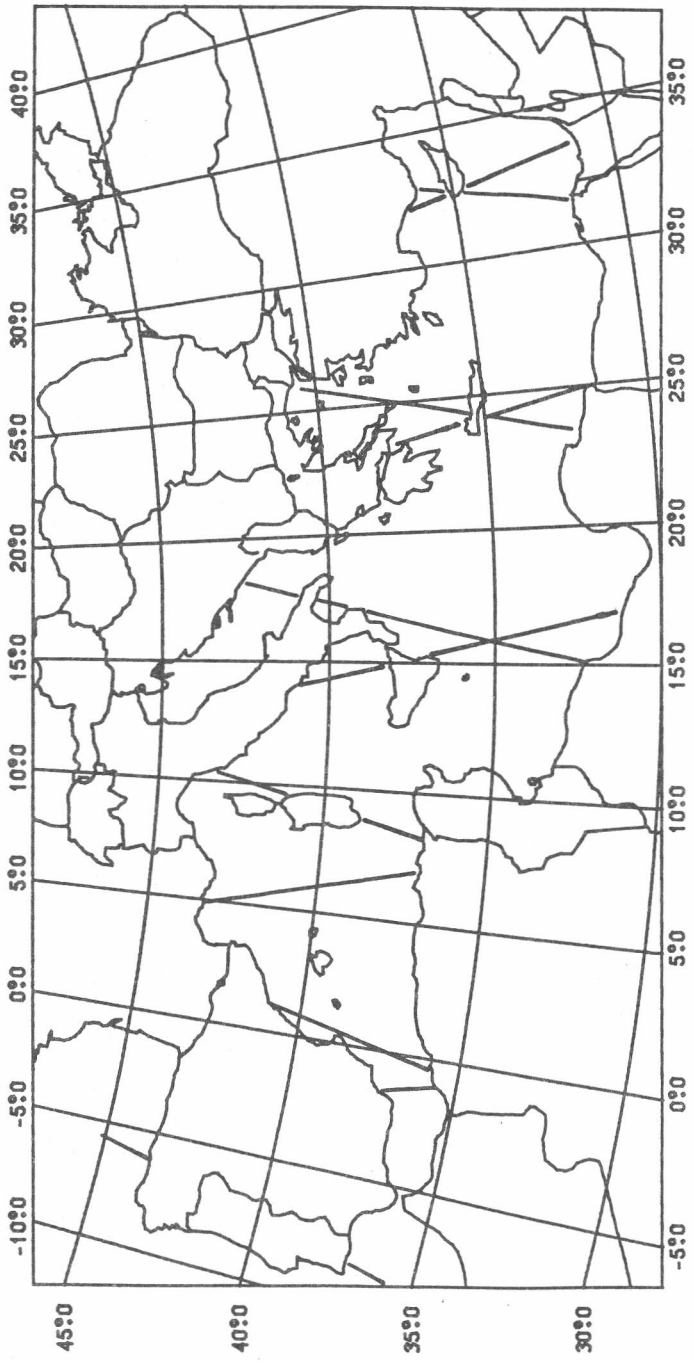
40:0
35:0
30:0
25:0
20:0
15:0
10:0
5:0
0:0
-5:0
-10:0
45:0
40:0
35:0
30:0
35:0
30:0
25:0
20:0
15:0
10:0
5:0
0:0
-5:0

Fig. 7

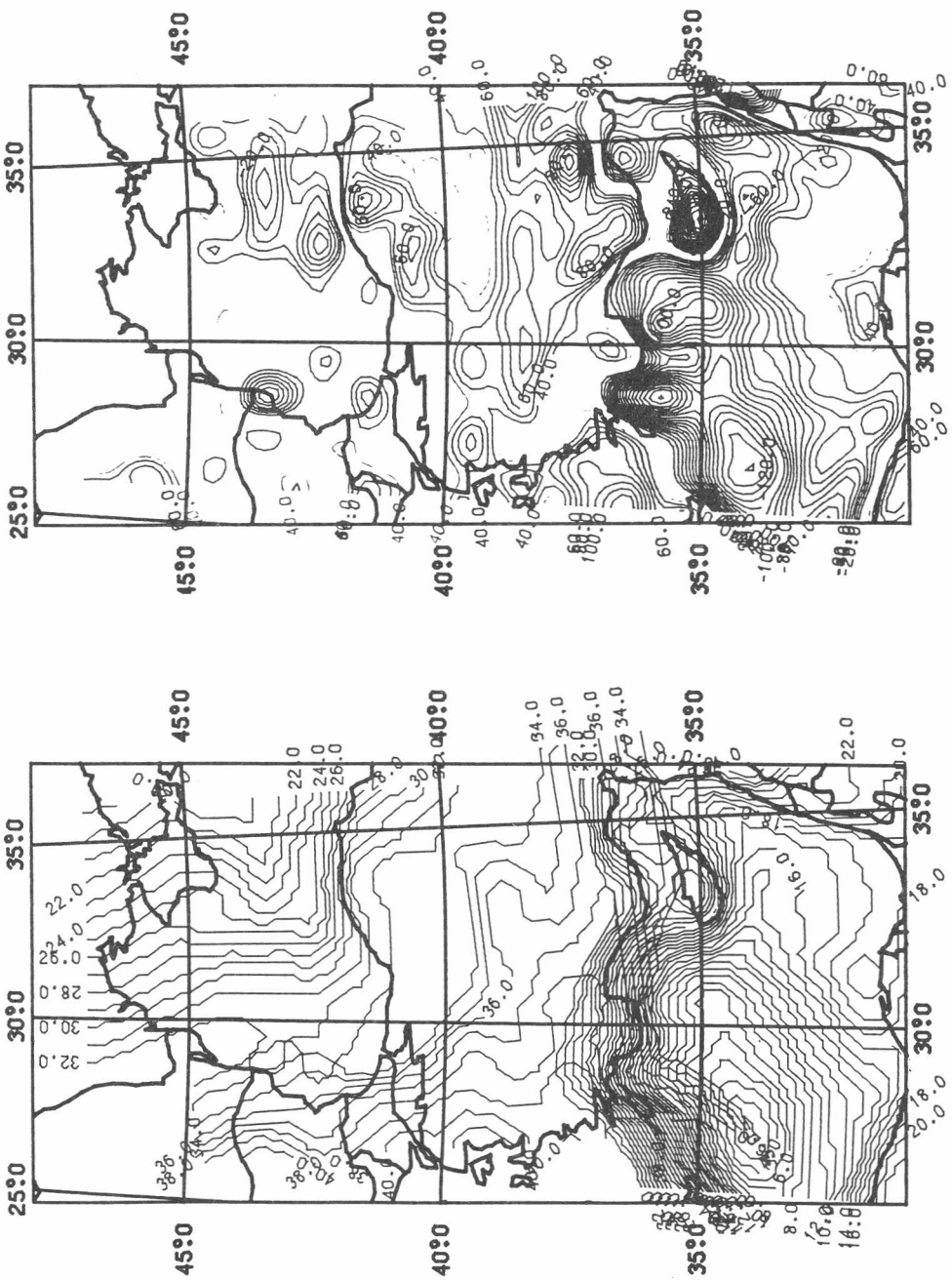

Fig. 8a

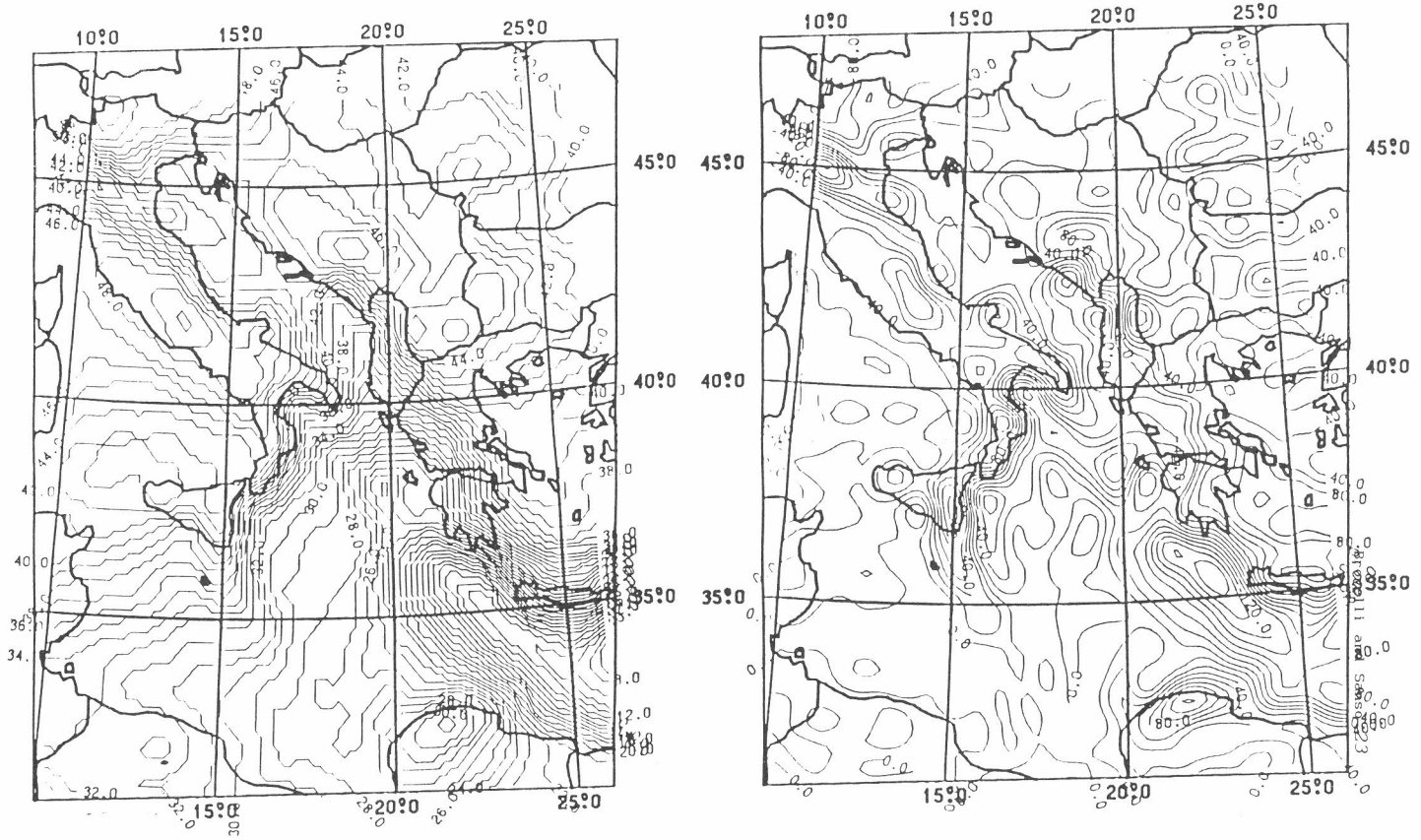

Fig. 8b

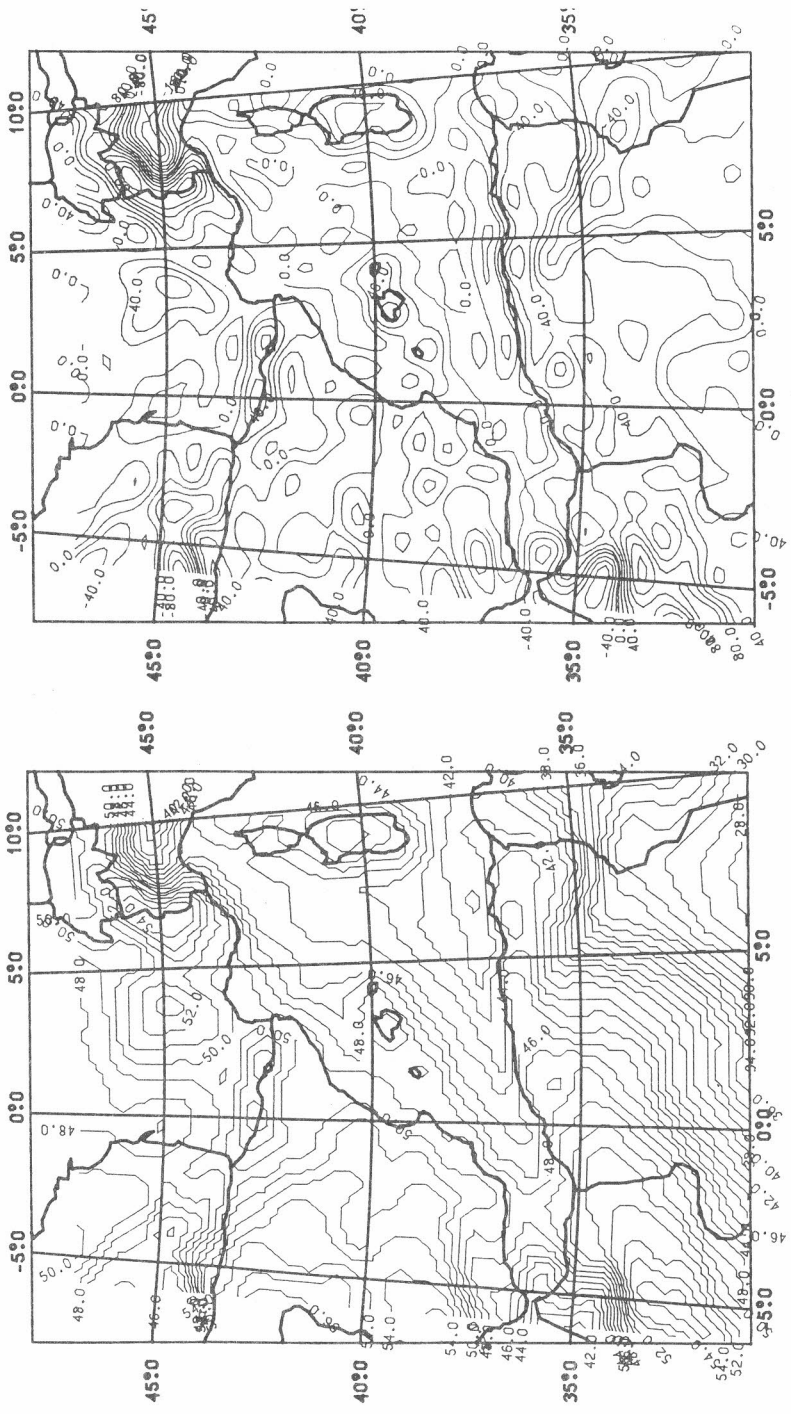

Fig. 8c

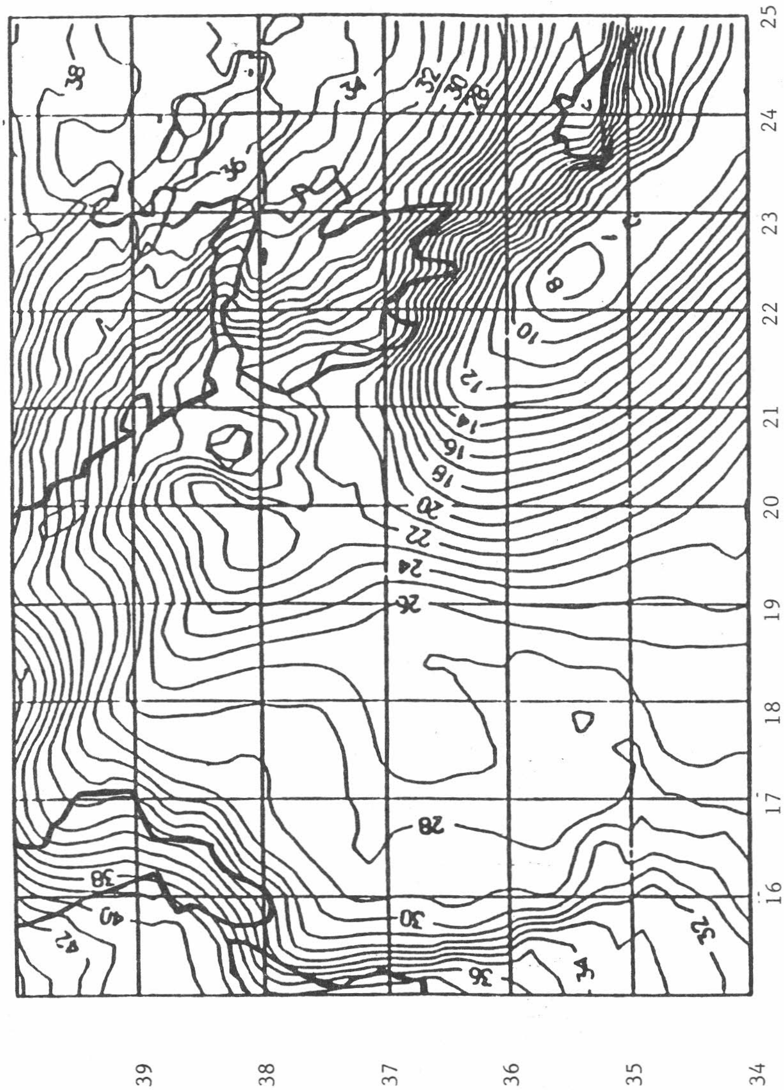

Fig. 9

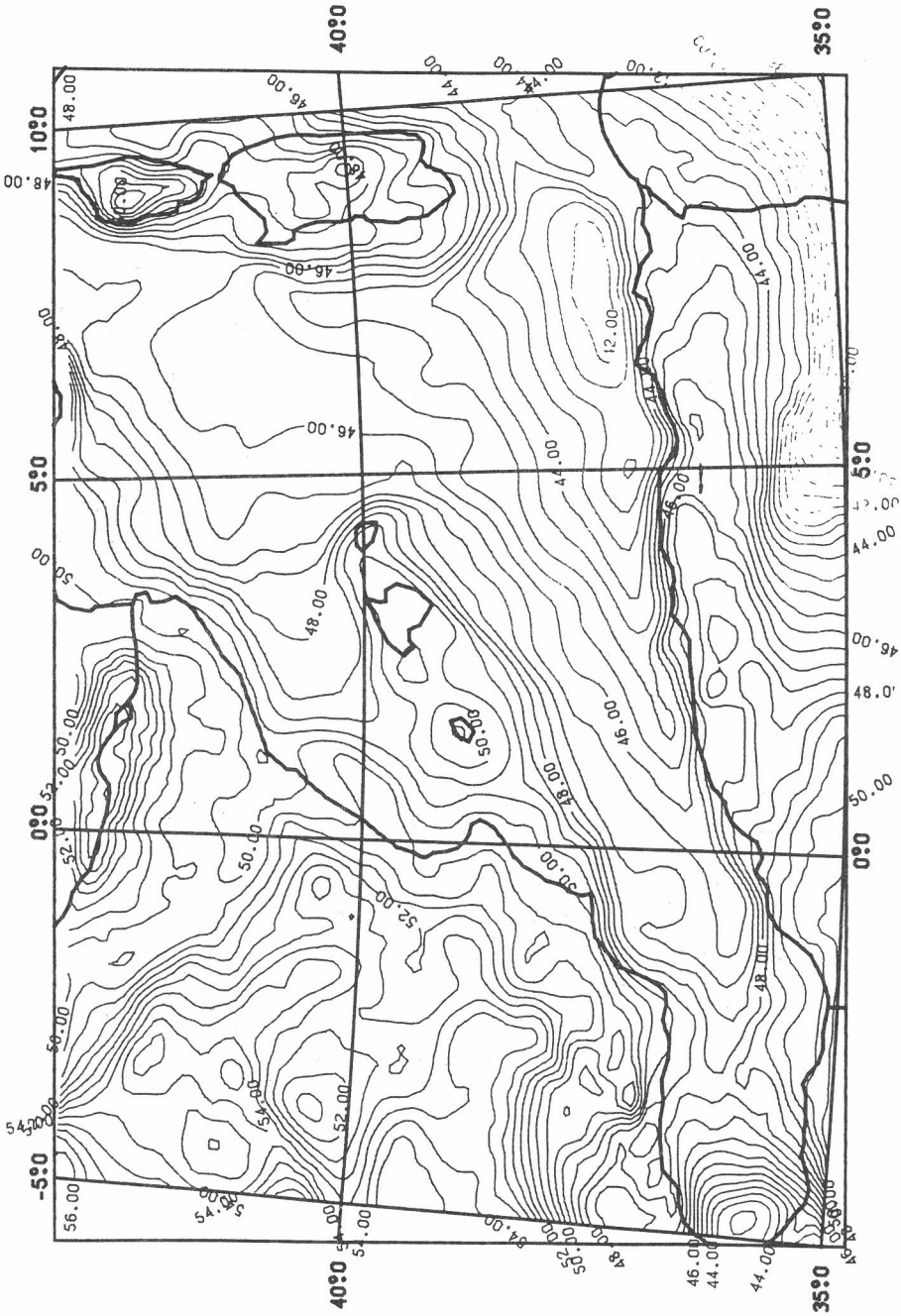

Fig. 10

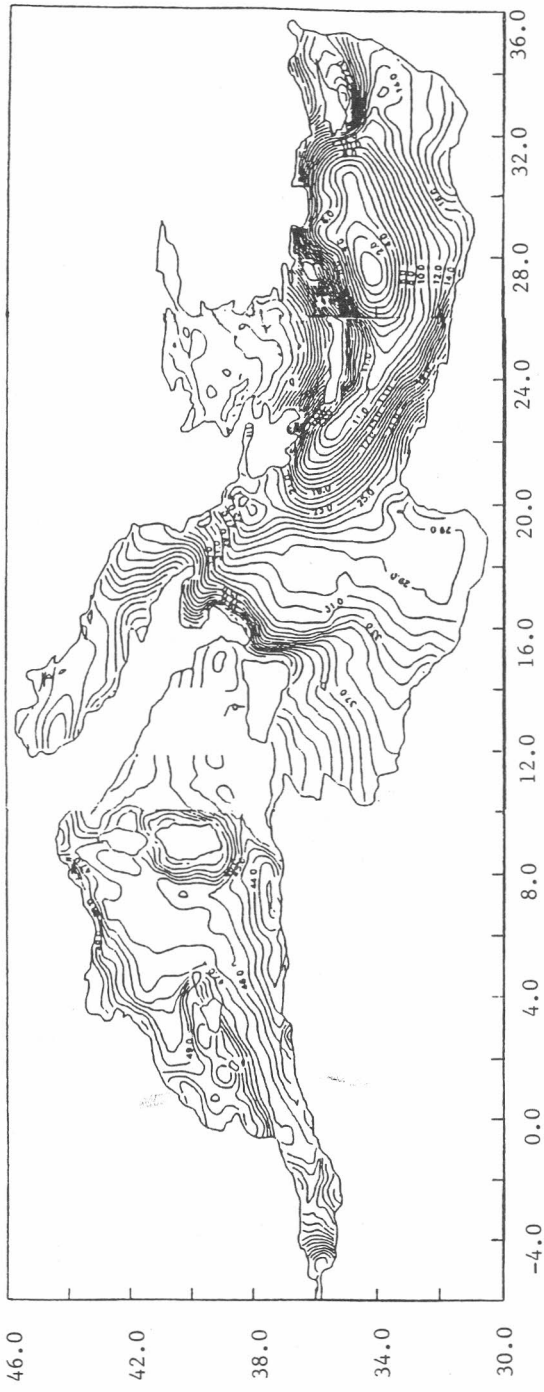

Fig. 11

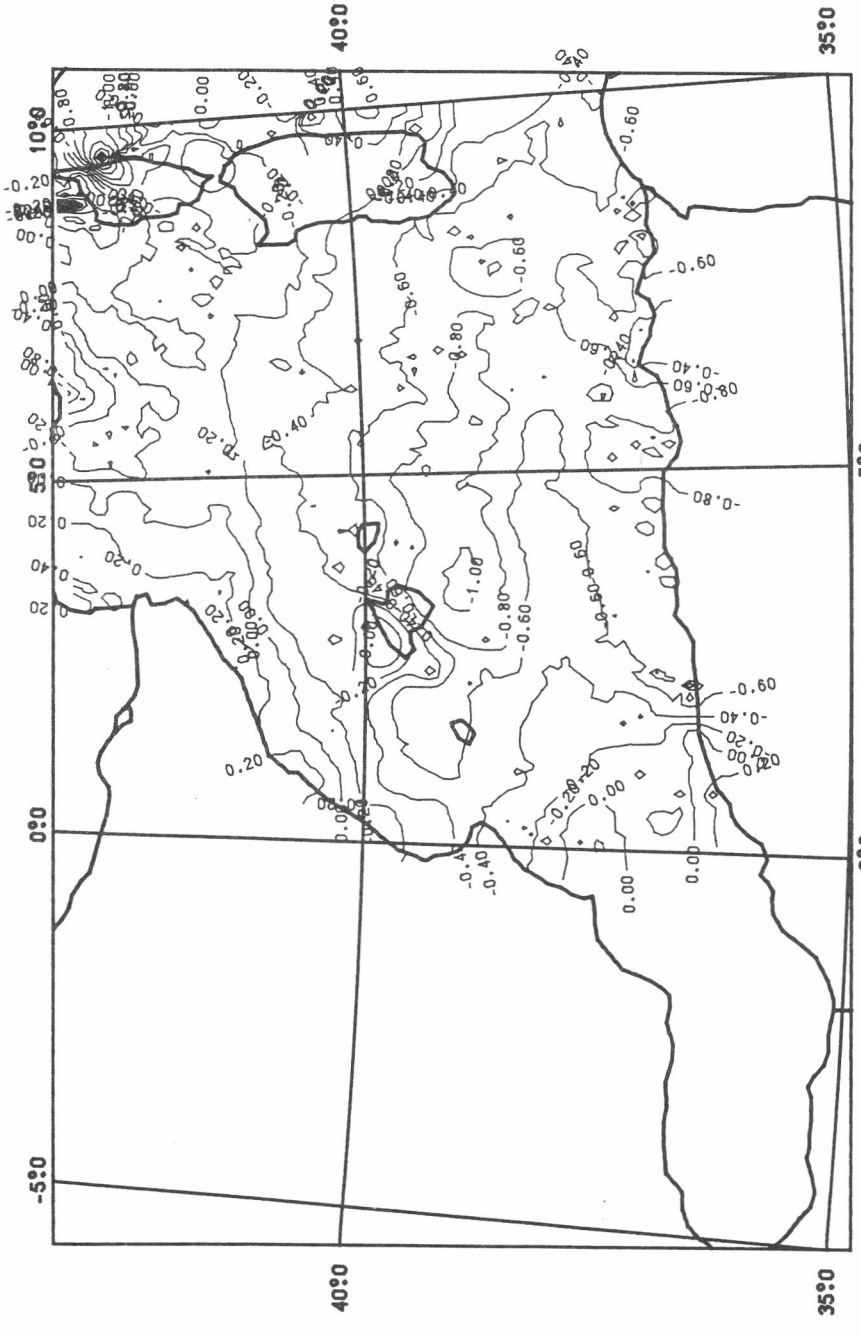

Fig. 12

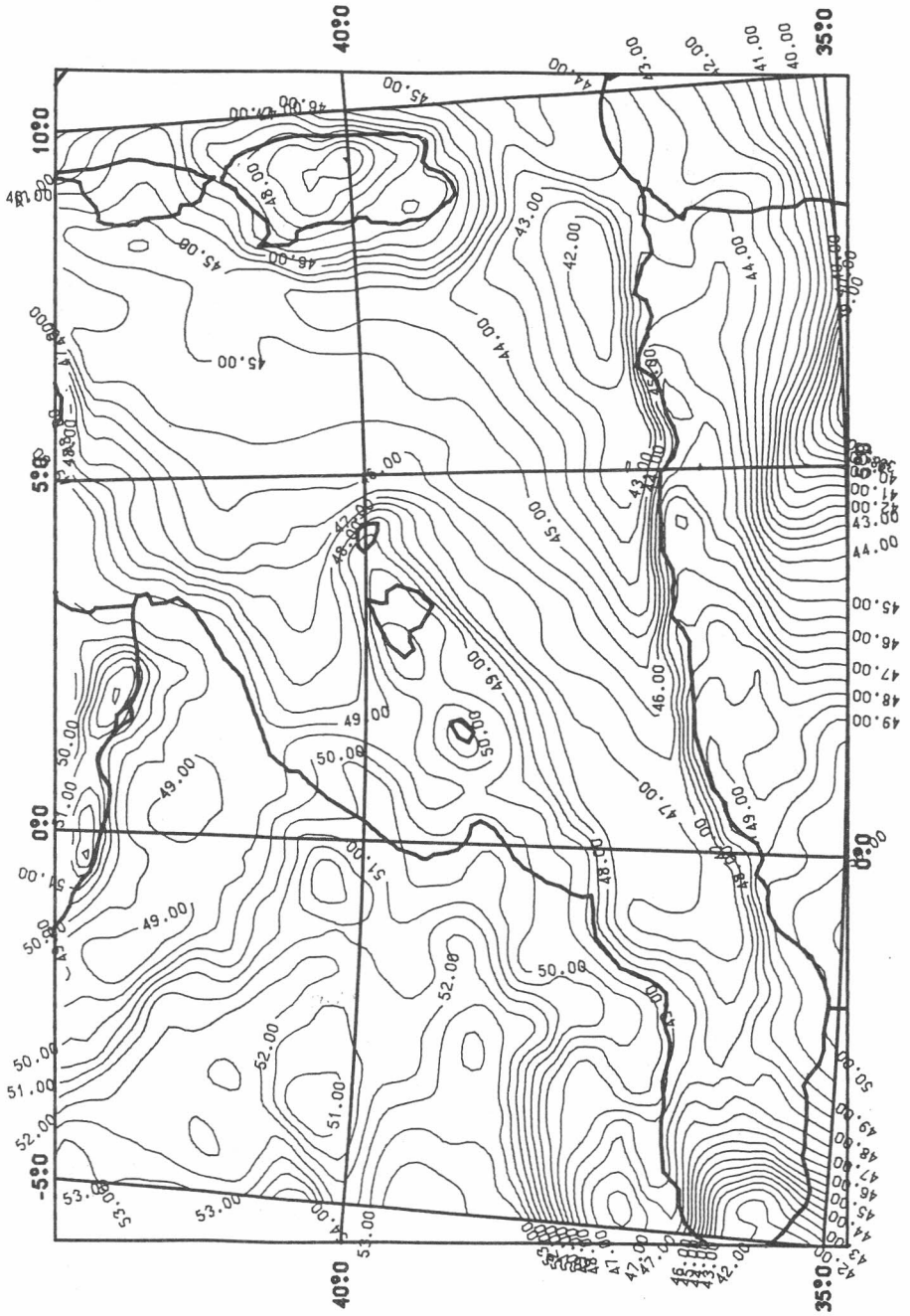

Fig. 13

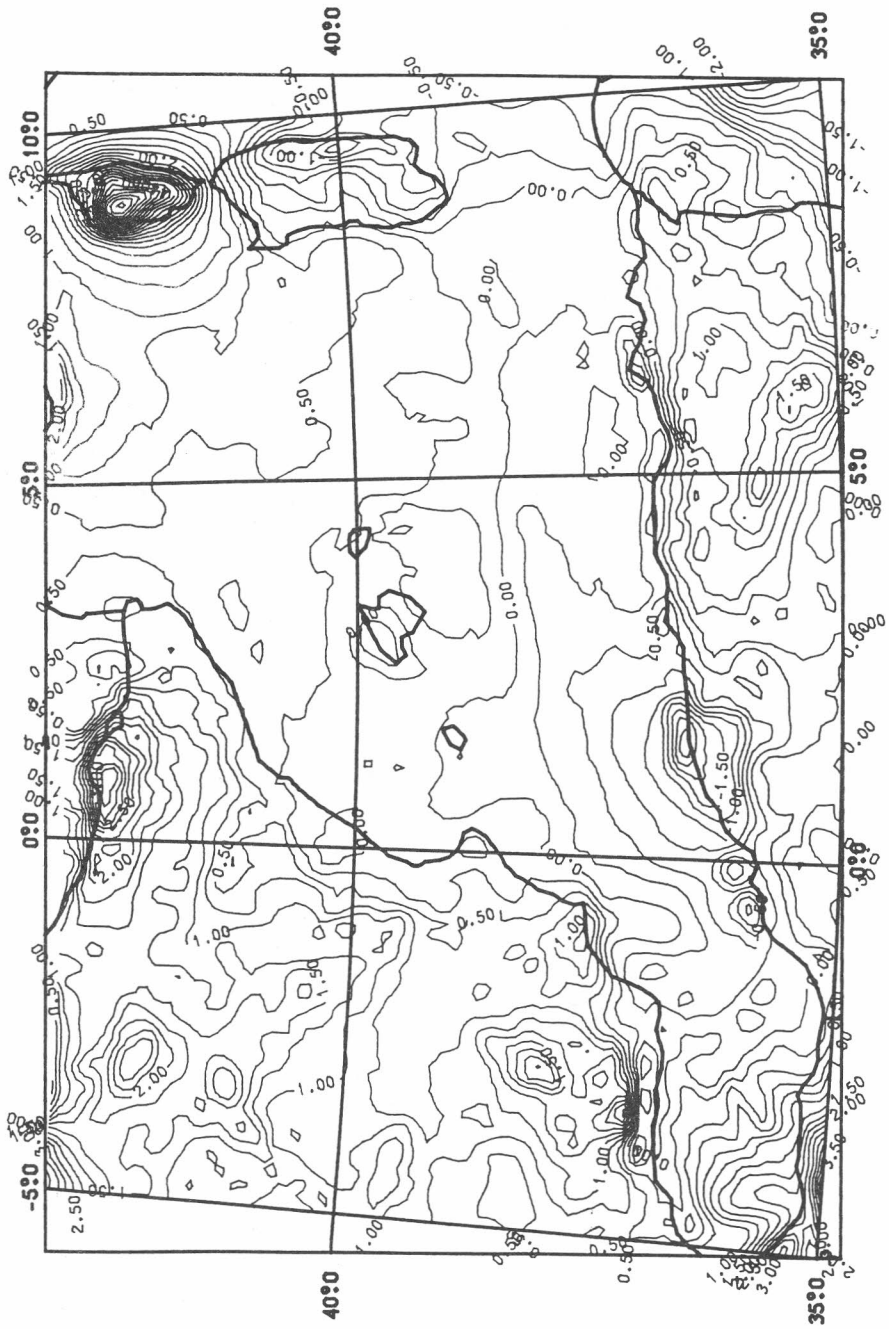

Fig. 14

References:

T.D. Allan and C. Morelli, 1971, A Geophysical Study of the Mediterranean Sea, Boll. Geofisica teorica e applicata, XIII, 50.

D. Arabelos, 1980, Untersuchungen zur gravimetrischen Geoidbestimmung,

dargestellt am Testgebiet Griechenland, Wissenschaftliche Arbeiten der Fachrichtung Vermessungswesen der Universit"at Hannover, Nr. 98, XIV 151, Hannover.

D. Arabelos and C.C. Tscherning, 1988, Gravity Field Mapping from Satellite Altimetry, Sea-Gravimetry and Bathymetry in the Eastern Mediterranean, Geophys J., Int. 92, pp. 195-206.

D. Arabelos, P. Knudsen, C.C. Tscherning, 1987, Covariance and Bias Treatment when Combining Gravimetry, Altimeter and Gradiometer Data by Collocation, Presented Intersection Symposium "Advances in Gravity Field Modelling", XIX General Assembly IAG, Vancouver, Canada, August 1987. Proceedings of the International Association of Geodesy (IAG) Symposia, Tome II, pp. 443-454.

D. Arabelos and I.N. Tziavos, 1989, The Hellenic geoid - new considerations and experiences". Ricerche di Geodesia Topografia e Fotogrammetria. Miscellanea per il 70' di Giuseppe Birardi, pp. 1-20, Milan.

G. Balmino, 1992, Orbit Choice and the Theory of Radial Orbit Error for Altimetry, Proceedings of the International Summer School of Theoretical Geodesy "Satellite Altimetry in Geodesy and Oceanography", Trieste, May 25- July 6, 1992, in print.

J.P. Barriot, 1987, La determination du geoide par altimetrie oceanique et gravimetrie. Quelques aspects du traitement et interpretation geologique sur l'Ocean Indien (partie Nord-Ouest) et Mediterranee Occidentale, PhD thesis, Academie de Montpellier, Universite des Sciences et Techniques du Languedoc.

R. Barzaghi, M.A. Brovelli, F. Sansó, 1990, Altimetry rank deficiency in crossover adjustment, in "Determination of the geoid: present and future", IAG Symposya 106, Springer- Verlag, pp. 108-118.

R. Barzaghi, M.A. Brovelli and P. Knudsen, 1992, Different crossover adjustments in the Mediterranean area, in print on Bollettino di Geofisica Teorica e Applicata.

G.P. Bottoni, R. Barzaghi, 1992, Fast Collocation, in print on Bull. Geod.

M.A. Brovelli and F. Migliaccio, 1992, The Direct Estimation of the Potential Coefficients by Biorthogonal Sequences, Proceedings of the International Summer School of Theoretical Geodesy "Satellite Altimetry in Geodesy and Oceanography", Trieste, May 25- July 6, 1992, in print.

R. Forsberg, 1985, Gravity field terrain effect computation, Bull. Geod n.59, pp. 342-360.

P. Knudsen and M.A. Brovelli, 1991, Co-linear and Cross-over Adjustment of GEOSAT ERM and SEASAT Altimeter Data in the Mediterranean Area, Proceedings of the EGS General Assembly, SE6, Wiesbaden, 22-26 April 1991, in print.

C. Morelli, 1970, Physiography, Gravity and Magnetism of the Tyrrhenian Sea, Boll. Geofisica teorica e applicata, XIII, pp. 275-309.

C. Morelli, M. Pisani, C. Gantar, 1975a, Geophysical Anomalies and Tectonics in the Western Mediterranean, Boll. Geofisica teorica e applicata, XVII, 67.

C. Morelli, C. Gantar, M. Pisani, 1975b, Bathymetry, Gravity and Magnetism in the Strait of Sicily and the Jonian Sea, Boll. Geofisica teorica e applicata, XVII, pp. 39-58.

C. Morelli, C. Gantar, M. Pisani, 1975c, Geophysical Studies in the Aegean Sea and in the Eastern Mediterranean, Boll. Geofisica teorica e applicata, XVII, pp. 128-168.

R.H. Rapp, 1989a, The Treatment of the Permanent Tidal Effects in the Analysis of Satellite Altimeter Data for SST, MAnuscripta Geodaetica, n. 14 (6).

R.H. Rapp, 1989b, Combination of Satellite, Altimetric and Terrestrial Gravity Data, on the Volume "Theory of Satellite Geodesy and Gravity Field Determination" Lecture Notes in Earth Sciences, Springer-Verlag, 261-284.

R.H. Rapp, 1992, Use of Altimeter Data in Estimating Global Gravity Models, Proceedings of the International Summer School of Theoretical Geodesy "Satellite Altimetry in Geodesy and Oceanography", Trieste, May 25- July 6, 1992, in print.

F. Sansó, 1992, Theory of Geodetic B.V.P.s Applied to the Analysis of Altimetric Data, Proceedings of the International Summer School of Theoretical Geodesy "Satellite Altimetry in Geodesy and Oceanography", Trieste, May 25- July 6, 1992, in print.

E.J.O Schrama, 1989, The role of orbit errors in processing of satellite altimetric data, Netherlands Geodetic Commission, Pubblication on Geodesy n. 33.

M.G. Sideris, 1987, Spectral methods for the numerical solution of Molodensky's problem, UCSE Rep. n. 20024 - The University of Calgari.

G. Strang van Hees, 1991, Stokes formula using Fast Fourier Techniques in "Determination of the geoid: present and future", Iag Symposia 106, Springer-Verlag, pp.405-408.

C.A. Wagner, 1989, Summer School Lectures on Satellite Altimetry, on the Volume "Theory of Satellite Geodesy and Gravity Field Determination" Lecture Notes in Earth Sciences, Springer-Verlag, pp. 285-334.

Y.M. Wang and R.H. Rapp, 1990, Revised Geosat Geophysical Data Records based on the OSU89 orbit improvement for the first year of the ERM, Internal Report, Dept. of Geod. Sc. and Surveying, The Ohio State University, Columbus.

C. Wunsch, 1992, Physics of the Ocean Circulation, Proceedings of the International Summer School of Theoretical Geodesy "Satellite Altimetry in Geodesy and Oceanography", Trieste, May 25- July 6, 1992, in print.

V. Zlotnicki, 1992, Quantifying Time - Varying Oceanographic Signals with Altimetry, Proceedings of the International Summer School of Theoretical Geodesy "Satellite Altimetry in Geodesy and Oceanography", Trieste, May 25- July 6, 1992, in print.

Altimeter Data from ERS-1 in the Mediterranean Sea

D. Arabelos, S.D. Spatalas, I.N. Tziavos

Department of Geodesy and Surveying
University of Thessaloniki
540 06 Thessaloniki, Greece

Abstract.

New, five months about, repeat ERS-1 altimeter data have been preliminary processed in the Mediterranean Sea with respect to selection criteria in order to avoid data influenced by errors caused mainly by orbit errors and altimeter signal uncertainties, and of course due to presence of land. After the removal of a number of erroneous observations and in order to assess the quality of the data a crossover analysis has been carried out and a crossover root-mean-square (rms) error discrepancy was found equal to 1.785 m. After a crossover adjustment model was applied introducing bias and tilt into the computations, the rms crossover discrepancy decreased to 0.046 m. Furthermore, a first collinear analysis was performed and some indicative results were outlined.

Introduction

The ERS-1 satellite has been launched during 1991 in order to investigate the environment. It has a sun-synchronous, near polar orbit, and operates in a 3 days, a 35 days and a 176 days cycle (ESRIN, 1992). Altimeter data for the Mediterranean Sea [$30^\circ \leq \phi \leq 50^\circ$, $-5^\circ \leq \lambda \leq 40^\circ$] from ERS-1 mission were recently available to us in the frame of the participation of the first of the authors in the ERS-1 project DK2. The time period covered by this data set is April 4, 1992 to August 31, 1992 (four repeat periods). Data were delivered as records in ascii format. Each of the records put in our disposal contains the revolution number, time (UTC since January 1, 1985, midnight), latitude, longitude, corrected sea surface height H_c, standard deviation of H_c, significant wave height H_w and standard deviation of H_w. The correction applied to sea surface height is given as follows (O. Andersen and C.C. Tscherning, personal communication):

$$H_c = H - (\text{ionosphere} + \text{dry} + \text{wet troposphere} + \text{solid Earth tide correction})$$

It is worth mentioning here that the sea surface heights have not been corrected for ocean tide effect.

Concerning the satellite orbits it is interesting to note that they have been computed using the GEM-T2 model instead the newer PG4491 model in order to enable mixing the altimeter measurements from GEOSAT and ERS-1. The ERS-1 orbital frequency is

6035.9287 secs. The duration of each Exact Repeat Mission (ERM) is 35 days or correspondingly 501 revolutions. In our test area and for the five months mission period a number of 25757 subsatellite points (one second mean values) is available. These points are distributed in the four ERM periods mentioned above.

From the altimeter data the influence of the OSU91A geopotential model complete to degree and order 360 and the influence of the OSU91 Sea Surface Topography (SST) complete to degree and order 10 have been subtracted. The results from the statistical analysis of the residual altimeter data are summarized in Table 1.

In our preliminary analysis of the first ERS-1 altimeter data the following selection criteria have been adopted:

- The test area has been restricted to the Mediterranean Sea omitting subsatellite points found above latitude 43° and western of longitude 0°, as well as parts of the tracks located above latitude 40° and eastern of longitude 27°.
- Short tracks (having less than 5 points or equivalent length less than about 33.5 km) were eliminated.
- Residual altimeter heights (ERS-1– OSU91A – OSU91SST) larger than 10 m were considered as outliers and have not been taken into account in the computations.
- Altimeter heights with a standard deviation larger than 0.25 m were also omitted from the further data elaboration.

Table 1. Results of ERS-1 altimeter data reduced to OSU91A1F and the OSU91 SST (unit=m)

ERM	No. of data	Min. value	Max. value	Mean value	Standard dev.
1	6157	-4.163	6.110	0.367	1.618
2	6864	-4.416	6.953	0.353	1.483
3	6142	-4.660	6.170	0.420	1.675
4	6594	-35.479	7.112	-0.787	4.491
4*	6450	-5.210	7.112	0.161	1.588

* ERM 4 after the removal of values (ERS-1 – OSU91A – OSU91 SST) > 10 m

According to the criteria constructed above a number of 5992 observations was detected and removed. From these observation only a number of 144 outliers has been detected (i.e., reduced values > 10 m). A number of 21 short arcs were detected and the 58 observations contained to these arcs were neglected. The rest ones are located outside of our test area or were detected as erroneous data using the standard deviation of the satellite points.

Following the above mentioned selection criteria a number of 19765 observations was resulted showing a mean value equal to 0.47 m and standard deviation equal to 1.364 m. These observations are distributed in 315 tracks (see Figure 1). From Figure 1 it is clear that the ERS-1 35 days repeat period provides altimetry with a significantly improved coverage compared with GEOSAT 17 days ERM data (see, e.g. Arabelos and Tziavos, 1990). The distance between the tracks in the ERS-1 mission is about the half of the corresponding distance of GEOSAT mission in the Mediterranean area.

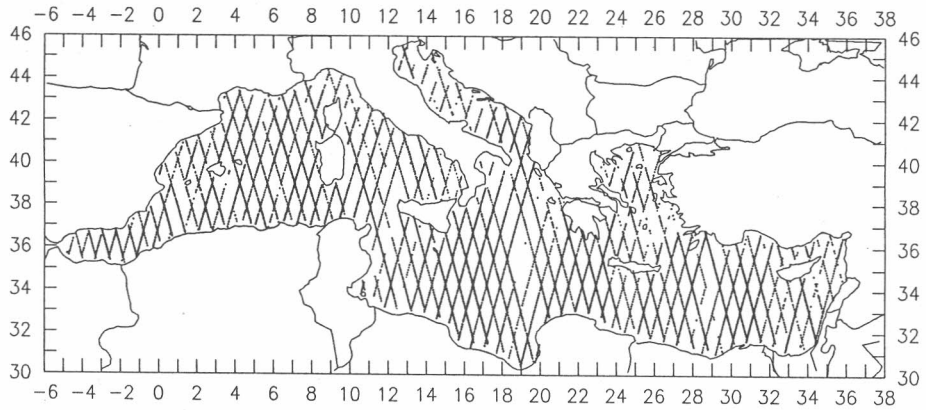

Figure 1. The distribution of ERS-1 altimeter data.

Data analysis

Crossover analysis

For the processing of the data selected by the method described above, a crossover analysis has been carried out. Owing to the large number of available data, we adopted crossover, when the distance between two neighbouring points of each of the two crossing tracks was less than 16.75 km. Finally, 842 crossovers were found belonging to 278 tracks (139 ascending and 139 descending). These crossovers were used in the crossover analysis, which the results are given in Table 2. From the results of Table 2 it seems that the ascending tracks present a small bias (offset equal to –0.188 m and a slightly larger mean tilt value (–0.271 m/100 km). The crossover analysis of the descending tracks shows a larger bias (0.763m) in comparison with the ascending tracks and a smaller tilt (0.137 m/ km) with respect again to the ascending tracks.

Table 2. Results of the crossover analysis of the ERS-1 altimeter data

		Ascending	Descending	All
Mean value (m)	before the	-	-	-0.906
R.M.S. (m)	adjustment	-	-	1.775
Mean bias (m)		-0.188	0.775	0.294
Mean tilt (m/100 km)		-0.271	0.125	-0.073
Mean value (m)	after the	-	-	0.000
R.M.S. (m)	adjustment			0.046

When the crossovers are treated simultaneously (both the ascending and descending tracks) the crossovers were found with a rms crossover discrepancy 1.775 m and a mean

value of differences –0.906 m. The mean value has been eliminated after the crossover analysis, while the rms crossover discrepancy has been considerably reduced (0.046 m). Concerning the bias (0.294 m) and tilt (–0.073 m/100 km) detected by the crossover analysis we could say that the descending tracks had larger bias (two times about) than the ascending ones. In Figures 2 and 3 the biases and tilts for both ascending and descending tracks are plotted. It is obvious from Figure 2 that the individual bias values are generally less than 3 m in absolute sense. From Figure 3 it is observed that tilt values rarely exceed 2 m/100 km.

Collinear analysis

Another treatment of the ERS-1 altimeter data has been carried out using observations from collinear tracks. A typical example of such an analysis is presented below,where three of the longest collinear tracks edited in this study are examined through a number of numerical tests. The starting point of these descending collinear tracks is ($\phi = 40^{\circ}.5$, $\lambda = 24^{\circ}.7$) and the end point is ($\phi = 32^{\circ}.9$, $\lambda = 22^{\circ}.4$). The track have a length of 128.4 secs, or 864.6 km.

In Figure 4 the three descending collinear tracks are plotted by a solid line and the mean track is presented by not connected triangles. The long straight line parts between subsatellite points are due to the lack of altimeter data due mainly to presence of land. In Figure 5 the average resulted track denoted by crosses has been depicted simultaneously with the orbits derived by adding (or subtracting) the standard deviation of the mean subsatellite points from their original values. It is worth to comment here that the standard deviation of the subsatellite points from the three individual tracks is generally small, while the signal (reduced sea surface height) presents a large variation.

In Figure 6 the differences of each subsatellite point from the corresponding mean value are plotted. The major part of these discrepancies is included between -6 cm and +6 cm. In Figure 7 the covariance function of the above mentioned discrepancies is presented with respect to the distance for each of the three individual collinear tracks as well as the covariance function of their mean values (denoted by $\times$). From this Figure we observe that the correlation length of the error covariances is considerably small. This means that the errors do not present a systematic behaviour and consequently these errors have rather a random character than a systematic one.

This preliminary analysis has shown that the quality of the ERS-1 altimeter data is extremely high and the future analysis of more repeat orbits will give best information concerning the geoid and different oceanographic effects, as, e.g. SST, ocean tides, etc. This will lead to a more fine representation and structure of the gravity field in the Mediterranean Sea.

Conclusions

In this paper a preliminary analysis of five months ERS-1 altimeter observations has been carried out. More specifically, a preprocessing of the data has been done in order to validate the observations and to assess their quality. The altimeter data have been edited

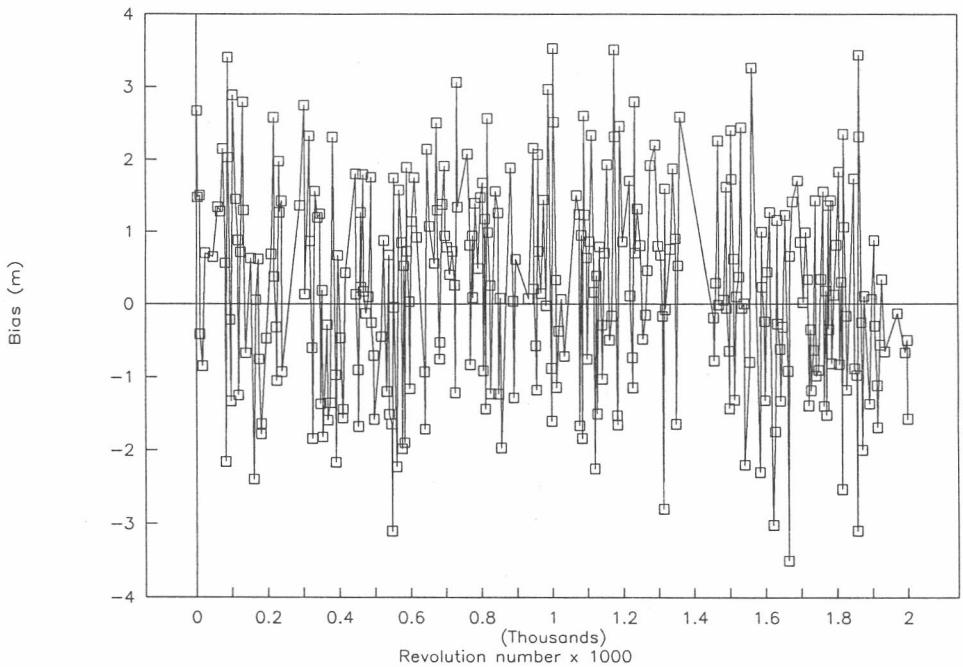

Figure 2. Biases of both ascending and descending tracks.

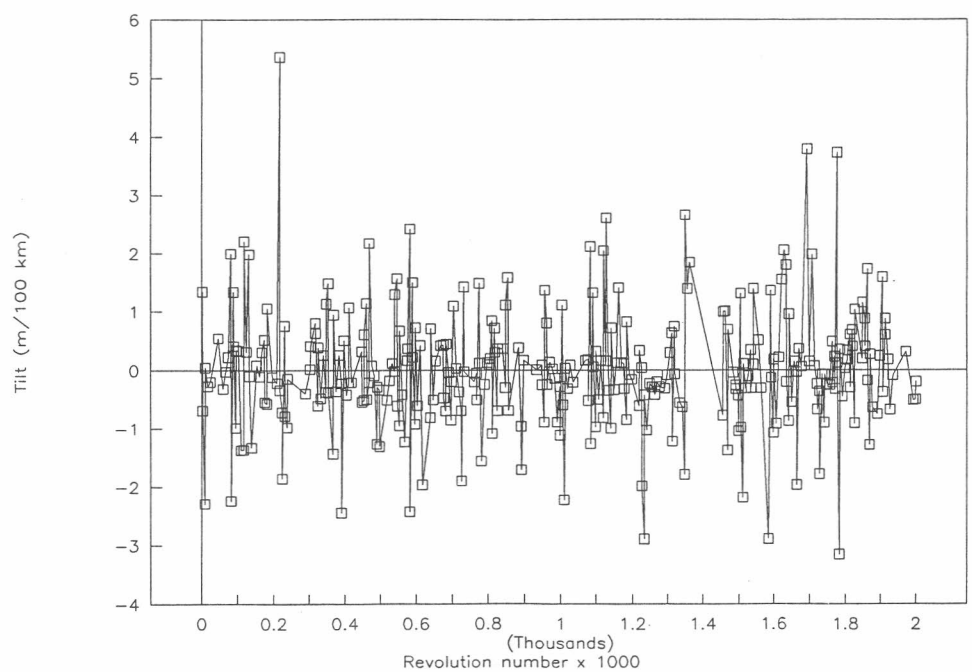

Figure 3. Tilts of both ascending and descending tracks.

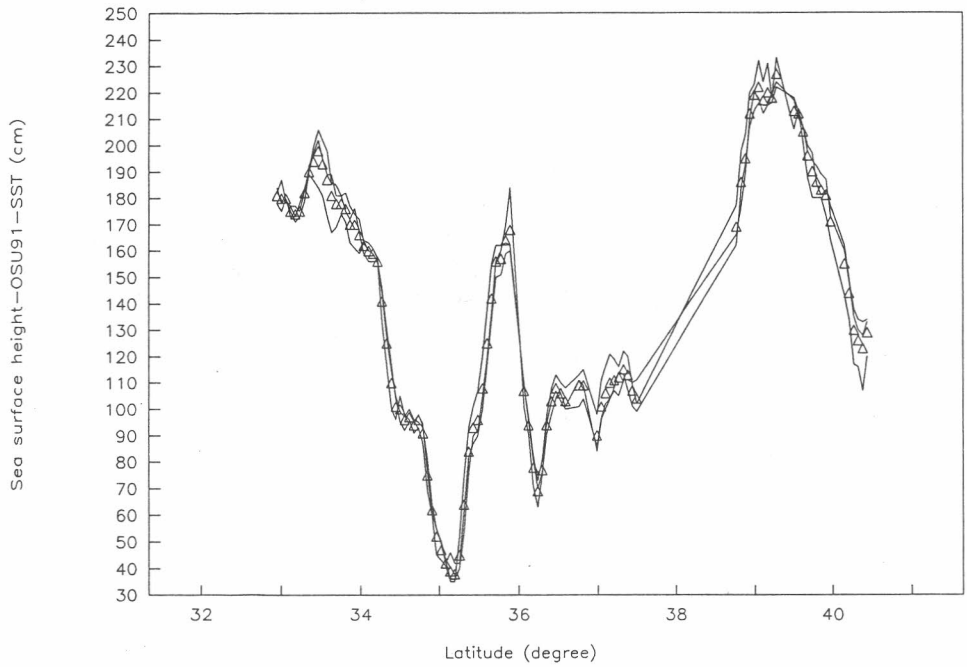

Figure 4. Collinear tracks and their mean.

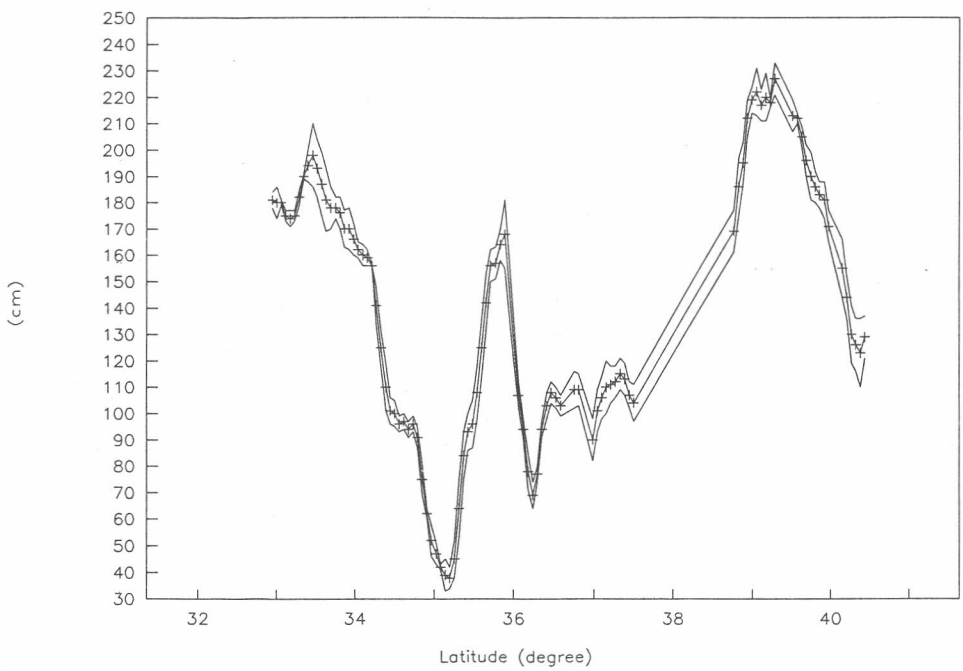

Figure 5. Mean (descending) satellite orbit. Upper line: mean+s.d., middle line: mean, lower line: mean-s.d.

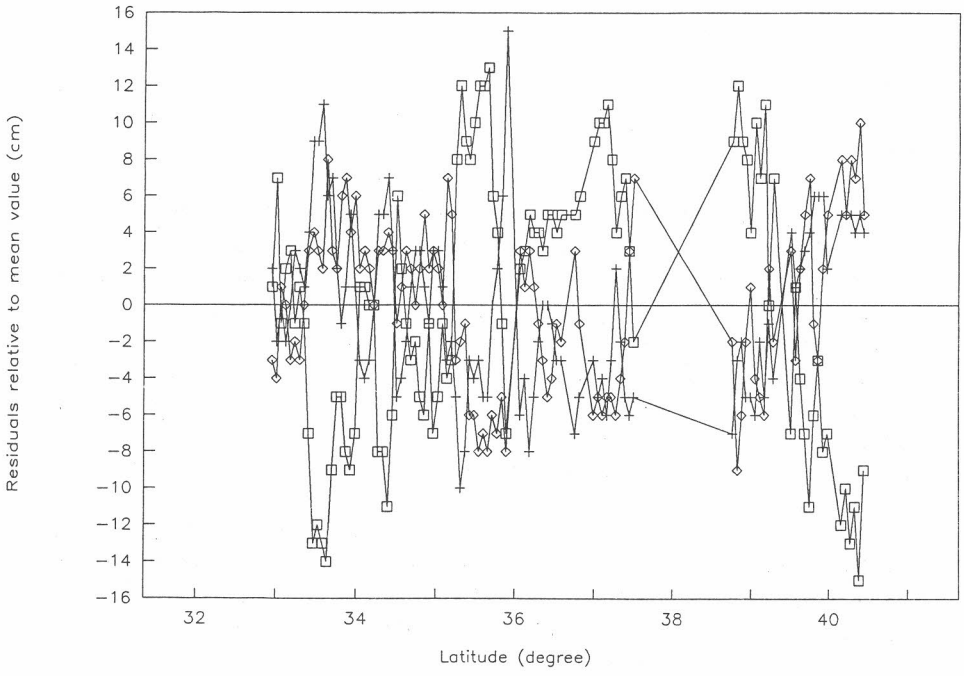

Figure 6 Differences of the three collinear tracks from their mean.

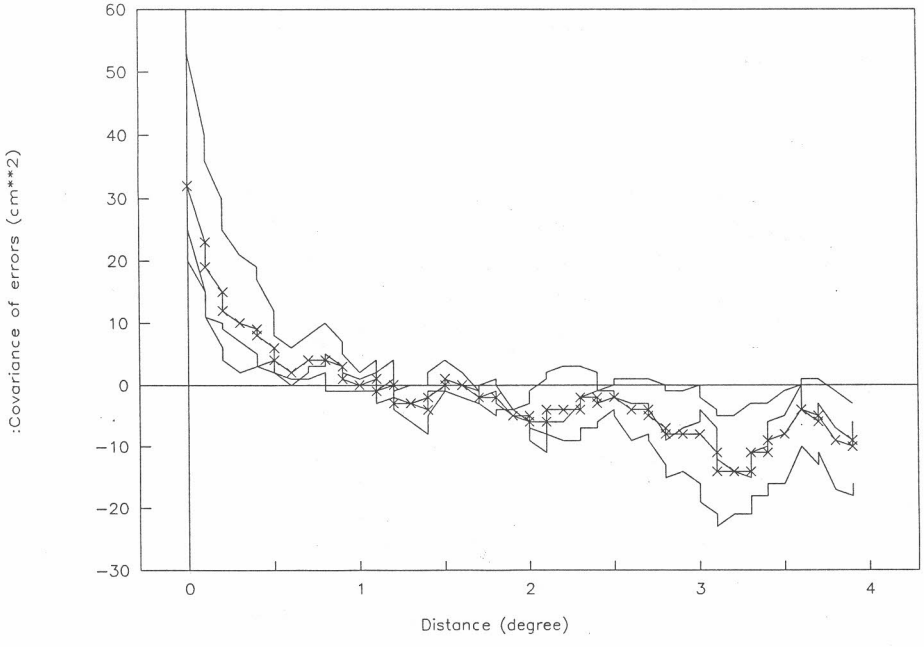

Figure 7. Error covariance functions of (a) the differences of the three collinear tracks from their mean (solid lines), (b) the mean values of the differences.

following a number of selection criteria in order to exclude erroneous data due to errors caused by orbit errors, altimeter signal uncertainties, and of course due to presence of land.

In a second stage of the processing of the ERS-1 altimeter data a crossover and collinear analysis were performed. The main conclusions from this analysis can be drawn in the following. The ERS-1 mission provides altimetry with a significantly improved coverage compared with GEOSAT 17 days ERM data. In the future, when the satellite enters more days repeat orbit, the coverage will be denser (Knudsen and Brovelli, 1991; Knudsen et al., 1992a; 1992b) and superior for a more accurate computation of mean sea surface heights, geoid heights and fine structure and representation of the gravity field. It is interesting to note here that the present coverage of ERS-1 in Mediterranean Sea can not be used for tidal studies in the test area and we await that the improved coverage to aid the investigation of tidal effect in the basin of the Mediterranean Sea (Arabelos and Spatalas, 1992).

The preliminary crossover and collinear analysis of the ERS-1 altimetry in the Mediterranean Sea indicated the high quality of the data in comparison with the data from previous satellite missions (e.g., GEOSAT). The results from the above analysis clearly demonstrate the potential of these new ERS-1 altimeter data which already permit the determination of the sea surface topography in the test area.

Acknowledgement We would like to thank ESA for releasing the ERS-1 altimeter data and the Geophysical Institute of the University of Copenhagen for making available to us these altimeter data files.

References

Arabelos D. and I.N. Tziavos: Sea surface heights in the Mediterranean sea from GEOSAT altimeter data. JGR Vol. 95, No C10, pp. 17947-17956, 1990.

Arabelos, D. and S. Spatalas: Tidal effects on satellite altimeter data in a closed sea area. Presented First Continental Workshop on the Geoid in Europe "Towards a Precise Pan-European Reference Geoid for the Nineties", Prague, May 11-14, 1992.

ESRIN: ERS-1 User Handbook, ESA SP-1148, May 1992.

Knudsen P. and M. Brovelli, 1991 : Collinear and crossover adjustment of GEOSAT ERM and SEASAT altimeter data in the Mediterranean Sea. Proc. Euro. Geophys. Soc. XVI Gen. Assembly, Wiesbaden, 22-26 April, in press.

Knudsen, P., O.B. Andersen, and C.C. Tscherning, 1992a : Altimeter data from ERS-1. Presented Dansk Telemalingsdag, 4. March 1992, DTH, Lyngby.

Knudsen P., O.B. Andersen and C.C. Tscherning, 1992b : Altimetric gravity anomalies in the Norwegian-Greenland Sea-Preliminary results from ERS-1 35 days repeat mission. Accepted for publication in Geophysical Research Letters.

UNIVERSIDAD COMPLUTENSE
DE MADRID

CONSEJO SUPERIOR DE
INVESTIGACIONES CIENTIFICAS

INSTITUTO DE ASTRONOMIA Y GEODESIA

MEDGEO92

PROGRESS IN THE GRAVIMETRIC GEOID COMPUTATIONS

M.J. SEVILLA, G. RODRIGUEZ-CADEROT and A.J. GIL

ABSTRACT

The research developed by the Madrid GEOMED Group in the field of the Gravimetric Mediterranean Geoid computation is outlined. The incorporation of new gravity data and the analysis of the merging zones allow to complete the gravimetric geoid in the whole area.

1. INTRODUCTION

Recently, new data has been added to the original dada bank which has been used to compute a geoid in the Mediterranean Sea following the same method as shown in Sevilla et al. (1992) and presented in the GEOMED Meeting held in Vienna in 1991. The new data has been provided by BGI corresponding to the area of limits $37<\phi<48$ and $10<\lambda<16$ .There are 1104 free-air anomalies irregularly distributed.

After having checked the new data, a comparison has been done to see their goodness which resulted in the same precision about 6 mgal. These gravity anomalies have been changed to IGSN71 and GRS80 systems and divided into several zones to be validated.

Having validated the data a new geoid has been computed in the area mentioned before and several analysis have been carried out as shown in the sequel.

MARE NOSTRUM 2, (1992), PP 43-54

2. SOURCE DATA BANK AND VALIDATION

The updated available Mediterranean gravimetry data bank is formed as show Table 1 and Figure 1.

TABLE 1. *Source Data Bank*

FILE	DESCRIPTION	NUMBER OF DATA	DISTRIBUTION
G1MED	Eastern Mediterranean $31<\phi<37,\ 26<\lambda<36$	3652	irregular
G2MED	Central Mediterranean $31<\phi<48,\ 10<\lambda<26$	15062	gridded
G2BGI	BGI Data $37<\phi<48,\ 10<\lambda<16$	1104	irregular
G3MED	Western Mediterranean $31<\phi<48,\ -6<\lambda<10$	8390	gridded

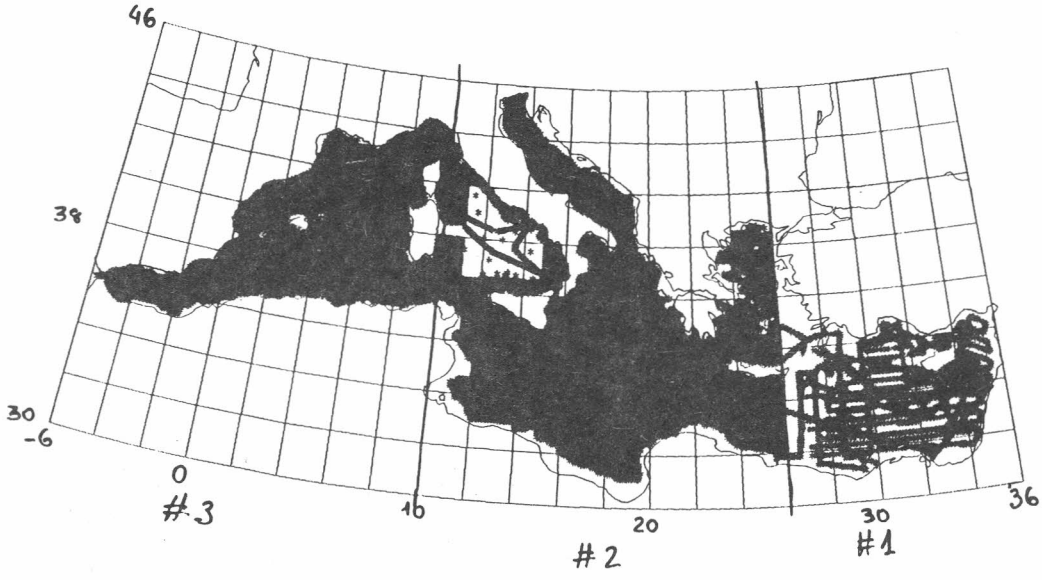

Figure 1. Distribution of the available gravity data in October 1992

In the new file G2BGI the measured gravity g is referred to IGSN71 system and the theoretical gravity γ to GRS67. The reference ellipsoid to which the coordinates of the points are referred, is unknown. The points are irregularly distributed. There were 87 duplicate points. These new free air anomalies have been validated using the IFE88E2 geopotential model. The complete results of validation are shown in the Table 2

TABLE 2. *Results of validation at october 1992*

	Number of points	Mean (mgal)	Standard deviation	Minimum	Maximum	Correlation
MEDIGRAV	**30<φ<46, -6<λ<36. (26949)**					
FREE AIR	26949	-10.09	45.79	-226.96	142.52	
OSU81	26949	-7.43	42.64	-173.34	122.45	
FREE AIR-OSU81	26949	-2.66	25.41	-125.84	136.40	
MEDGRA92	**30<φ<46, -6<λ<36. (26575)** (validated, 374 outliers detected)					
FREE AIR	26575	-10.42	45.46	-226.96	124.00	
OSU81	26575	-7.58	42.48	-173.34	122.45	
FREE AIR-OSU81	26575	-2.84	24.96	-125.84	122.80	
PREDICTION	26575	-10.32	45.16	-228.57	127.37	
FREE AIR-PRED.	26575	-0.10	4.14	-23.85	30.59	
G1MED	**31<φ<37, 16<λ<36. (4244)** (With margin points)					
FREE AIR	4244	-50.31	56.02	-220.48	113.79	
OSU81	4244	-40.18	57.08	-172.74	118.69	
FREE AIR-OSU81	4244	-10.14	32.51	-133.97	104.91	
G1MED	**31<φ<37, 26<λ<36. (3652)**					
FREE AIR	3652	-47.83	53.35	-220.48	113.79	
OSU81	3652	-38.23	54.90	-172.74	117.25	
FREE AIR-OSU81	3652	-9.60	33.03	-133.97	104.91	
G1MED	**31<φ<37, 26<λ<36. (2587)** (gridded)					
FREE AIR	2587	-45.95	53.24	-216.31	96.78	
OSU81	2587	-36.68	55.17	-172.49	116.35	
FREE AIR-OSU81	2587	-9.27	30.99	-125.84	102.02	
G1MED	**31<φ<37, 26<λ<36. (2583)** (gridded-validated, 4 outliers detected)					
FREE AIR	2583	-45.94	53.25	-216.31	96.78	0.63
OSU81	2583	-36.59	55.12	-172.49	116.35	
FREE AIR-OSU81	2583	-9.35	30.93	-125.84	102.02	0.07
PREDICTION	2583	-45.68	53.45	-215.15	93.58	
FREE AIR-PRED.	2583	-0.26	4.71	-28.57	30.60	1.00
G1MED	**31<φ<37, 26<λ<36. (2566)** (gridded-validated, 21 outliers detected)					
FREE AIR	2566	-45.81	53.16	-216.31	96.78	0.63
OSU81	2566	-36.36	55.05	-172.49	116.35	
FREE AIR-OSU81	2566	-9.44	30.61	-125.84	102.02	0.06
PREDICTION	2566	-45.57	53.40	-215.15	93.58	
FREE AIR-PRED.	2566	-0.24	4.32	-19.66	19.65	1.01
G2MED	**31<φ<46, 10<λ<26. (15062)** (Original data)					
FREE AIR	15062	-10.68	50.42	-226.96	142.52	
OSU81	15062	-8.03	47.62	-173.34	122.45	
FREE AIR-OSU81	15062	-2.66	24.12	-114.45	136.40	

G2MED 31<ϕ<46, 10<λ<26. (14861) (validated, 201 outliers detected)

FREE AIR	14861	-11.13	50.21	-226.96	124.00	0.52
OSU81	14861	-8.28	47.58	-173.34	122.45	
FREE AIR-OSU81	14861	-2.85	23.55	-114.45	114.63	0.15
PREDICTION	14861	-10.98	49.83	-228.57	121.39	
FREE AIR-PRED.	14861	-0.14	4.55	-33.82	31.65	0.99

G2MED 31<ϕ<46, 10<λ<26. (14806) (validated, 256 outliers detected)

FREE AIR	14806	-11.03	50.12	-226.96	124.00	0.52
OSU81	14806	-8.17	47.53	-173.34	122.45	
FREE AIR-OSU81	14806	-2.86	23.50	-114.45	114.63	0.15
PREDICTION	14806	-10.89	49.77	-228.57	121.39	
FREE AIR-PRED.	14806	-0.14	4.30	-23.85	25.66	0.99

G2MEDBGI 31<ϕ<46, 10<λ<26. (15972) (Original data plus BGI data)

FREE AIR	15972	-8.63	50.06	-226.96	142.52	
OSU81	15972	-6.51	47.19	-173.34	122.45	
FREE AIR-OSU81	15972	-2.12	24.64	-114.45	136.40	

G2MEDBGI 31<ϕ<46, 10<λ<26. (15753) (validated, 219 outliers detected)

FREE AIR	15753	-9.16	49.79	-226.96	124.00	0.52
OSU81	15753	-6.82	47.11	-173.34	122.45	
FREE AIR-OSU81	15753	-2.34	24.07	-114.45	122.80	0.16
PREDICTION	15753	-9.02	49.41	-228.57	127.37	
FREE AIR-PRED.	15753	-0.14	4.59	-33.82	31.65	0.99

G2MEDBGI 31<ϕ<46, 10<λ<26. (15698) (validated, 274 outliers detected)

FREE AIR	15698	-9.05	49.71	-226.96	124.00	0.52
OSU81	15698	-6.71	47.06	-173.34	122.45	
FREE AIR-OSU81	15698	-2.34	24.03	-114.45	122.80	0.16
PREDICTION	15698	-8.92	49.35	-228.57	127.37	
FREE AIR-PRED.	15698	-0.13	4.37	-23.85	30.59	0.99

G3MED 35<ϕ<45, -6<λ<10. (8390)

FREE AIR	8390	-1.81	24.95	-131.92	84.19	
OSU81	8390	-0.17	18.55	-55.57	50.16	
FREE AIR-OSU81	8390	-1.64	24.63	-114.83	79.15	

G3MED 35<ϕ<45, -6<λ<10. (8327) (validated, 63 outliers detected)

FREE AIR	8327	-2.04	24.73	-131.92	79.79	0.41
OSU81	8327	-0.29	18.50	-55.57	50.16	
FREE AIR-OSU81	8327	-1.75	24.45	-114.83	77.84	0.04
PREDICTION	8327	-2.07	24.24	-121.50	74.74	
FREE AIR-PRED.	8327	0.03	3.77	-27.09	32.56	0.98

G3MED 35<ϕ<45, -6<λ<10. (8311) (validated, 79 outliers detected)

FREE AIR	8311	-2.08	24.67	-131.92	79.79	0.41
OSU81	8311	-0.33	18.49	-55.57	50.16	
FREE AIR-OSU81	8311	-1.75	24.43	-114.83	77.84	0.04
PREDICTION	8311	-2.08	24.24	-121.50	74.74	
FREE AIR-PRED.	8311	0.00	3.59	-19.02	23.93	0.98

3. GEOPOTENTIAL MODELS IN THE MEDITERRANEAN SEA

The computations of free air gravity anomalies have been made by using three geopotential models namely IFE88E3, OSU89B and OSU91A, then these anomalies have been compared to the observed ones to see the goodness of the models. The results are presented in Tables 3, 4, and 5. The statistic is repeated for the gravity points in the Mediterranean Sea with and without removing the suspected data provided from validation

TABLE 3. *Row data*

Mediterranean Sea (26949 points)

	MEAN	SD	MINIMUM	MAXIMUM	RANGE	ZEROS
LATITUDES	37.33	3.16	31.08	45.58	14.50	0
LONGITUDES	14.85	9.00	-5.75	35.58	41.33	0
DEPTHS	-1639.16	1149.76	-4700.00	0.00	4700.00	617
FREE-AIR ANOMALIES	-10.09	45.79	-226.96	142.52	369.48	2
IFE88E2 ANOMALIES	-9.22	44.44	-220.43	137.13	357.56	5
OSU89B ANOMALIES	-9.40	41.49	-177.36	121.07	298.43	2
OSU91A ANOMALIES	-9.33	41.56	-179.57	118.53	298.10	3
FREE-AIR-IFE88E2	-0.87	16.33	-119.51	114.30	233.81	8
OSU91A-OSU89B	-0.07	1.82	-6.05	6.51	12.56	61

Free-air regression line: 21.52012 + 0.01928*h
Standard deviations: 40.07 (of the coefficients: 0.43, 0.00)
Free-air correlation coefficient: 0.484
Free-air minus ife88e2 regression line: 0.62496 + 0.00091*h
Standard deviations: 16.29 (of the coefficients: 0.17, 0.00)
Free-air minus ife88e3 correlation coefficient: 0.064
Gross errors detected: 0

TABLE 4. *Validated data (flag 1)*

Mediterranean Sea (26663 points)

	MEAN	SD	MINIMUM	MAXIMUM	RANGE	ZEROS
LATITUDES	37.31	3.17	31.08	45.58	14.50	0
LONGITUDES	14.84	9.02	-5.75	35.58	41.33	0
DEPTHS	-1646.26	1150.73	-4700.00	0.00	4700.00	608
FREE-AIR ANOMALIES	-10.50	45.56	-226.96	124.00	350.96	2
IFE88E2 ANOMALIES	-9.47	44.38	-220.43	137.13	357.56	5
OSU89B ANOMALIES	-9.64	41.39	-177.36	121.07	298.43	2
OSU91A ANOMALIES	-9.57	41.46	-179.57	118.53	298.10	3
FREE-AIR-IFE88E2	-1.02	15.83	-119.51	101.15	220.66	8
OSU91A-OSU89B	-0.07	1.82	-6.05	6.51	12.56	60

Free-air regression line: 21.01652 + 0.01914*h
Standard deviations: 39.88 (of the coefficients: 0.43, 0.00)
Free-air correlation coefficient: 0.483
Free-air minus ife88e2 regression line: 0.41842 + 0.00087*h
Standard deviations: 15.80 (of the coefficients: 0.17, 0.00)
Free-air minus ife88e3 correlation coefficient: 0.064
Gross errors detected: 286

TABLE 5. *Validated data (flag 2)*

M e d i t e r r a n e a n S e a (26575 points)

	MEAN	SD	MINIMUM	MAXIMUM	RANGE	ZEROS
LATITUDES	37.32	3.17	31.08	45.58	14.50	0
LONGITUDES	14.83	9.01	-5.75	35.58	41.33	0
DEPTHS	-1646.42	1151.31	-4700.00	0.00	4700.00	604
FREE-AIR ANOMALIES	-10.42	45.46	-226.96	124.00	350.96	2
IFE88E2 ANOMALIES	-9.39	44.30	-220.43	137.13	357.56	5
OSU89B ANOMALIES	-9.56	41.31	-177.36	121.07	298.43	2
OSU91A ANOMALIES	-9.49	41.38	-179.57	118.53	298.10	3
FREE-AIR-IFE88E2	-1.02	15.74	-119.51	101.15	220.66	8
OSU91A-OSU89B	-0.07	1.82	-6.05	6.51	12.56	60

Free-air regression line: 21.03456 + 0.01910*h
Standard deviations: 39.78 (of the coefficients: 0.43, 0.00)
Free-air correlation coefficient: 0.484
Free-air minus ife88e2 regression line: 0.39730 + 0.00086*h
Standard deviations: 15.71 (of the coefficients: 0.17, 0.00)
Free-air minus ife88e3 correlation coefficient: 0.063
Gross errors detected: 374

These tables confirm that the election of the IFE88E2 model to make the geoid calculation in this area is correct.

4. COVARIANCES OF THE NEW ZONES

To complete the report given in Sevilla et al., (1992) we present in the Tables 6 and 7 the covariance functions obtained from the new data. These update the covariance calculations. These tables include the covariance functions of the two blocks that we have named Alternative 1 and Alternative 2 and which use will be explained in the sequel.

TABLE 6. *Empirical Covariances*

Zone Number	Number of points	Mean (mgal)	Variance ($mgal^2$)	Correlation length(a m)	First zero length(a m)
100	54	2.61	472.70	3.70	7.07
101	77	-2.14	474.40	4.63	10.91
102	196	0.07	646.90	7.40	20.08
103	219	-3.22	839.80	7.60	17.17
104	245	-4.00	649.40	7.64	19.91
126	181	2.42	513.20	4.30	13.00
127	164	-0.76	609.00	5.31	11.78
128	252	-3.19	841.70	7.72	17.03
129	287	-11.25	981.20	11.06	22.41
130	364	-6.36	708.40	9.79	18.16
157	226	-10.93	710.70	7.80	51.29
158	326	-11.21	823.10	11.91	25.69
159	506	-1.49	474.90	10.45	19.90
187	390	-1.29	500.90	8.84	18.18
188	472	-1.29	535.70	8.64	15.77

ALT-1	392	-1.05	670.75	8.10	15.52
ALT-2	703	-6.06	790.47	11.90	17.52

TABLE 7. *Fitted covariances*

Zone Number	Variance signal	Variance noise	Order	A ($mgal^2$)	$R - R_B$ (km)
100	463.46	0.49	719	1751.967	-3.497
101	467.21	1.03	496	1175.007	-3.996
102	636.90	6.00	269	758.687	-3.804
103	832.82	3.15	317	1144.077	-3.758
104	646.68	0.09	258	612.560	-2.862
126	506.36	3.99	414	546.593	-2.237
127	604.13	1.11	454	2855.670	-6.503
128	832.99	5.36	314	1232.294	-4.090
129	976.30	1.49	246	2084.206	-7.203
130	701.50	4.92	323	2984.357	-9.156
157	707.43	0.12	93	243.956	-0.833
158	820.17	0.37	210	1501.499	-7.296
159	469.11	4.87	284	1586.663	-8.926
187	496.18	3.43	312	1352.471	-6.981
188	533.39	1.22	377	2913.165	-9.130
ALT-1	670.11	0.29	346	1090.18	-4.06
ALT-2	788.77	1.69	309	2643.23	-7.79

A = scale factor of degree variance model
R_B = Bjerhammar radius

5. ZONES PATCHING CRITERIA

5.1. CHOICE OF BJERHAMMAR SPHERE RADIUS

The prediction of the geoid must be done by choosing a unique Bjerhammar sphere radius which defines the harmonicity domain of the function approximating the gravity field. There are large discrepancies in the values of this radius for each single zone as shown in Table 7. So, it is difficult to take a unique value.

To the election of the Bjerhammar radios we have applied several criteria based in the use of the mean value of the zones considered normal zones. This normal zones are the rest zones after having removed the zones included in the following cases.

1.- Coastal zones with fewer than 200 points.
2.- Zones with observed gravity minus implied model anomaly larger 5 mgal.
3.- Zones with standard deviation of reduced anomalies greater than observed ones.
4.- Zones whit standard deviation of implied model anomalies larger than observed ones.
5.- Zones with fewer than 250 points in any region.
6.- Zones with rough gravimetry, i.e. with standard deviation of free-air anomalies greater than 35 mgal.

7.- Zones with large correlations to depths.
8.- Very deep zones with values over 2000 meters.
9.- Zones with negative noise.
10.- Zones with data irregularly distributed.

The value for R_B - R is the mean value of the normal zones.

$$R_B - R = -4.6105 \text{ km}$$

5.2. THE ZONES PATCHING. COMPARISON OF GEOID UNDULATIONS

As a general rule, the mean value is considered in the common boundary of two zones. This is applied when

a) The difference of gravity anomalies is under 4 mgal.
b) The difference of geoid undulations is under 15 centimeters.

When this is not satisfied, the following criteria are applied:
The general criterion in to take the closest result to the observation data, i.e. with the least residual anomalies. As the prediction points are not in correspondence with the observation ones the criteria is based in the comparison between the closest points or the comparison of the mean values in each prediction zone.

Others criteria are:

a) Take the prediction of the zone whose covariance function has a better behavior
b) Take the zone with more points inside or in the corresponding zone used for prediction
c) Take the zone with no coast.
d) Take the zone with least prediction error.
e) If the differences are larger It is not sufficient to treat only the common line, It is necessary to extend the prediction zones to get enough overlapping.
f) If the former do not solve the problem, news dimensions of the zones and news covariance functions must be taken.

5.3 RESULTS OF COMPARISON OF NEIGHBORING ZONES

Comparisons in the four boundaries of each zone have been done. The most of them give differences under 15 cm. Those differences greater than this value were analyzed individually, and in each case some action was taken to get a new value under the 15 cm. Nevertheless, in some areas this results are not completely satisfactory, showing the parts of the Mediterranean Sea which have some different characteristics.

The next Table shows: ZONES, number of the zones compared; DIFFERENCES, number of centimeters in the differences; POINTS, number of points with large differences and number of compared points; ACTION, shows the characteristics of the problematic zones in order to explain the differences obtained, and the action taken to correct o flaged as especial zones for particular geophysical analysis.

ZONES	DIFFERENCES	POINTS	ACTION	RESULTS
14- 28	16 a 18	4 de 12	14 coast zone	Admitted
15- 16	18 y 32	2 de 7	Coastal points	Admitted
24- 38	16 y 20	2 de 12	24 coasts zone	Admitted
38- 39	18 y 20	2 de 13	39 coast zone	Admitted
50- 51	16	2 de 13	BGI zone	Admitted
51- 72	20 y 22	2 de 12	BGI zone	Admitted
63- 90	18	1 de 12	Point next to island	Admitted
64- 65	18	2 de 13	Point next to island	Admitted
70- 71	16	1 de 13	70 island zone	Admitted
71- 72	18 a 26	3 de 13	BGI zone	Admitted
71- 98	16 y 18	2 de 13	BGI zone	Admitted
74-101	16 a 18	3 de 13	BGI zone/Alternative 1	Admitted
75-102	32 a 78	8 de 8	Coastal zone BGI/Alternative 1	Admitted
78-106	22 a 26	4 de 11	Coastal points	Admitted
81- 82	21 a 26	4 de 9	Coastal zone	Admitted
83-111	16 a 38	5 de 11	83 island inside and few data	Admitted
90- 91	20 a 28	5 de 9	Island zone	Admitted
100-101	18	2 de 13	Sicily zone/Alternative 1	Admitted
100-126	18 a 28	8 de 12	Sicily zone/Alternative 1	Admitted
101-102	14 a 28	4 de 13	Sicily zone/Alternative 1	Admitted
103-129	18 a 24	2 de 9	Calabria zone/Alternative 1	Admitted
104-130	32 a 40	5 de 5	Coastal zone/Alternative 2	
	20 a 50	4 de 5	Conflictive zone	Admitted
105-131	20 a 25	2 de 13	Coastal zone	Admitted
124-125	16 a 18	2 de 13	Sicily zone	Admitted
125-126	16 a 26	4 de 13	Sicily zone/Alternative 1	
	16 a 25	8 de 13	Sicily zone/Alternative 1	Admitted
126-127	16 de 18	3 de 10	Sicily zone/Alternative 1	Admitted
126-155	21 a 28	2 de 5	Sicily zone/Alternative 1	Admitted
127-128	16 a 22	3 de 11	Sicily zone/Alternative 1	Admitted
128-129	26 a 60	5 de 12	Sicily zone/Alternative 1	Admitted
129-130	24 a 32	4 de 4	Calabria zone/Alternative 2	Admitted
129-158	29 a 105	5 de 6	Calabria zone/Alternatives 1 and 2	
	33 a 88	5 de 6	Conflictive zones	Admitted
135-136	20 a 24	3 de 3	Coastal zone	Admitted
137-138	18 a 26	7 de 13	Coastal zone	Admitted
137-166	18 a 20	3 de 12	Coastal zone	Admitted
156-186	18 a 20	2 de 13	Coastal zone	Admitted
157-158	44 a 154	13 de 13	Sicily zone/Alternative 2	Admitted
157-187	36 a 54	2 de 2	Sicily zone/Alternative 2	Admitted
158-159	18 a 72	4 de 13	Sicily zone/Alternative 2	Admitted
158-188	18 a 54	6 de 12	Sicily zone/Alternative 2	
	20 a 29	5 de 11		Admitted
166-196	14 a 22	1 de 12	Coastal zone	Admitted
168-169	16 a 26	4 de 12	Island zone. Boundary G1-G2MED	Admitted
168-198	22 a 36	6 de 12	Island zones	Admitted
169-170	25	1 de 1	Coastal zone	Admitted
173-174	26	1 de 7	Coastal points	Admitted
177-178	24	1 de 6	Coastal points	Admitted
187-188	18	1 de 13	Coastal points	Admitted
194-195	22	1 de 9	Coastal points	Admitted
198-199	18 a 26	8 de 13	Island zone. Boundary G1-G2MED	Admitted
200-232	18 a 22	4 de 8	Island zone	Admitted

205-237	16 a 18	3 de 13	Island zone	Admitted
207-239	18	1 de 10	Island zone	Admitted
232-233	18 a 20	2 de 13	Island zone	Admitted
234-235	18	1 de 13	Island zone	Admitted
236-262	16 a 20	2 de 13	Island zone	Admitted
239-240	162 de 13		Coastal zone	Admitted
254-255	14 a 24	2 de 13	Crete zone	Admitted
256-257	16 a 22	5 de 13	Crete zone. Boundary G1-G2MED	Admitted
256-281	16 a 24	2 de 12	Boundary G1-G2MED	Admitted
257-258	20 a 70	9 de 13	Few data. Boundary G1-G2MED	Admitted
257-282	22	1 de 12	Few data	Admitted
258-259	18 a 26	3 de 13	Few data	Admitted
258-283	16	1 de 12	Few data	Admitted
262-263	18	1 de 13	Cyprus zone	Admitted
275-276	18 a 24	3 de 13	Coastal zone	Admitted
281-282	18 a 22	4 de 13	Few data. Boundary G1-G2MED	Admitted
291-292	18	3 de 12	Coastal zone	Admitted
306-322	18	1 de 12	Coastal zone	Admitted
322-323	16 a 18	2 de 4	Coastal zone	Admitted

5.4. ALTERNATIVES USED IN ZONES WITH PROBLEMS

There are two regions with a lot of problems as shown in the last Table. These zones were joint in two blocks in order to avoid these problems. This solves the numerical part but no the geodetic one. These two zones were called Alternative 1 and 2.

ALTERNATIVE 1

1. This block is formed by zones 100, 101, 102, 103, 126, 127, 128 and 129, it is between the limits $38<\phi<40$ y $12<\lambda<15.5$.
2. A covariance function is computed.
3. The geoid is predicted in this block.
4. A new check is done in the boundaries.

ALTERNATIVE 2

1. This block is formed by zones 104,128,129,130, 157, 158, 159, 187 and 188
2. A covariance function is computed.
3. The geoid is predicted in zones 129,130,158 and 159.
4. A new check is done in the boundaries.

The geoid in these two regions is shown in Figures 2: 2a geoid from single zones and 2b the geoid with the alternatives

5.5 GLOBAL RESULTS IN THE ZONE PATCHING

There are 151 points whit differences between 16 and 30 centimeters distributed in 57 boundaries of 571, and 10 points with differences between 30 and 88 cm in 2 boundaries. 154 boundaries give differences under 15 cm.

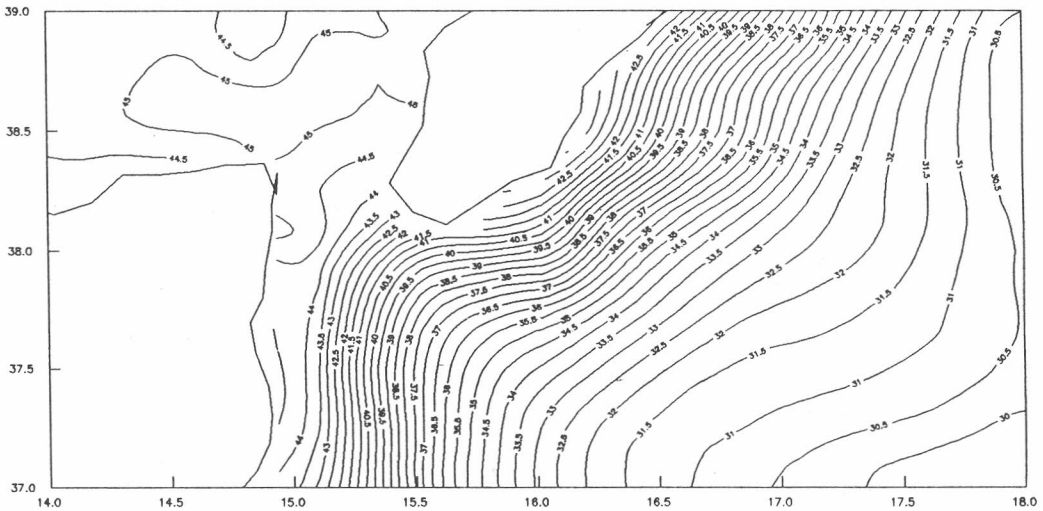

Figure 2a. Geoid from single zones

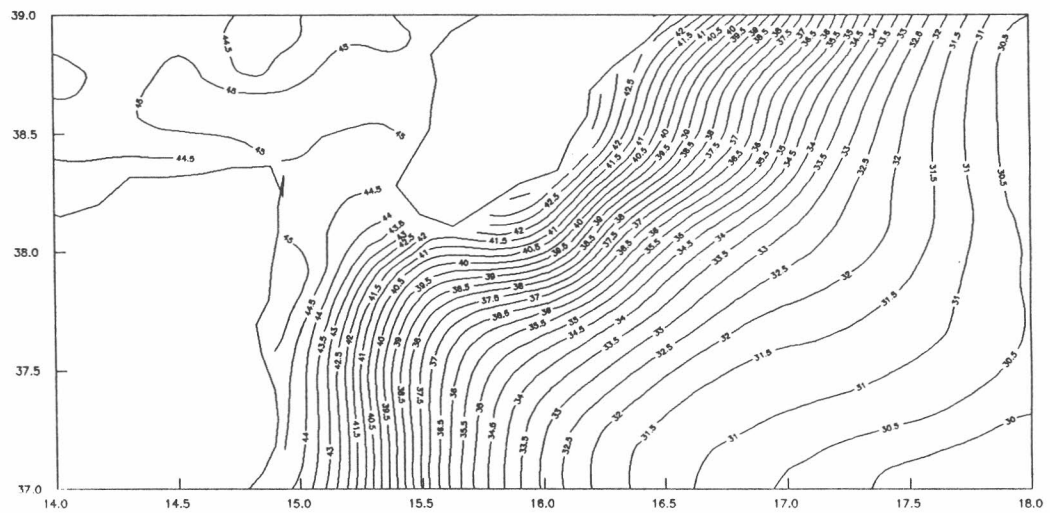

Figure 2b. Geoids from Alternative 2

6. NEW RESULTS

TABLE 6. *Statistical information MEDIGE092*

LIMITS: $30.5<\phi<45.7$, $-6.0<\lambda<35.6$
NUMBER OF PREDICTED POINTS: 35226

	Mean (cm)	Standard deviation	Minimum	Maximum	Range
LATITUDES	37.18	3.32	30.58	45.67	15.08
LONGITUDES	16.60	9.43	-6.00	35.58	41.58
GEOID PREDICTION	33.38	13.76	0.19	50.97	50.78
IFE88E2 GEOID	33.38	13.76	0.15	50.93	50.78
(IFE-PRE) GEOID	-0.00	0.20	-1.38	1.30	2.68
PREDICTION ERROR		0.04	0.06	0.00 0.76	0.76

7. REFERENCES

SEVILLA, M.J., G.RODRIGUEZ-CADEROT and A.J.GIL (1992): A gravimetric geoid un the Mediterranean Sea. Mare Nostrum Num. 1, pp.37-83. Milan

OCEAN TIDE CHARTS IN THE MEDITERRANEAN SEA

R. Vieira and C. de Toro

Instituto de Astronomía y Geodesia (C.S.I.C.-U.C.M.)
Facultad de Ciencias Matemáticas
Ciudad Universitaria, 28040 MADRID. SPAIN.

ABSTRACT

We present in this paper a synthesis of the first stages of modeling the main constituents of the ocean tides in the Mediterranean sea. We have initiated our work with the construction of the M2 harmonic chart for the whole sea. At the present stage we have obtained the results corresponding to its western basin, from the Gibraltar Strait till the islands of Corsica and Sardinia.

1. INTRODUCTION

The need of a good modeling of the ocean tides in areas close to the Iberian Peninsula came out as a consequence of the Earth Tide investigations carried out by the I.A.G. since 1973. Since 1981, the ocean effects, which greatly disturbs the observations of the gravimetric, clinometric and extensometric tides, especially in stations close to the coast, have been determined on the bases of the NSWC global models (Schwiderski, 1980) of eleven most important harmonics of the tidal potential. However, these charts need to be completed for two reasons: first, because Schwiderski, in his models, does not consider some seas such as the Mediterranean and, second, because it is generally problematic that the global charts can reflect some of the geographic and hydrodinamic characteristics with important influence on the tides in the coastal areas. For these reasons, like other groups of investigators used to do in their close areas, we started an investigation for the creation of the so called Iberia charts. The investigations were later extended to the atlantic area of the Canary Islands (Vieira et al. 1983, 1986, 1991; Toro, 1989).

MARE NOSTRUM 2, (1992), pp 55-74

The charts built up to now are based on tidal observations in coastal and deep stations, in the nearby areas of the studied zone, as well as in distant areas. The handling of a great number of records has made necessary a data base whose design and logical organization has been built up by taking on account the different applications of those data. Now a days, the data bank is integrated by the information of 291 tidal stations among which 105 coastal stations located in the Mediterranean sea, 20 are in the Gibraltar Strait and the remaining are located in the atlantic region next to the Iberian Peninsular and the Canary Islands; 53 of the later ones correspond to pelagic observations. The number of the records in the data bank in its actual state is of 30975.

In the Iberia and Canary charts we have imposed as a boundary condition the phase and amplitude isolines to link without discontinuity with the charts of the global model NSWC (Schwiderski, 1983). This is a logical consequence of the certified accuracy of such charts and the recommendations of different International Commission to use them as a standard tool for geodesic and geophysical applications. Obviously, in the case of the Mediterranean sea, we are only interested in linking through Gibraltar Strait with the near atlantic area.

With this work we are offering the results corresponding to a first modeling of the main semidiurnal component with lunar origin M2 for the western area of the Mediterranean sea between Gibraltar and the 8^{o} E meridian. As we have already commented, in this first trial model we have only used tidal data from the coast as we do not have information available from pelagic observations from the Mediterranean sea. In spite of it, when continuing this work, once its influence evaluation will be carried out, we will take into account some other factors such as bathymetry, shape of the basin, the amplifying effects and non-linear interactions between the harmonics in shallow waters, etc.

2. SETTING LIMITS AND DIVISION AREAS

The area of our interest includes not only the Mediterranean sea, which is not modeled by Shwidersky, but also the atlantic regions near the Iberian Peninsula and the Canary islands. Confining our work to the Mediterranean sea, we have carried out a division by zones taking mainly

into account what we can call natural barriers (figure 1). This zonal division is also indicating the progression in our modeling work, initiated by the indicated figure as the first one, which corresponds to western Mediterranean. Obviously, the lack of homogeneity in the number and quality of the data as well as the singularities of each area, mainly due to its bathymetry, will give rise to the definitions of the corresponding reliable parameters in the modeling process.

3. DESIGN AND LOGICAL STRUCTURE OF TIDAL DATA BASE

To build up the tidal data base has been, up to the moment, one of the main problems of the works we are carrying out. This is due to the difficulty to obtain the information, the lack of its uniformity and the versatility with which we want to provide the data base in relation with the variety of applications in the geodesy, oceanography and geophysics.

With the intention to obtain a flexibility and optimize the range of applications, the base has been provided with a set of characteristics which we summarize in the following points:

1.- Data bank is made of an exhaustive and ordered collection of information, jointly loaded avoiding harmful and unnecessary redundancies. Presently the number of stations included in the bank proceeding from many different sources is 291 (figure 2).

2.- The ENDIF program has been carried out to include new observations and modify or extract those already loaded. This program allows a permanent actualization of the data bank.

3.- Its logical structure (figure 3) allows an easy restructuring which is of a great utility if there is new information to add for some other applications. However, in its actual state it collects almost all existing data.

4.- Access to information is obtained with a suitable speed which allows to have the requested answer immediately delivered.

The 291 tidal stations presently included in the data bank come from the following sources:

* International Association for the Physical Sciences of the Ocean (IAPSO) of the IUGG.(Cartwrigth et al., 1979, 1985).

* Instituto Español de Oceanografía (Frutos Fernandez, 1973; García Lafuente et al., 1987).
* International Hydrographic Bureau (IHB).
* International Hydrographic Organization. IHO Tidal Constituent Bank.
* Instituto Hidrográfico de la Marina (IHMC).
* Silva (IHMC), personal comunication.
* Instituto Hidrográfico de Portugal (IHP). Tabla de Mares.
* Liverpool Tidal Institut (LTI).
* Cartwright, D.E., Edden, A.C., Spencer, R. and Vassie, J.M., 1980.
* Admiralty Tides Tables. The Hydrographer of the Navy, 1993.

The information with an overall of 30975 records has been collected in 10 different files (table 1) which were the sources to build up the data bank through the UNIM program. Among some other utilities, this program allows:

- To determine the Time Zone.
- To easy the observation epoch.
- To inform about the predominant tidal regime in the station area.
- To unify all the units adopted by the different organisms as information sources.
- To transform the observed phase lags through expressions

$$G_i(\phi,\lambda) = \psi^G_{ie} - \psi^P_i$$

$$k_i(\phi,\lambda) = G_i(\phi,\lambda) + m\lambda = \psi^P_{ie} - \psi^P_i$$

$$g_i(\phi,\lambda) = G_i(\phi,\lambda) + \omega_i S(\phi,\lambda)$$

where

m is the order of spherical harmonics,

ω_i the angular hour velocity of the corresponding harmonic

S the time zone

G_i the phase lag of the partial oceanic tide with respect to the equilibrium tide in Greenwich,

k_i the phase lag of the partial oceanic tide with respect to the equilibrium tide in the observation point,

g_i phase lag with respect to the equilibrium tide in Greenwich when we have expresed the observation time in local time.

- Provides the amplitude in centimeters and the various phase lag G, k, g for every one of the 60 harmonic included in the bank.
- Informs about the method of analysis used and the number of days used in such analysis.
- Provides the information about data variances and about residuals for every frequency band. These two statistics allow us to evaluate the ratio signal/noise and, therefore the standard deviation of the harmonic constants.
- It includes as an output of the program some other complementary information which can be of interest for some applications of the tidal bank such as:
  * the altitude in centimeters of the mean level over the hydrographic zero of the local chart of a higher scale (Z_o),
  * the link with the leveling network (ENR),
  * designation of the reference and the height (S_o) above it of the mean sea level observed,
  * the Altitude Unity (UA) and
  * the Common Establishment of the Port (EP).

4. APPLICATION PROGRAMS

The following are three application programs we have created (figure3):

SAEDIF program which allows complete or partial access to the information loaded in the bank with a bibliographic format.

SANIM program which provides the information about the mean levels Z_o and the heights S_o over the reference of the observed mean level.

SAMAR program, which allows the loading in CMS files of the information necessary to initiate the modeling process of a given harmonic.

Some other programs are not included in the diagram of figure 3, as they do not affect the building up process of the data bank and its applications. However, they are interesting for the investigations like those related to the analysis of ocean tidal observations. With this idea in mind, the authors have carried out in the I.A.G. two programs which are based on two different methodologies of analysis.They are: the MO88 program, mainly based on the least square technique and the LEMAG program

which uses the Fourier analysis. Both programs are operative and with them we have analyzed some of the tidal data series incorporated in the BAMAG bank of the I.A.G.

5. MODELING

The modeling process initiates from the information provided by the data base of the SAMAR program.

First of all, by starting with the DERAP program we proceed to study and eliminate, when necessary, the harmonic constants which we can consider aberrant, either as a consequence of mistakes or, more often, due to the singularities of given tide records. It is well know that many of the tide records of the coast are located in ports, bays, river estuaries, etc., places where the local phenomena produce amplitude and phase values which are representative of such place and its surroundings. For that reason, they are singular observations which we must eliminate from the process of regional or global modeling we are working on, although they may have a great importance at a local level. The criteria followed for this selection is to consider that in a radius of around 100 km the spatial distribution of the gradients from different parameters should be homogeneous and uniform except for places such as straits where such regimes may substantially vary over lesser distances.

A second elimination program also carried out through the DERAP program consists of comparing every one and all of the parameters observed and calculated in one station (H, He, ψ, ψe, G, k, g) to those of other stations located in an area of one degree in latitude and longitude. The LEMAG program allows to calculate the theoretical parameters such as amplitudes and phases of the equilibrium tide for every one of the tidal stations (table 2). On figures 4 and 5 the spatial distribution of the harmonic constants which passed through the different tests for singularities detection can be seen.

We have processed the values of the amplitudes and the phases through a graphic program and we have plotted the isoamplitude and isophase lines for the western Mediterranean area, from the Gibraltar Strait till the natural barrier made by the Islands of Corsica and Sardinia and the group of small islands and bathymetric heights which we can consider that shape

and close the western area of the "Mare Nostrum".

In parallel we have proceeded a subdivision of the area in trapeze shaped zones of 0.5 x 0.5 degrees and smaller ones in the coast band, in order to take into account, in this way, the real boundaries of this coast. The number and the dimensions of the spherical polygons for the area we are considering are:

197 -- 0°.5000 x 0°.5000
81 -- 0°.2500 x 0°.2500
156 -- 0°.1250 x o°.1250
2 -- 0°.0625 x 0°.0625

The central points of all polygons shape the digital network of the chart to which values are assigned by interpolation between the amplitude and phase lines next to that very center. The group of these values ordered by geographic coordinates forms the digital chart of the studied area (figures 6 and 7). The whole modeling process is carried out through the MODEL ARMONI program which allows to create a file which contains for every polygon the average amplitude of the tide, measured in centimeters, the average differences with respect to the equilibrium tides in Greenwich meridian measured in degrees, and the geographic coordinates of the center and surface of the polygon calculated from the DESUP program.

REFERENCES

Admiralty Tide Tables, 1993. Volume 1: European Waters, including Mediterranean Sea. Pub. The Hydrographer of the Navy (UK), NP 201-93 438 pp.

Cartwright, D.E. Zetler , B.D., and Hamon, B.V., 1979. Pelagic Tidal Constant. IAPSO Pub. Sc. 30, 65 pp.

Cartwright, D.E., Edden, A.C., Spencer, R. and Vassie, J.M., 1980. The tides of the Northeast Atlantic Ocean. Phil. Trans. R. Soc. Lond. A., vol. 298.

Cartwright, D.E. and Zetler ,B.D., 1985. Pelagic Tidal Constant 2. IAPSO. Pub. Sc. 33, 59pp.

García Lafuente, J., Castillejo, F. and García, M., 1987. Resultados de la red mareográfica del Estrecho de Gibraltar. Rev. de Geofísica (1987) 43, 37-56.

Frutos Fernández, 1973. Constantes armónicas de marea de la zona del Estrecho de Gibraltar. Bol. IEO, 169.

Frutos Fernández, 1973. Constantes armónicas de marea de las Islas Baleares, Canarias y Costa Occidental de Africa.Bol. IEO, 170.

Schwiderski, E.W., 1980. Ocean Tides, Part. I: Global Ocean Tidal Equations. Marine Geodesy 3: 161.

Schwiderski, E.W., 1980. Ocean Tides, Part. II: A Hydrodinamical Interpolation Model. Marine Geodesy 3: 219.

Schwiderski, E.W., 1980. On Charting Global Ocean Tides. Rev. Geophysics and Space Physics 18, 1, 243-268.

Schwiderski, E.W., 1983. Atlas of Ocean Tidal charts and maps, I, The semidiurnal lunar tide M2. Marine Geodesy, 6, 219-265.

Toro, C., 1989. Determinación y evaluación de las variaciones periódicas de la gravedad y de las desviaciones de la vertical en la Península Ibérica producidas por las mareas oceánicas. Ph.D. Thesis, Fac. CC. Matemáticas. Universidad Complutense de Madrid, 378 pp.

Vieira, R., Toro, C. and Sukhwani, P.K., 1983. Ocean effects on Gravity Tides in the Iberian Peninsula. In: J.T. Kuo (Sc.Ed.), Proc. 9th Int. Symp. Earth Tides, New York 1981. Schweizerbart'she Verlag., Stuttgart, 403-410.

Vieira, R., Toro, C. and Megias, E., 1986. Ocean Tides in the nearby of the Iberian Peninsula. Part I: M2 Iberia Map. In : R. Vieira (Sc. Ed.), Proc. 10th Int. Symp. Earth Tides, Madrid 1985. Consejo Superior de Investigaciones Científicas, 679-696.

Vieira, R., Toro, C. and Fernandez, J., 1986. Ocean Tides in the nearby of the Iberian Peninsula. Part II: S2 Iberia Map. In: R. Vieira (Sc. Ed.), Proc. 10th Int. Symp. Earth Tides, Madrid 1985. Consejo Superior de Investigaciones Científicas, 697-706.

Vieira, R., Fernandez, J., Toro, C. and Camacho, A.G., 1991. Structural and oceanic effects in the gravimetric tides observations in Lanzarote (Canary Islands). In: J. Kakkuri (Sc. Ed.), Proc. 11th Int. Symp. Earth Tides, Helsinki 1989. Schweizerbart'sche Verlag., Stuttgart, 217-230.

INDEX OF THE ILLUSTRATIONS

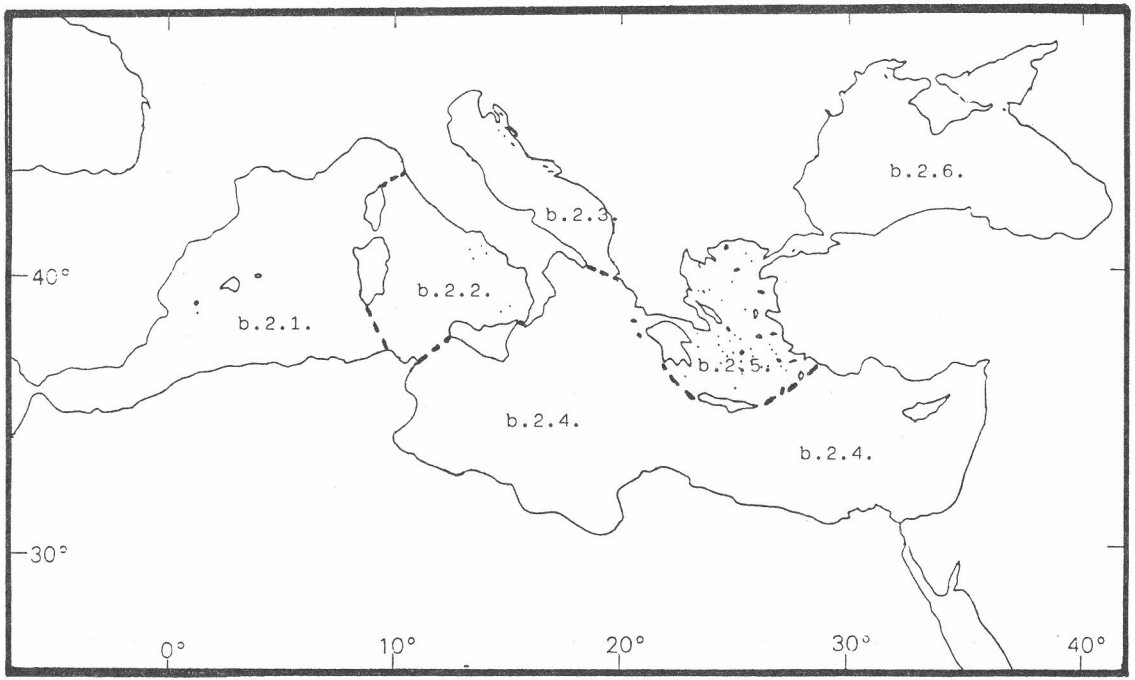

Figure 1. MEDITERRANEAN SEA. MODELING AREAS.

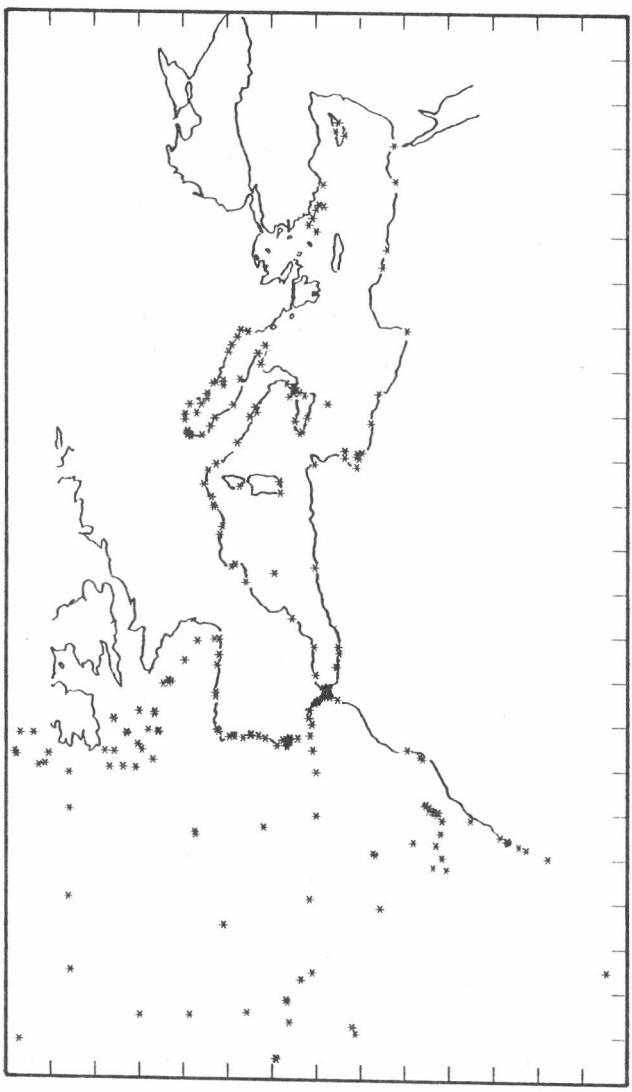

Figure 2. MAREOGRAPHIC DATA

Figure 3. BLOCK SCHEME OF THE MAREOGRAPHIC DATA BASE.

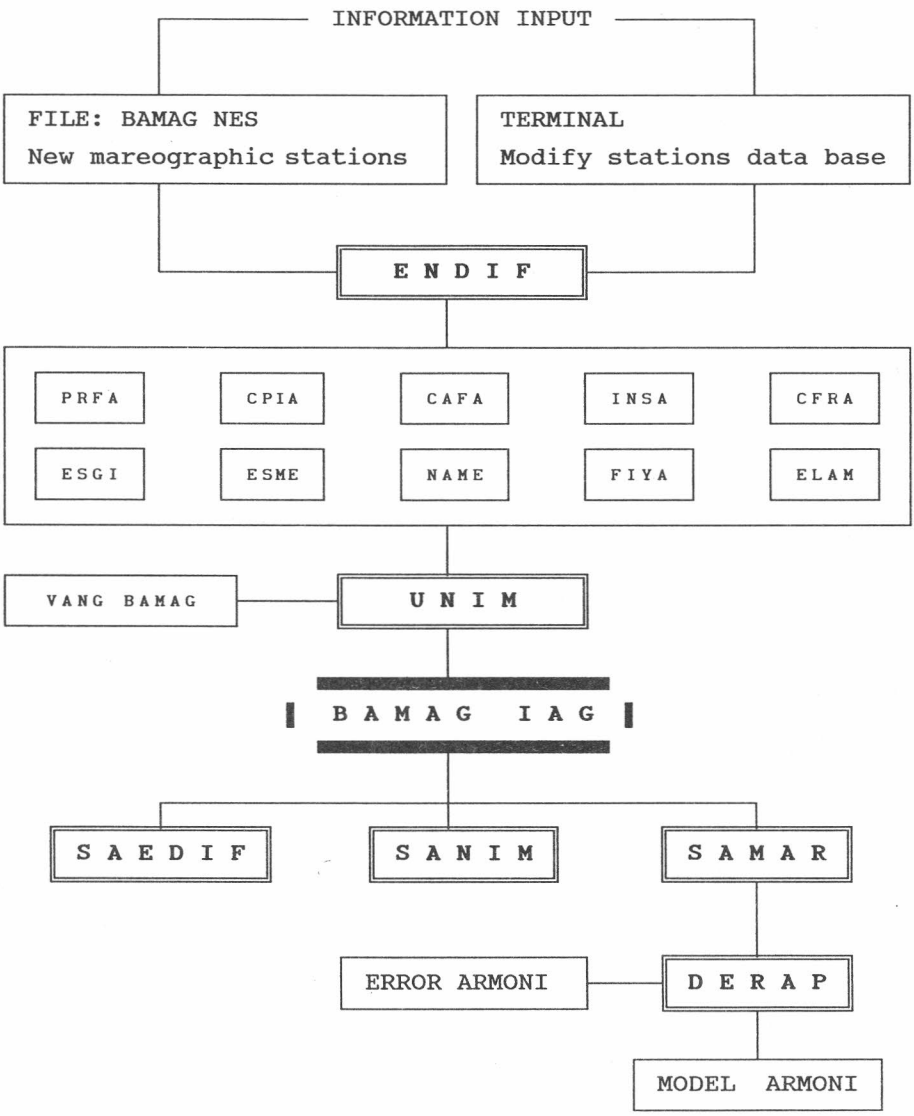

Table 1. MAREOGRAPHIC DATA BANK. LOGICAL DESCRIPTION OF THE SOURCE FILES.

CODE	DESIGNATION FILE	TIDE GAUGES NUMBER	RECORDS	DESCRIPTION
20	PRFA	53	5800	Pelagic Tidal Constants. Northeast Atlantic Ocean.
11	CPIA	48	5296	Shore mareographic stations located along the atlantic Iberian Peninsula coast.
12	CAFA	14	1487	Shore stations located along the atlantic African coast.
13	INSA	29	3114	Atlantic island stations.
14	CFRA	22	2303	French atlantic stations.
15	ESGI	20	2185	Gibraltar strait.
16	ESME	7	760	Spanish stations in the Mediterranean Sea.
17	NAME	20	2098	Mediterranean African coast: from Gibraltar strait to Syria - Turkey border, including spanish stations.
18	FIYA	66	6886	Mediterranean shore stations of France, Monaco, Italy, Yugoslavia and Albania.
19	ELAM	12	1046	Greece tide gauges, mareographic stations in the Mediterranean coast of Minor Asia and Black Sea area.

Table 2. M2 COMPONENT. STRAIT OF GIBRALTAR AND MEDITERRANEAN SEA.

MAREOGRAPHIC STATION	ZONE	LATITUDE	LONGITUDE	D/S	H(CM)	G(GR)
15001 ALGECIRAS (1)	11.1.2011.111	36.1333	-5.4500	.0	31.3	52.0
15002 ALGECIRAS (2)	11.1.2011.111	36.1167	-5.4333	.0	33.5	51.5
15003 ALGECIRAS (3)	11.1.2011.111	36.1333	-5.4500	.0	32.3	43.8
15004 BARBATE	11.1.1033.111	36.1833	-5.9167	.0	45.8	62.1
15005 CABO ESPARTEL	11.1.2011.111	35.7650	-5.9433	.0	75.8	67.0
15006 CABO TRAFALGAR	11.1.2011.111	36.1717	-6.0300	.0	76.2	53.5
15007 CEUTA (1)	11.1.2011.111	35.9050	-5.2983	.0	29.9	47.5
15008 CEUTA (2)	11.1.2011.111	35.8833	-5.2667	.0	28.8	55.0
15009 GIBRALTAR	11.1.2011.111	36.1333	-5.3500	.0	29.8	46.2
15010 SANDY BAY (GIBRALTAR)	11.1.2011.111	36.1333	-5.3333	.0	27.0	46.0
15011 PUNTA ALBOASA	11.1.1033.111	35.8333	-5.7000	.0	52.0	69.0
15012 PUNTA CAMARINAL	11.1.1033.111	36.0833	-5.8000	.0	65.0	49.0
15013 PUNTA CARNERO	11.1.2011.111	36.0717	-5.4283	.0	31.1	47.5
15014 PUNTA CIRES	11.1.2011.111	35.9117	-5.4800	.0	36.4	46.5
15015 PUNTA GRACIA	11.1.2011.111	36.0900	-5.8100	.0	64.9	49.0
15016 PUNTA KANKOUSH	11.1.2011.111	35.8417	-5.7000	.0	51.8	69.0
15017 TANGER (1)	11.1.1033.111	35.7500	-6.0167	.0	68.9	69.9
15018 TANGER (2)	11.1.1033.111	35.7833	-5.8000	.0	68.2	66.7
15019 TARIFA (1)	11.1.1033.111	36.0033	-5.6067	.0	41.5	57.0
15020 TARIFA (2)	11.1.1033.111	36.0033	-5.6067	.0	40.2	41.1
16001 ALICANTE	11.1.2211.113	38.3333	-.4833	.0	2.0	58.0
16002 ALMERIA	11.1.2211.112	36.8333	-2.4833	.0	9.0	51.0
16003 BARCELONA	11.1.2211.113	41.5167	2.0000	.0	4.4	207.2
16004 CHAFARINAS	11.1.2211.116	35.1833	-2.4333	.0	11.7	99.6
16005 MALAGA	11.1.2211.112	36.7167	-4.4167	.0	16.3	60.5
16006 PALMA DE MALLORCA	11.1.2211.115	39.5500	2.6333	.0	2.8	210.2
16007 ROSAS	11.1.2211.113	42.2333	3.2667	.0	5.5	250.4
17001 ALHUCEMAS (1)	11.1.2211.116	35.2333	-3.8833	.0	18.5	60.7
17002 ALHUCEMAS (2)	11.1.2211.116	35.3333	-3.8667	.0	17.9	54.7
17003 VILLA NADOR	11.1.2211. 16	35.0900	-2.9167	.0	6.0	163.0

MAREOGRAPHIC STATION	ZONE	LATITUDE	LONGITUDE	D/S	H(CM)	G(GR)
17005 ALGER	11.1.2211.116	36.7833	3.0667	.0	2.4	219.3
17006 LA GOULETTE	11.1.2222.117	36.8167	10.3167	.0	8.0	249.0
17007 GABES	11.1.2244.117	33.8833	10.1167	.0	48.0	121.9
17008 HOUMT ADJIM	11.1.2244.117	33.7167	10.7500	.0	31.0	103.0
17009 SFAX	11.1.2244.117	34.7333	10.7667	.0	42.0	77.0
17010 HOUMT SOUK	11.1.2244.117	33.8833	10.8667	.0	31.0	104.0
17011 RAS TOURG-EN-NESS	11.1.2244.117	33.8167	11.0500	.0	27.0	69.0
17012 ZARZIS	11.1.2244.117	33.5000	11.1167	.0	22.0	77.0
17013 EL ABASSIA	11.1.2244.117	34.7167	11.2500	.0	26.0	83.0
17014 TRIPOLI (TARABULUS)	11.1.2244.117	32.9000	13.1833	.0	13.0	65.0
17015 MISURATA	11.1.2244.117	32.3667	15.2167	.0	7.0	53.0
17016 MESA EL BREGA	11.1.2244.117	30.4167	19.5833	.0	5.0	60.0
17017 MERSA TOBRUK	11.1.2244.118	32.0833	23.9667	.0	1.0	285.0
17018 BARDIA	11.1.2244.118	31.7667	25.1667	.0	3.0	236.0
17019 ALEJANDRIA	11.1.2244.118	31.1667	29.8500	.0	7.0	245.0
17020 PORT SAID	11.1.2244.118	31.2667	32.3167	.0	12.0	240.0
18001 PORT VENDRES	11.1.2211.114	42.5167	3.1000	.0	5.0	288.0
18002 MARSELLA	11.1.2211.114	43.3000	5.3667	.0	7.0	217.0
18003 TOLON	11.1.2211.114	43.1167	5.9333	.0	3.0	266.0
18004 NIZA	11.1.2211.114	43.7000	7.2833	.0	7.0	244.0
18005 MONTE CARLO	11.1.2211.114	43.7333	7.4167	.0	4.0	259.0
18006 AJACCIO	11.1.2211.119	41.9333	8.7500	.0	7.0	250.0
18007 CAGLIARI	11.1.2222.119	39.2000	9.1000	.0	8.0	236.0
18008 CARLO FORTE	11.1.2212.114	39.1500	8.3000	.0	6.0	231.0
18009 IMPERIA	11.1.2211.120	43.8833	8.0167	.0	8.0	237.0
18010 GENOVA	11.1.2211.120	44.4000	8.9000	.0	8.0	222.0
18011 LA ESPEZIA	11.1.2211.120	44.0667	9.8500	.0	9.0	215.0
18012 LIVORNO	11.1.2212.120	43.5500	10.3000	.0	8.0	232.0
18013 CIVITAVECCHIA	11.1.2222.120	42.1000	11.7833	.0	11.0	239.0
18014 GAETA	11.1.2222.120	41.2167	13.5833	.0	11.0	234.0
18015 NAPOLES	11.1.2222.120	40.8333	14.2667	.0	11.0	237.0
18016 ISCHIA	11.1.2222.120	40.7333	13.9333	.0	12.0	232.0

MAREOGRAPHIC STATION	ZONE	LATITUDE	LONGITUDE	D/S	H(CM)	G(GR)
18017 TROPEA	11.1.2222.120	38.6833	15.9000	.0	15.0	242.0
18018 VILLA SAN GIOVANNI	11.1.2224.120	38.1833	15.6333	.0	3.0	85.0
18019 REGGIO CALABRIA	11.1.2224.120	38.1167	15.6500	.0	6.0	62.0
18020 TAORMINA	11.1.2244.121	37.8167	15.2833	.0	9.0	57.0
18021 MESSINA	11.1.2224.121	38.2167	15.5667	.0	5.0	2.0
18022 CAPO PELORO	11.1.2224.121	38.2667	15.6500	.0	5.0	238.0
18023 LIPARI	11.1.2222.120	38.4833	14.9667	.0	12.0	232.0
18024 MILAZZO	11.1.2222.121	38.2167	15.2500	.0	12.0	234.0
18025 PALERMO	11.1.2222.121	38.1333	13.3333	.0	11.0	232.0
18026 MARSALA	11.1.2224.121	37.8000	12.4333	.0	7.0	207.0
18027 MAZARA DEL VALLO	11.1.2224.121	37.6333	12.5833	.0	4.0	128.0
18028 PORTO EMPEDOCLE	11.1.2244.121	37.2833	13.5333	.0	5.0	76.0
18029 CATANIA	11.1.2244.121	37.4833	15.1000	.0	6.0	61.0
18030 VALLETTA	11.1.2244.122	35.8833	14.5167	.0	7.0	48.0
18031 TARANTO	11.1.2244.120	40.4667	17.2167	.0	6.0	71.0
18032 OTRANTO	11.1.2234.120	40.1500	18.5000	.0	7.0	73.0
18033 BRINDISI	11.1.2233.120	40.6500	17.9667	.0	9.0	73.0
18034 VIESTE	11.1.2233.120	41.8833	16.1833	.0	8.0	61.0
18035 ORTONA	11.1.2233.120	42.3500	14.4167	.0	7.0	64.0
18036 ANCONA	11.1.2233.120	43.6167	13.5000	.0	7.0	303.0
18037 PESARO	11.1.2233.120	43.9167	12.9167	.0	13.0	288.0
18038 PORTO CORSINI	11.1.2233.120	44.5000	12.2833	.0	15.0	274.0
18039 CHIOGGIA	11.1.2233.120	45.2333	12.3000	.0	22.0	273.0
18040 MALAMOCCO	11.1.2233.120	45.3333	12.3167	.0	23.0	267.0
18041 VENECIA	11.1.2233.120	45.4333	12.3333	.0	24.0	285.0
18042 GRADO	11.1.2233.120	45.6833	13.3833	.0	23.0	276.0
18043 TRIESTE	11.1.2233.120	45.6500	13.7500	.0	26.5	302.5
18044 SAN GIULANO	11.1.2233.120	45.4667	12.2833	.0	24.0	306.0
18045 TORCELLO	11.1.2233.120	45.5000	12.4167	.0	19.6	345.8
18046 PALIAGAO	11.1.2233.120	45.5167	12.3833	.0	19.8	12.8
18047 TORSON DI SOTO	11.1.2233.120	45.5000	12.4167	.0	20.8	342.8
18048 MILLECAMPI	11.1.2233.120	45.3000	12.1833	.0	16.9	18.4

MAREOGRAPHIC STATION	ZONE	LATITUDE	LONGITUDE	D/S	H(CM)	G(GR)
18049 PORTO PIAVE VECCHIA	11.1.2233.120	45.4867	12.5783	.0	22.3	307.2
18050 CAVALLINO	11.1.2233.120	45.5000	12.4167	.0	10.7	39.8
18051 PULA	11.1.2233.123	44.8667	13.8333	.0	15.0	236.0
18052 RIJEKA (FIUME)	11.1.2233.123	45.3333	14.4333	.0	10.0	220.0
18053 SENJ	11.1.2233.123	45.0000	15.9000	.0	10.0	211.0
18054 MALI LOSINJ	11.1.2233.123	44.5333	14.4667	.0	8.0	211.0
18055 ZALIV PANTERA	11.1.2233.123	44.1500	14.8500	.0	4.0	165.0
18056 ZADAR	11.1.2233.123	44.1333	15.2000	.0	6.0	203.0
18057 SIBENIK	11.1.2233.123	43.7333	15.9000	.0	6.0	106.0
18058 ROGOZNICA	11.1.2233.123	43.5333	15.9833	.0	6.0	111.0
18059 SPLIT	11.1.2233.123	43.0500	16.0833	.0	8.0	100.0
18060 KOMIZA	11.1.2233.123	43.0500	16.0833	.0	7.0	79.0
18061 OTOK SVTAC	11.1.2233.123	43.0333	15.7667	.0	7.0	93.0
18062 DUBROVNIK	11.1.2233.123	42.6667	18.0667	.0	9.0	86.0
18063 MELJINE	11.1.2233.123	42.4500	18.5500	.0	9.0	70.0
18064 BAR	11.1.2233.123	42.0667	19.0833	.0	9.0	80.0
18065 SHENGJIN	11.1.2233.123	41.8167	19.5833	.0	9.0	79.0
18066 DURRES	11.1.2233.123	41.3167	19.4500	.0	9.0	73.0
19001 NISOS LEROS	11.1.2255.124	37.1667	26.8333	.0	3.0	304.0
19002 NISOS ASTIPALAIA	11.1.2255.124	36.6333	26.3833	.0	3.0	295.0
19003 NISOS KOS	11.1.2255.124	36.8833	27.3167	.0	4.0	271.0
19004 NISOS SIMI	11.1.2255.124	36.6167	27.8667	.0	4.0	269.0
19005 RODHOS	11.1.2244.124	36.4500	28.2333	.0	5.0	250.0
19006 LINDHOS	11.1.2244.124	36.1000	28.1000	.0	6.0	249.0
19007 MEYISTI	11.1.2244.125	36.1500	29.6000	.0	7.0	245.0
19008 KYRENIA	11.1.2244.126	35.3333	33.3167	.0	10.1	8.6
19009 LIMASSOL	11.1.2244.126	34.6667	33.0500	.0	10.0	235.0
19010 FAMAGUSTA	11.1.2244.126	35.1167	33.9500	.0	11.0	236.0

Figure 4. MEDITERRANEAN SEA. TIDAL CONSTITUENT M2. AMPLITUDE H (cm).

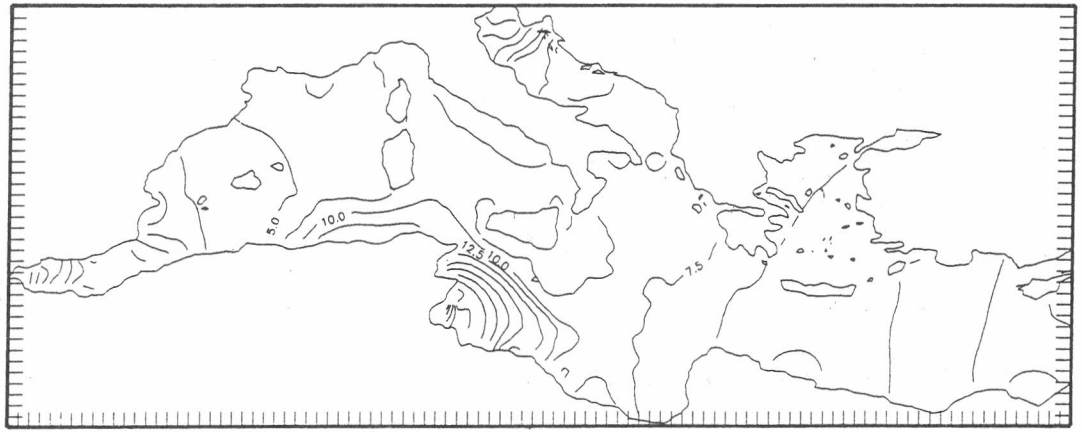

Figure 5. MEDITERRANEAN SEA. TIDAL CONSTITUENT M2. PHASE LAG G (degrees).

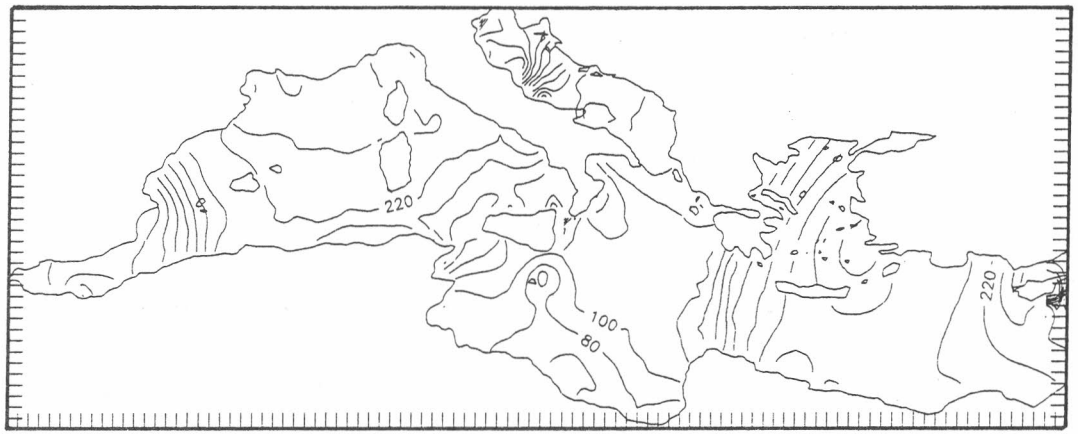

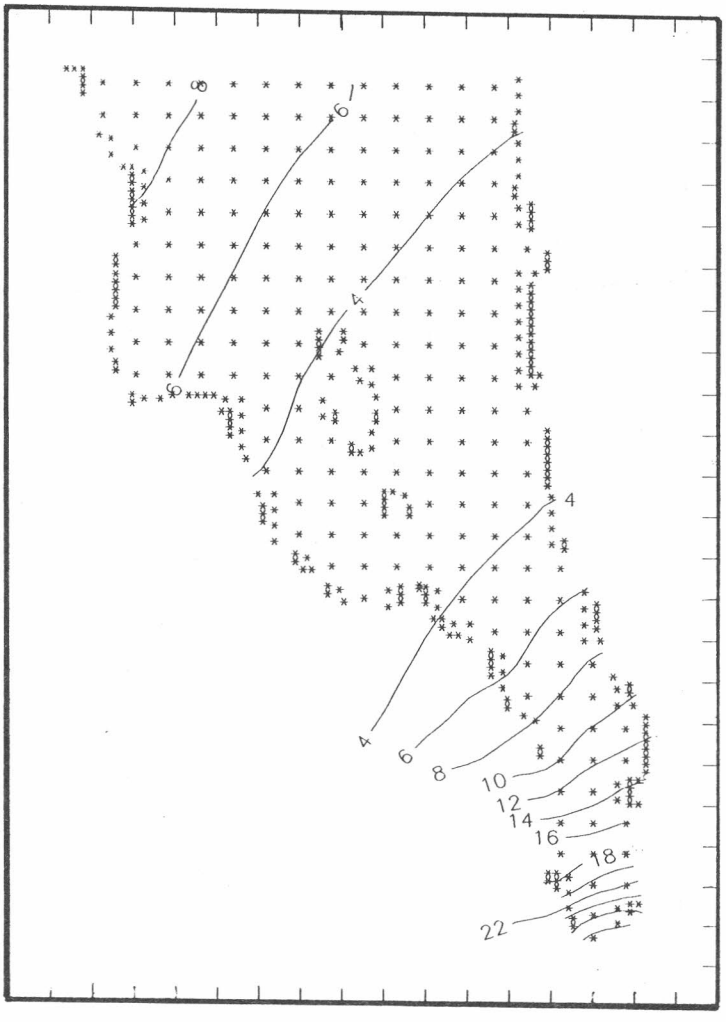

Figure 6. WEST MEDITERRANEAN SEA. TIDAL CONSTITUENT M2. AMPLITUDE H (cm).

Figure 7. WEST MEDITERRANEAN SEA. TIDAL CONSTITUENT M2. PHASE LAG G (degrees).

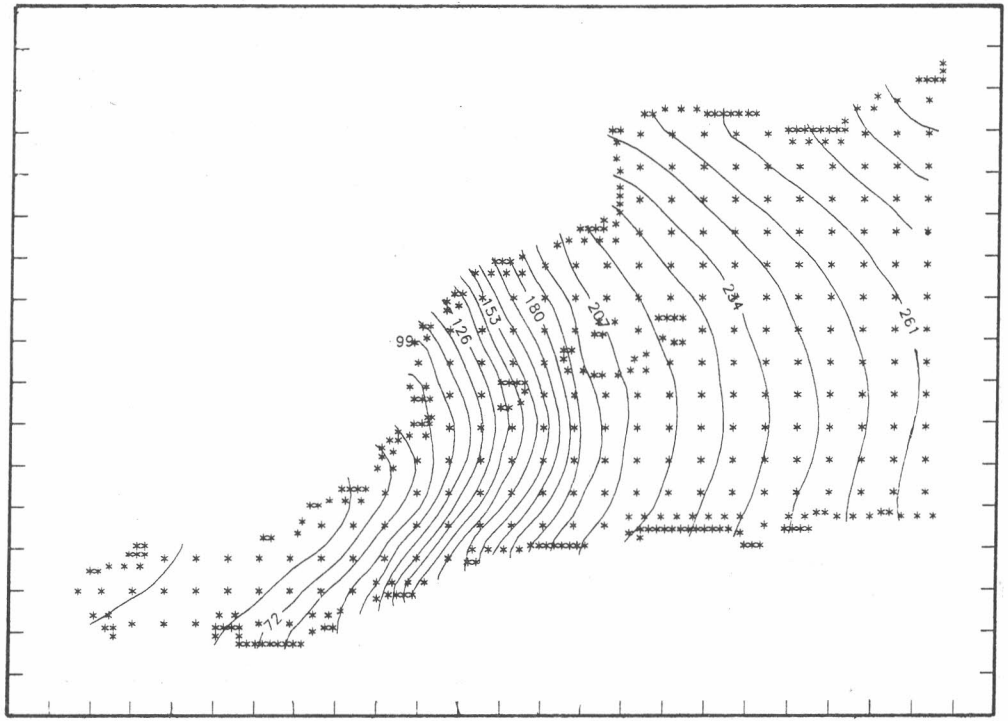

CROSSOVER ADJUSTMENT OF SATELLITE ALTIMETER DATA

W. Fürst
W. Hausleitner
E. Höck
W.-D. Schuh
H. Sünkel

Institute of Mathematical Geodesy
and Geoinformatics
Graz University of Technology
Steyrergasse 30, A-8010 Graz, Austria

Abstract

In the frame of the GEOMED project various problems related to crossover adjustment are investigated. Interpolation techniques which are currently in use, are dealt with numerically. The dependence of the rank of the linear system of equations for crossover adjustment on the area size and on the geographical location is studied. Three methods to repair the rank deficiency are investigated and the pro's and con's are identified.

1 Introduction

In order to exploit the information which is contained in satellite altimeter data from satellite missions such as SEASAT, GEOSAT, ERS-1 or TOPEX-POSEIDON as much as possible, the satellite's orbit must be known with utmost accuracy. A method of orbit correction which is being widely applied is the method of crossover adjustment of altimeter data. Such an adjustment procedure requires altimeter data at the intersection of northgoing and southgoing satellite groundtracks and a proper procedure to solve the singular linear system of equations. The present contribution addresses these two issues.

In particular interpolation techniques are compared against each other regarding the interpolation accuracy depending on the size of the data gap, the smoothness of the interpolator, and the

MARE NOSTRUM 2, (1992), pp 75-90

smoothness properties of the function to be interpolated.

The system of linear equations which results from the adjustment of the crossover discrepancies is rank deficient with two eigenvalues being numerically zero in any case and one or two eigenvalues being very close to zero, depending on the size and on the geographical location of the data area in consideration.

Three methods to repair the rank deficiency are compared against each other, the track fixing method, the geoid fitting method, and the singular value decomposition technique supplemented by surface fitting. The quality of these methods is judged on numerical investigations which are based on GEOSAT exact repeat mission (ERM) data.

2 Interpolation of crossover points

Before crossover adjustment of satellite altimeter data can be pursued, crossover points and corresponding crossover discrepancies must be available. The identification of a crossover point is a simple matter of intersection between a northgoing and a southgoing satellite groundtrack. The assignment of proper altimeter data to such an intersection point is less trivial, unless altimeter measurements are performed exactly at the intersection point (which is indeed a very unlikely event). Therefore, the data have to be interpolated at the crossover points using some kind of interpolation technique.

Numerical investigations with available satellite altimeter data such as SEASAT and GEOSAT data using existing software have revealed some weeknesses which are related to the applied interpolation technique. Since the quality of the crossover adjustment results depend to some extent on the input data (crossover data), an investigation of simple interpolation procedures suggested itself.

In particular two alternative interpolation methods have been investigated: linear interpolation as applied in existing satellite altimeter processing software, and alternatively, cubic interpolation. Obviously interpolation results are not only dependent on the interpolator (linear, cubic, or more sophisticated) and on the data gap which is spanned by interpolation. Interpolation results depend also to a large extent on the properties of the underlying function to be interpolated (smooth versus rugged). In order to account for these facts, the two interpolators mentioned above have been used both for smooth and rugged geoid profiles with the interpolator spanning between 3 and 31 data points. The interpolated values were compared against the given data (which, of course, were not used in the interpolation procedure).

The respective results are summarized in Table 1 in terms of mean, rms and maximum interpolation error. In Figure 1 mean interpolation errors are presented for two geoid profiles, a smooth one (lower curve) and a rugged one (upper curve). The histograms in Figure 2 provide a comparison of interpolation errors between linear and cubic interpolation bridging a single data gap. The interpolation errors are broken down according to their size.

Qualitatively the results are in agreement with what one should expect: cubic interpolation is superior over linear interpolation and is therefore recommended to be used for the interpolation of altimeter data in any case. A smooth profile may be bridged by cubic interpolation up to a gap of about 10 data points with sufficient accuracy, while only about 7 points may be bridged in a rugged profile. The interpolation error increases with increasing length of the data gap with a much higher rate for a rugged profile than for a smooth one.

Quantitatively it is obvious that interpolation errors over a moderately small data gap are of the order of about 4 cm with an rms of about 5 - 7 cm and maximum absolute values of several decimeters, depending on the smoothness of the geoid profile.

Interpolation	linear 3 points	cubic 5 points	cubic 7 points	cubic 13 points	cubic 31 points
Mean	4	4	4	7	19
RMS	6	5	5	10	27
Maximum	52	32	39	83	173

Table 1: Interpolation errors depending on interpolation technique and size of data gap

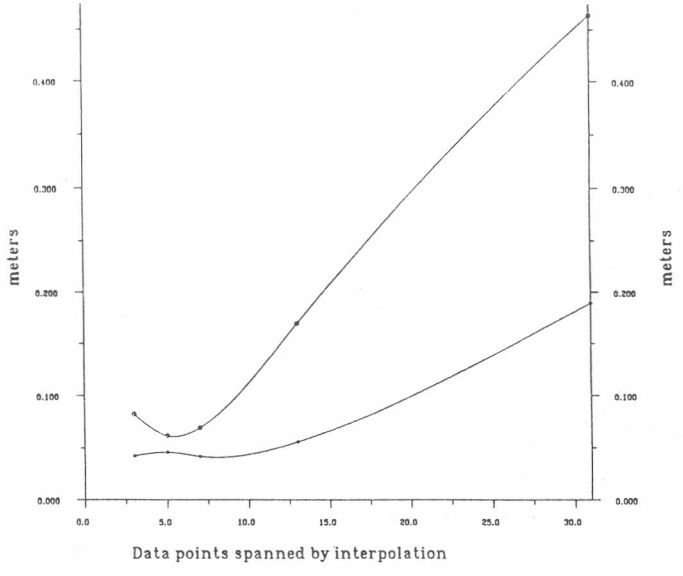

Figure 1: Interpolation error depending on smoothness of interpolated profile and on size of data gap

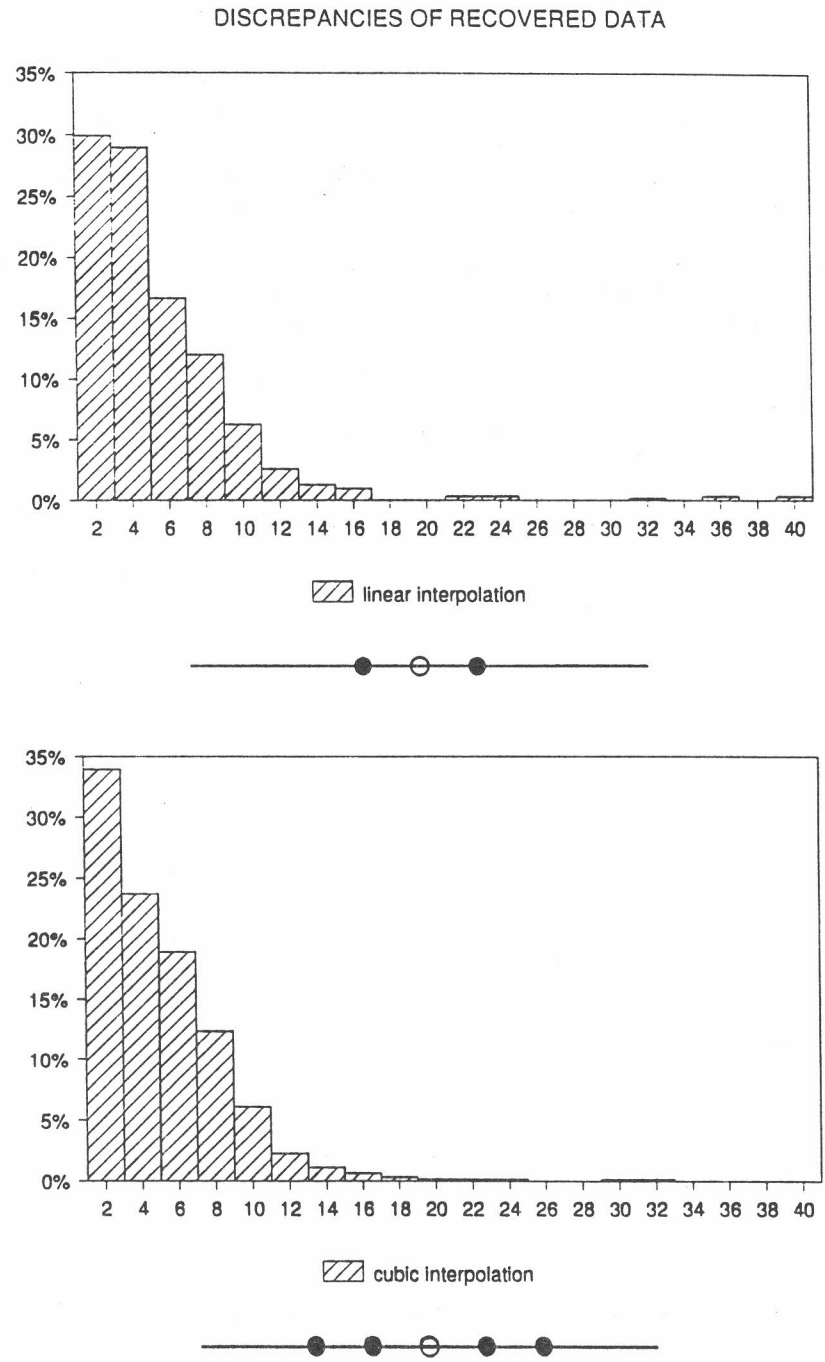

Figure 2: Interpolation error: linear versus cubic interpolation (1 data gap only)

3 Crossover adjustment - the principle

The crossover technique relies on the requirement that a measured geoid height at a given geographical location must be independent of the tracking instant. Crossover differences d_{ij} of corrected altimeter data are therefore essentially identical to the radial orbit error of the respective satellite tracks:

$$d_{ij} = h_i - h_j = d_i - d_j + \epsilon_i - \epsilon_j \tag{1}$$

with

h_i, h_j ... Measurement at the crossover location of the satellite tracks i und j
d_i, d_j ... Orbit errors of the satellite tracks at the crossover location
ϵ_i, ϵ_j ... Measurement error

It is well known that in sufficiently small areas the radial orbit error may be modelled by either a time- or a distance-dependent polynomial, leading to the following observation equations at the crossover points:

$$v_{ij} = \sum_{e=0}^{k} \alpha_{ie}(t_i - t_{i0})^e - \sum_{e=0}^{l} \alpha_{je}(t_j - t_{j0})^e - d_{ij} + \epsilon_i - \epsilon_j \tag{2}$$

with

k, l ... Degree of chosen polynomials
α ... Polynomial coefficients
$(t - t_0)$ ... Time parameter

Since differences of measurements are used as observations and those differences are invariant with respect to certain transformations, the corresponding adjustment problem is singular.

The parameters λ_i , used in the bias and tilt model, represent relative geographical longitudes of the crossover points, counted from the mean geographical longitude of the respective satellite track:

$$\Delta h_{ij} = (a_i + b_i\lambda_j) - (a_j + b_j\lambda_i) + r_{ij} \tag{3}$$

with

Δh_{ij} ... Height difference at the crossover point of the tracks i and j
a_i, b_i, a_j, b_j ... Bias and tilt parameters
λ_i, λ_j ... Relative geographical longitudes of crossover point
r_{ij} ... Residual

The bias and tilt coefficients a_i and b_i and a_j and b_j, respectively, have to be determined such that the residuals r_{ij} of crossover height differences are minimized in the least squares sense. The observation equations

$$\Delta h = Ax + r \tag{4}$$

with the vector of unknown parameters x (bias, tilt) leads to a least squares adjustment problem which is singular and has a rank deficiency to be dealt with in the next chapter.

4 Rank deficiency: global versus local

The adjustment problem of crossover differences is known to be singular. The singularity is characterized by four vanishing eigenvalues in the planar case, while in the spherical case the rank deficiency is just two. In our particular situation of the Mediterranean Sea we have neither a planar case nor a full spherical case. Therefore, two eigenvalues will be zero and two others very small, but numerically not zero.

In order to understand the behaviour of the smallest eigenvalues, two investigations have been performed using simulated GEOSAT ERM tracks:

a) The latitude dependence of the smallest eigenvalues was studied for a diamond shaped system consisting of 6 × 6 crossover points. The diamond was located at various latitudes between 0° and 72° . The location of the diamonds is depicted in Figure 3. The behaviour of the eigenvalues no. 4 and 5 (eigenvalues are here ordered with increasing magnitude), depending on the geographical location of the diamond, is presented in Figure 4. The first three eigenvalues are not presented here - they are practically zero.

   It is obvious that the 4th eigenvalue is almost zero in the neighborhood of the equator, increasing towards the middle latitude range, and again approaching zero towards the pole (due to the degeneration of the diamond). Also the 5th eigenvalue decreases when the diamond moves towards the pole.

b) The dependence of the smallest eigenvalues on the size of a diamond shaped crossover system, consisting of between 10 × 10 and 80 × 80 crossover points, with the diamond centered at latitude $\phi = 20°$, was studied. Three out of a total of eight diamonds are depicted in Figure 5. The behaviour of the eigenvalues no. 3, 4, and 5, depending on the size of the diamond, is presented in Figure 6. The first two eigenvalues are not presented here - they are practically zero.

   It is obvious that the 3rd eigenvalues increases only little with the size of the diamond, while the 4th eigenvalue becomes significantly greater than zero with increasing diamond size.

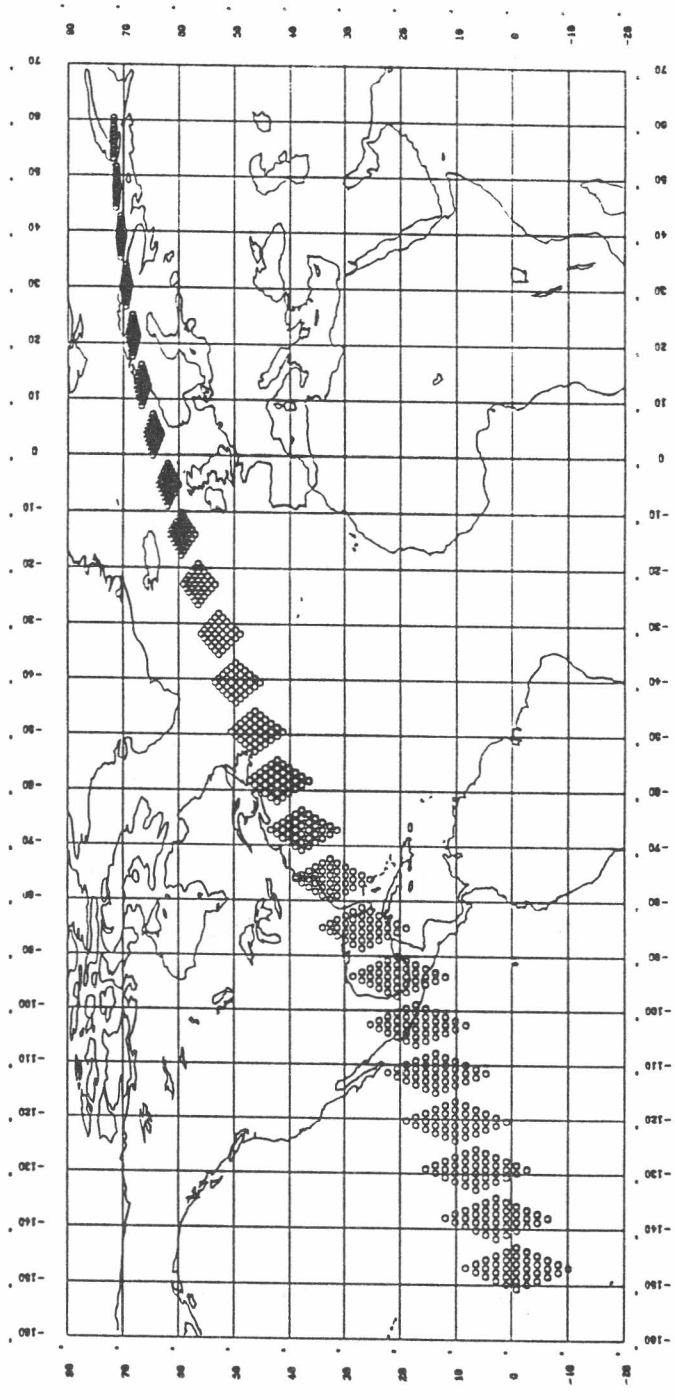

Fig. 3: Crossover diamonds (simulated GEOSAT ERM tracks)

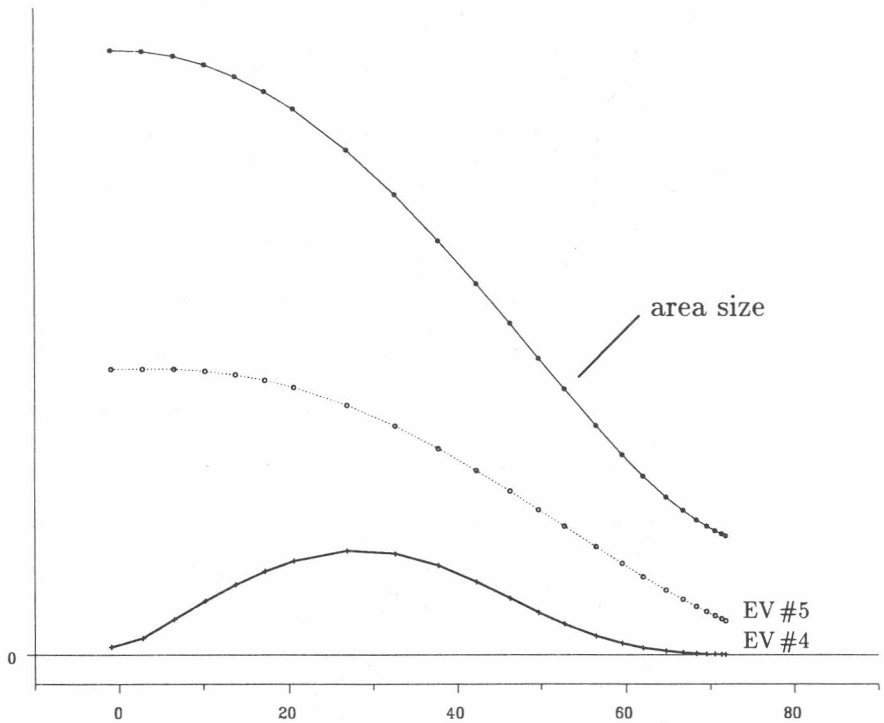

Fig. 4: Smallest eigenvalues dependent on latitude of crossover diamond

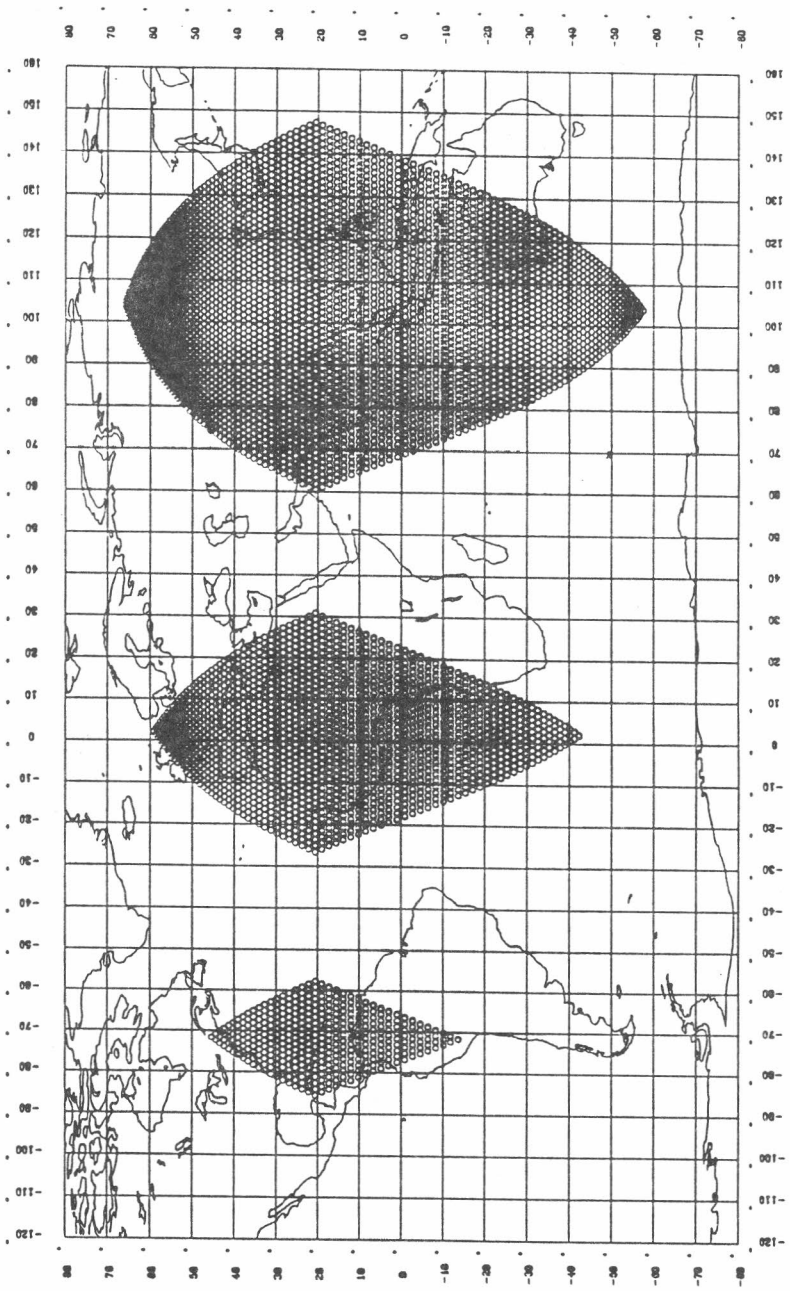

Fig. 5: Crossover diamonds (simulated GEOSAT ERM tracks)

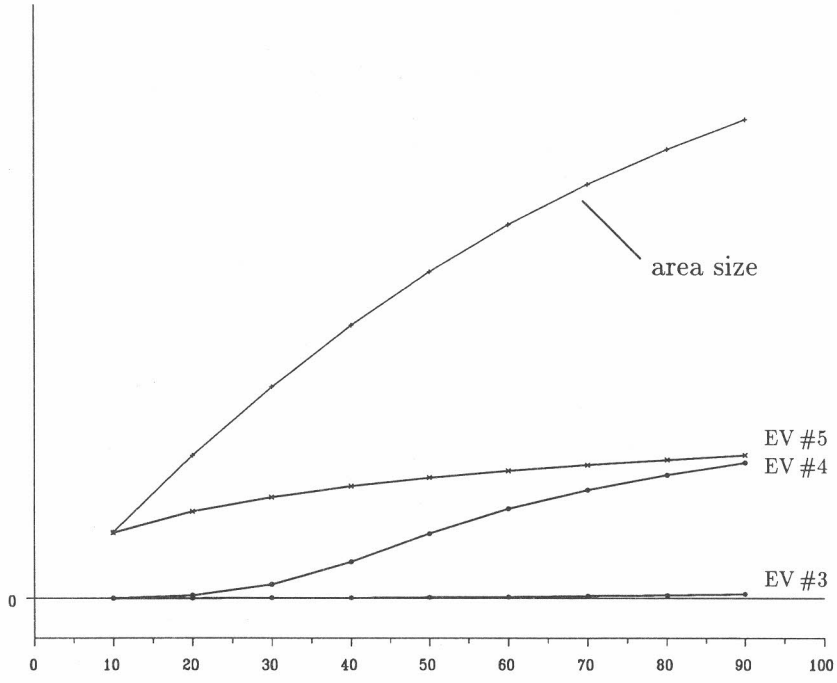

Fig. 6: Smallest eigenvalues dependent on size of crossover diamond

5 Solution of rank deficient systems

As mentioned above the adjustment problem of crossover differences has a rank deficiency between two and four. The rank deficiency can be repaired either by hard or by soft methods.

Rank deficiency repair using fixed tracks

One method of rank deficiency repair consists in the fixing of orbit tracks. In order to obtain a nonsingular solution it is necessary to fix either two northgoing or two southgoing tracks. By such a rank deficiency repair method a behaviour is imposed on the entire track system and therefore on the orbit corrections which is purely dictated by the two chosen tracks. Therefore, such a method is called a hard rank deficiency repair technique. As a matter of fact, the quality of this correction depends on the quality of the chosen (reference) tracks.

Rank deficiency repair using a reference geoid model

Another rank deficiency repair method consists in a regression analysis such that the offset between the altimeter determined ocean surface and an available geoid model is minimized along each track. Here the orbit correction, as induced by the crossover adjustment, is dictated by the used geoid model in the area of consideration. Therefore, also this method is a hard rank deficiency repair technique. As a matter of fact, the quality of this correction depends on the quality of the chosen (reference) geoid model. Note that the reference tracks in the previous case are replaced by the reference geoid in the present case.

The combined adjustment of the crossover differences and the fitting of the altimeter data to a given reference geoid model may be achieved by a combined minimization procedure which is controlled by a weighting parameter ω.

Adjustment of Crossover differences	Regression analysis (by track)
$\Delta h_{ij} = (a_i + b_i\lambda_j) - (a_j + b_j\lambda_i) + r_{ij}$	$\Delta\hat{h}_k = a_i^0 + b_i^0\lambda_k + R_{ik}$
$\sum(r_{ij})^2 \rightarrow Min$	$\sum(R_{ik})^2 \rightarrow Min$

$$a_i = a_i^0, b_i = b_i^0 \tag{5}$$

$$\sum(r_{ij})^2 + \omega \sum(R_{ik})^2 \longrightarrow MIN \tag{6}$$

$$(A^T Q^{-1} A + \omega\, \hat{A}^T \hat{A})\, x = A^T Q^{-1} \Delta h + \omega\, \hat{A}^T \Delta\hat{h} \tag{7}$$

with

Q^{-1} ... Diagonal matrix of a priori covariances
$\hat{A}$ ... Design matrix of regression model ($\hat{A}^T\hat{A}$ ... block diagonal matrix).

The design matrix follows from the chosen bias and tilt parameters which are used for the correction of the satellite tracks. The effect of the weighting parameter ω which controls the stability of the solution is demonstrated in Figure 7: A small weighting parameter minimizes primarily the crossover differences, while a large value for ω minimizes the offset of the corrected altimeter data from the used geoid model. An optimal weighting factor is obviously of the order of about 10^{-6} .

The main drawbacks of this solution are the non-transparence of the rank deficiency, particularly in topologically strongly structured areas such as the Mediterranean Sea, and the mixing of altimeter information with the reference system.

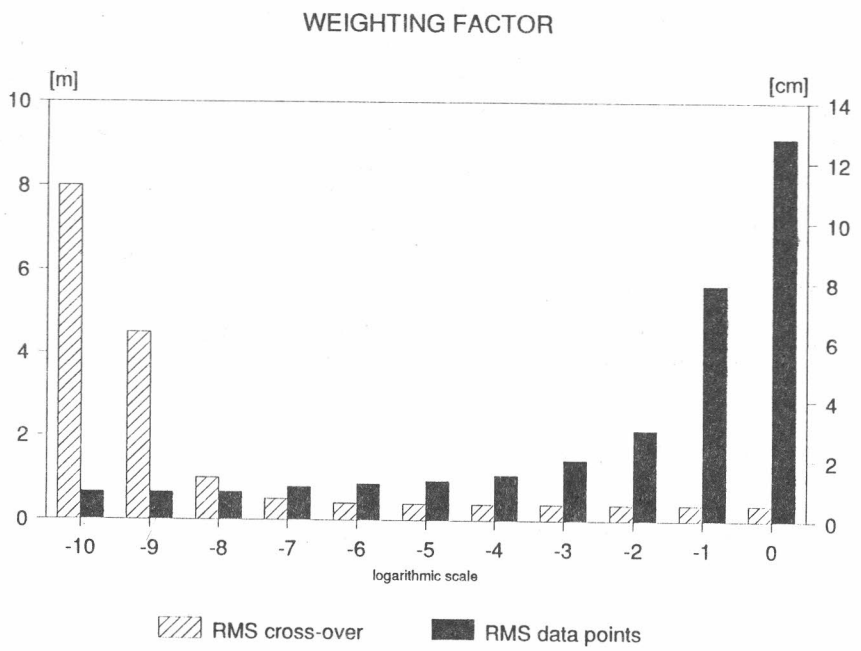

Fig. 7: Effect of weighting factor on crossover minimization and geoid fitting

Rank deficiency repair by singular value decomposition

An entirely different rank deficiency repair procedure is rendered possible by a singular value decomposition (SVD). The SVD method enables a representation of the entire solution space without imposing any restrictions. It is therefore called a soft rank deficiency repair technique. The final solution may be obtained by transformation of the so adjusted track system onto any reference surface.

Compared to the two hard solutions presented above, the solution of the adjustment problem employing SVD is enabled by a direct processing of the error equations. It relies on the orthogonal decomposition of the design matrix in terms of

$$A = U\Sigma V^T \tag{8}$$

with

U ... Orthogonal matrix of left eigenvectors u_i
V ... Orthogonal matrix of right eigenvectors v_i
Σ ... Diagonal matrix of nonnegative eigenvalues σ_i

The solution manifold is delivered by SVD through

SVD

Pseudoinverse A^+ for the construction of a particular solution x_p (least norm)

Complete representation of the nullspace (homogeneous solution x_h)
$N(A) = \{v_j \mid \sigma_j = 0\}$

The general solution is then provided by

$$x_g = x_p + x_h = \sum_{\sigma_i \neq 0} \frac{u_i^T \Delta h}{\sigma_i} v_i + \sum_{v_j \in N(A)} \alpha_j v_j \tag{9}$$

The crossover differences are minimized by x_p . The transformation of the corrected altimeter data onto an arbitrary reference surface (by incorporating the nullspace) leads to the minimum condition

$$\sum(\Delta\tilde{R}_{ik})^2 \rightarrow Min \tag{10}$$

with

$$\Delta\tilde{R}_{ik} = h_{ref,k} - h_{corr,k} \tag{11}$$

and

h_{corr} ... Corrected heights (using the parameter vector x_g)
h_{ref} ... Heights of reference surface

The solution of the adjustment problem delivers the unknown parameters $\alpha_j, \quad j = 1, dim(N(A)$ and provides a solution which minimizes both the crossover differences and the offset of the corrected altimeter derived surface from the reference surface.

Compared to the previous solution the SVD solution requires a high numerical effort and may cause problems in areas with very short tracks. However, these drawbacks are well balanced by the very advantageous properties of the SVD solution in terms of transparence and flexibility.

In the following Table 2 the result of numerical investigations using crossover adjustment solutions with various rank deficiency repair techniques are summarized. Here "v" stands for residual, "P" for the used weight matrix (derived from the altimeter noise of 2 - 10 cm, as provided in the GEOSAT ERM data files), "C" stands for crossover observation, "T" for observed altimeter data" and "CT" for altimeter data at the crossover points. The numbers given in the table are meters.

$\sqrt{\frac{v_c^T v_c}{n_c}}$	$\sqrt{\frac{v_c^T P_c v_c}{n_c}}$	$\sqrt{\frac{v_{ct}^T v_{ct}}{n_{ct}}}$	$\sqrt{\frac{v_{ct}^T P_{ct} v_{ct}}{n_{ct}}}$	$\sqrt{\frac{v_t^T v_t}{n_t}}$	$\sqrt{\frac{v_t^T P_t v_t}{n_t}}$
0.926	25.787	1.103	46.126	1.021	49.761
$C\_Norm + \omega \ T\_Norm$					
0.045	1.073	0.580	23.475	0.577	28.175
$SVD(rank4) + null \ space \ datum$					
0.045	1.073	0.588	23.656	0.578	28.154
$T\_surface + T\_Track = \Delta l$ $\sqrt{\omega} \ curve_0 = 0$					
0.055	1.329	0.033	1.015	0.022	0.671

Table 2: Results of various crossover adjustment solutions

6 Conclusions

The numerical investigations have clearly shown that the nonlinear (cubic) interpolation is superior over the linear interpolation of altimeter data, particularly in rugged, but also in smooth geoid areas. Therefore, cubic interpolation is recommended for the interpolation of altimeter data at the crossover points.

The rank deficiency of the linear system of equations, resulting from the adjustment of crossover discrepancies, depends on the area size and on the geographical latitude of the area in consideration. Two eigenvalues are always zero (even in the theoretical case of a complete coverage of the sphere), while one to two eigenvalues may become very close to zero under certain circumstances.

Three methods to repair the rank deficiency have been investigated: a conventional technique which uses fixed tracks (both northgoing or both southgoing), a method which fits the tracks to a given reference geoid model, and a singular value decomposition solution supplemented by a transformation onto a reference surface.

As usual, all techniques have their advantages and disadvantages. The latter technique is very transparent and flexible because the rank of the linear system is exactly analized and the nullspace provided, the orbit parameter information is strictly separated from the subsequent transformation onto the reference surface. Its main drawback is the very high computational effort. Despite this fact SVD can be recommended for the solution of further crossover adjustment problems.

References

[1] ARABELOS, D. and I.N. TZIAVOS: *Geoid mapping in the Mediterranean Sea using heterogeneous data.* In: Mare Nostrum I - Geomed Report 1, Politecnico di Milano, Milano, 1992.

[2] BARZAGHI, R., M. BROVELLI, F. SANSÒ, and C.C. TSCHERNING: *Geoid computation in the Mediterranean Area.* In: Mare Nostrum I - Geomed Report 1, Politecnico di Milano, Milano, 1992.

[3] HAUSLEITNER, W. and E. HÖCK: *Kreuzungspunkt - Ausgleichung von Satelliten-Altimeterdaten.* In: Geodätisches Seminar Planneralpe 1992, Proceedings, (Eds.: H. Sünkel and M. Wieser), Mathematical Geodesy and Geoinformatics, Graz University of Technology, 1992, pp. 179 - 195.

[4] KNUDSEN, P., O.B. ANDERSEN, and C.C. TSCHERNING: *Altimetric gravity anomalies in the Norwegian-Greenland Sea - preliminary results from the ERS-1 35 days repeat mission.* Geophysical Research Letters, Vol. 19, No. 17, pp. 1795 - 1798, 1992.

[5] SCHRAMA, E.J.O.: *The role of orbit errors in processing of satellite altimeter data.* Publication on Geodesy, New Series, No. 33, Netherlands Geodetic Commission, Delft, 1989.

[6] WAKKER, K.F., B.A.C. AMROSIUS, R.C.A. ZANDBERGEN, and G.H.M. GELDORP: *Precise orbit computation, gravity model adjustment and altimeter data processing for the ERS-1 altimetry mission.* European Space Agency Contract Report, Delft University of Technology, Delft, 1987.

[7] ZANDBERGEN, R.C.A.: *Satellite altimeter data processing. From theory to practice.* Delft University Press, 1990.

First analysis of gross-errors in ERS-1 altimeter data in the Mediterranean Sea.

by

C.C.Tscherning and M. S. Seierup
Geophysical Department
Haraldsgade 6
DK-2200 Copenhagen N, Denmark.

Abstract: Radar altimeter data from the first 35-day repeat tracks of ESA's ERS-1 satellite have been analyzed for gross-errors in an area covering the Mediterranean Sea. Pairs of values which after the subtraction of the OSU91A geoid were more than 0.3 m different were extracted for a first inspection. If the difference could not be explained by the depth variations, and did not occur on repeat tracks then the largest value was marked as an outlier. Using this procedure approximately one per mille of the data was identified as possible gross-errors.

1. Introduction.

Satellite radar altimeter data include just as all geophysical data gross-errors. These errors are generally due to an erroneous land mask, so that data which are supposed to be collected at sea really are partly at sea and partly on land, see e.g. Tscherning (1990).

It is in the nature of gross-errors, that they may not be errors, but be real observations. They should therefore not be eliminated, but have assigned a large error estimate (down-weighted) or simply flagged as gross-errors. We will in the following describe the procedure we have used to detect possible gross-errors of ERS-1 altimeter measurements in the Mediterranean Sea, which is the area of interest for the GEOMED project.

Our analysis has been limited to the area bounded by latitude 30° in South and 47° in North, -5° in West and 40° in East which fully includes the Mediterranean Sea. We describe here the analysis of the tracks from the first four 35-day repeat periods. There were totally 23279 data points in the area from this period. The data distribution corresponding to the first 35-day repeat period is shown in Fig. 1.

2. Method for gross-error detection used.

Gross-errors will here be measurements, where the by us estimated error largely exceeds the error estimate associated with the data as supplied by ESA. This error estimate expresses

MARE NOSTRUM 2, (1992), pp 91-97

a scatter of the data, which originally is formed as the mean value of 20 0.05 sec values. This means that the quantity also includes information about the signal variation in the 1 sec period.

We have in earlier investigations in the Norwegian Sea (see Knudsen et al.(1992a,b)) used the criteria that the scatter should be below 0.20 m in order to identify a possible gross-error. However, due to the strong variation of the gravity field in the Mediterranean Sea large values could simply signify a strong local geoid variation. We therefore decided not to use the value of the scatter in order to identify a possible gross-error.

A gross-error may be masked by a large bias. We therefore subtracted the contribution of OSU91A (Rapp et al.,1991) from the data. Values which after this subtraction numerically exceeded 10 m were then deleted, since we in this area expect the standard deviation of the values (after subtraction of OSU91A) to be below 3 m (cf. Arabelos & Tziavos, 1992, Table 9).

The data were then divided in segments, where a new segment was identified if the distance to the last point was more than 22 km, corresponding to approximately 3 sec time difference. This gave 977 segments in the area to be further analyzed.

They were analyzed by comparing consecutive pairs of points, so that pairs where the difference was larger than 0.3 m were marked for further analysis. Such a difference corresponds to a deflection of the vertical of slightly more than 3", which generally only occurs due to large variations in the bottom topography. Converted to gravity units it corresponds to a change of about 20 mgal over the distance of 22 km. This again correspond to a Bouger plate effect produced by a change in the bottom topography of 200 m.

Since we had to our disposal the bottom topography with a 5' resolution (ETOPO5), we could then compare the topographic signal with the altimetric visually, see Fig. 2. However, this procedure was not always succesful due to the bad quality of the bathymetric information.

Inspecting Fig. 3, it is clear that the bottom topographic information is erroneous. The part of the measurements from degree 42 to degree 43.5 must surely be caused by the topography, but nothing shows up. Here we should remember that older bathymetric measurements were not very reliable at large depths. 200 m height changes were difficult to measure at 3000 m depth.

However, the procedure turned out to be useful, since some large data variations clearly were caused by the topographic variations.

This procedure could have been improved using an improved geoid model, computed from gravity data and topographic data as described in (Tscherning, 1990), and it will be tried later.

We have, however, from the repeated measurements several estimates of the height of the sea surface. And it is obvious, that if large spikes are not repeated (and if we are not close to the coast), then there is something wrong. The comparison of repeat tracks is illustrated in Fig. 4 and 5, where gross-errors easily are seen.

3. Detected gross-errors.

Following the above described procedure 349 of the 977 tracks were found to include point pairs with numerical differences exceeding 0.3 m. Of these only 16 were identified as having gross- errors, and totally 46 points were identified, see Table 1. 17 of these values had assigned a standard deviation larger than 0.20 m. (Of the total dataset 20 % has assigned a standard deviation larger that 0.20 m).

Table 1. Gross-errors detected in the Mediterranean area from the first 4 35-day repeat tracks. The track number 1 is the first track in the 1 35 day repeat period.

Observation time	track no.		Observation time	track no.
230289643.8	0074		230289727.5	0074
230549266.5	0117			
232147011.0	0382	to	232147023.7	0382
232581703.8 *	0454		232581704.7 *	0454
232581734.2 *	0454		232835079.7	0496
232879191.1	0503		233313706.7	0575
234736395.8	0811		235649592.9	0962
235734196.5	0976		235943516.1	1011
235943518.1	1011		235949655.7	1012
235949656.7	1012		235949657.7	1012
237500901.6	1269	to	237500920.7	1269
237894861.7	1334		237894925.9	1334
237894932.7	1334		237985528.6	1349
237985529.6	1349		239408213.2	1585
239408216.2	1585		239711720.6	1635
239711727.5	1635		239790155.7	1648
240490356.8	1764			

NOTE ! points with an * are located in the Atlantic.

However, of the tracks, a large number (406) included 3 or less datapoints. Here more errors may be hidden. These points must be further analyzed using supporting data such as gravity data and other altimeter data (from other ERS-1 tracks or other missions).

The list of suspected errors will be updated when new data are analyzed and stored on a computer with access possible via Internet. We would appreciate if other investigators send us information about other values which they would regard as possible gross-errors.

4. Conclusion.

Approximatly 1 per mille possible gross-errors have been detected in the ERS-1 altimeter data from the first tracks analyzed. This is very typical for geophysical data. The cause of these errors is still unclear, since it only in a few cases seems to be related to a wrong land mask.

The second author of this paper has had the tedious task of inspecting all graphs showing possible errors. We hope that the task will be nearly 100 % automatized in the near future. Then we will also be prepared to inspect the global set of altimeter data with the purpose of detecting gross-errors.

Acknowledgement: This is a contribution to the GEOMED project sponsored by EC contract no. SC1*-CT92-0808. The ERS-1 data has been made available by ESA through the project DK-2.

References:

Arabelos, D. and I.N.Tziavos: Geoid mapping in the Mediterranean Sea using heterogeneous data. GEOMED Rep. no. 1, pp. 82 - 102, Milano, 1992.

Knudsen, P., O.Ba.Andersen and C.C.Tscherning: A preliminary ERS-1 altimeter data analysis in the Northern North-Atlantic Ocean. Pres. EGS XVII General Assembly, G5, Edinburgh, April 1992.

Knudsen, P., O.Ba.Andersen and C.C.Tscherning: Altimetric gravity anomalies in the Norwegian-Greenland Sea - Preliminary Results from the ERS-1 35 days repeat mission. Geophys. Res. Letters, Vol. 19, no. 17, pp. 1795-1798, 1992.

Rapp, R.H., Y.M.Wang and N.K.Pavlis: The Ohio State 1991 Geopotential and Sea Surface Topography Harmonic Coefficient Models. Rep. of the Dep. of Geodetic Science and Surveying n. 410, The Ohio State University, Columbus, 1991.

Tscherning, C.C.: A strategy for gross-error detection in satellite altimeter data applied in the Baltic-Sea area for enhanced geoid and gravity determination. Proc. 11th General meeting Nordic Geodetic Commission, Copenhagen, May 1990, pp. 90-106, Kort-og Matrikelstyrelsen, Copenhagen, 1990.

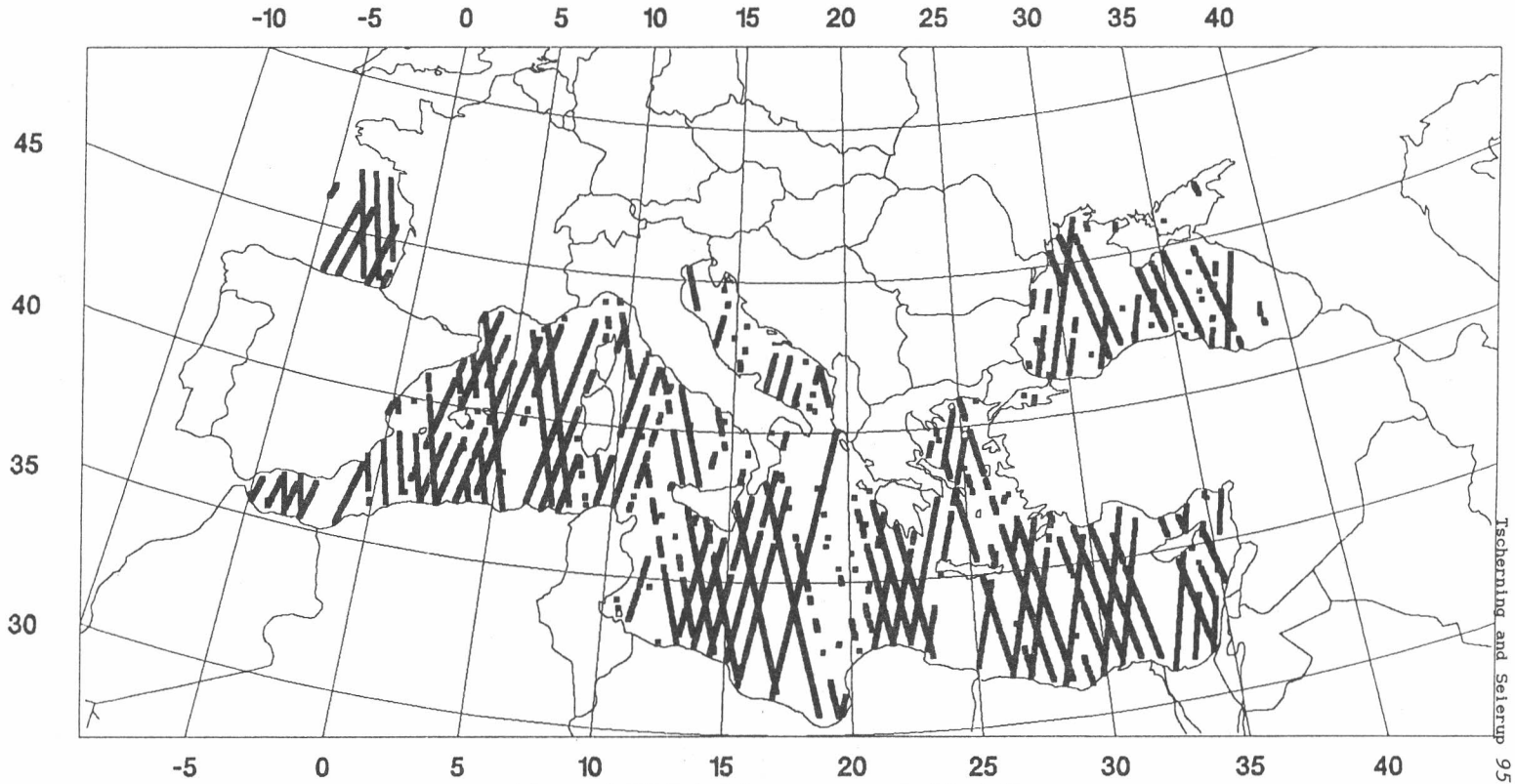

Figure 1. ERS-1 data coverage in Med. Sea.

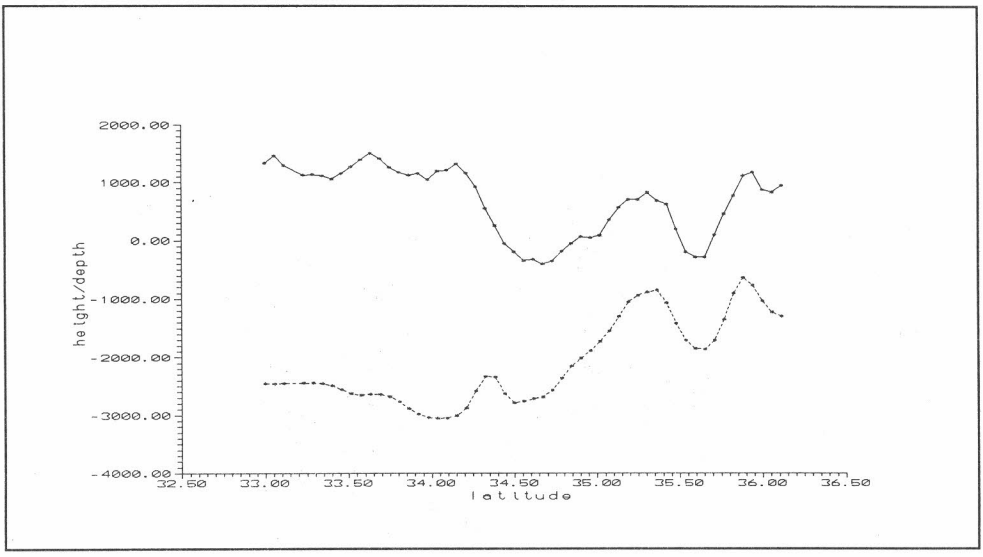

Figure 2. This figure shows a segment of track 2221, where the variations in the track (full line)
and the seafloor topography (dotted line) corresponds nicely.
Note that the track height is exaggerated by a factor 1000.

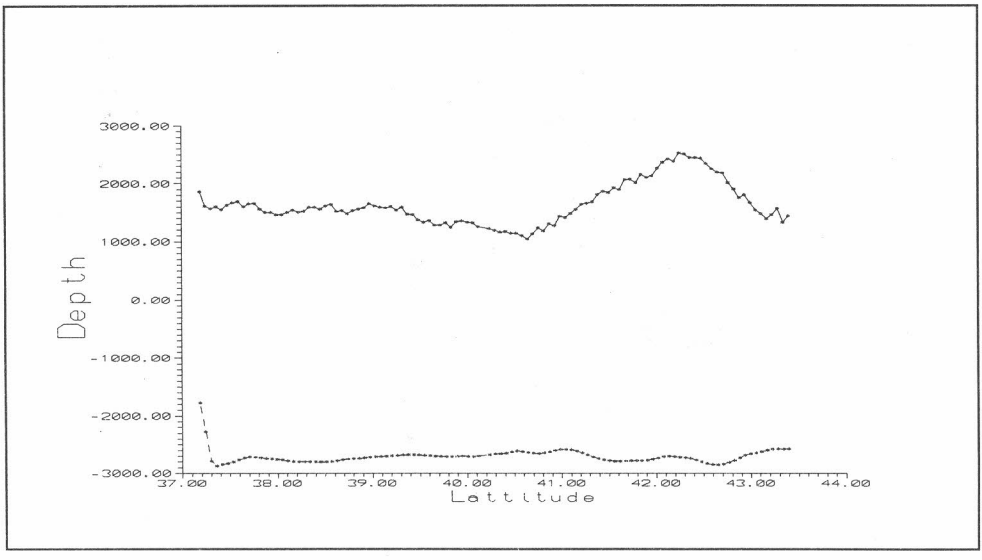

Figure 3. This shows a graphical comparison between track 89 and the seafloor topography.
Note that the ssh-values of the track (full line) are exagerated by a factor 1000.

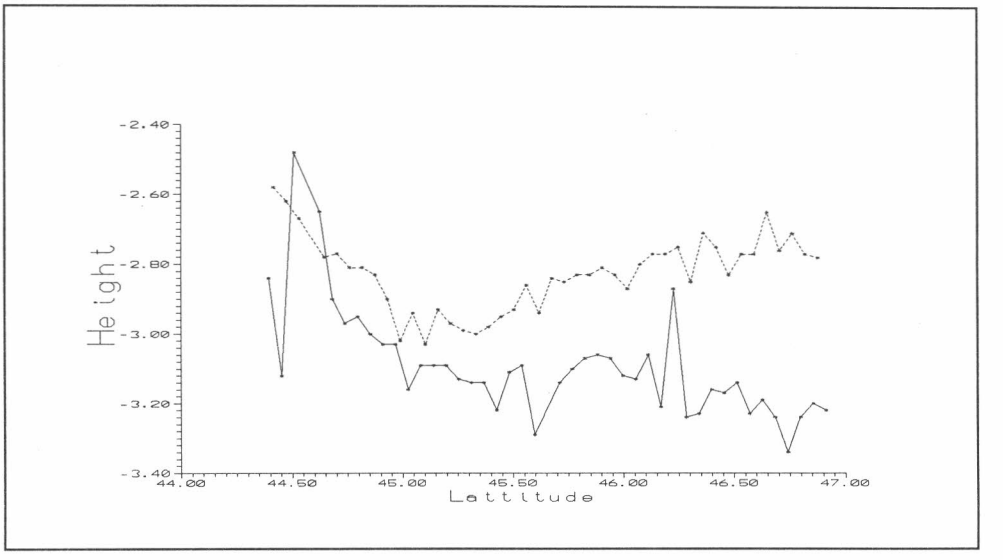

Figure 4. This is a graph comparing two tracks, 454 & 955 (full & dotted line). Two errors are clearly seen on track 454, namely the start of the graph at 44.30 and the spike at 46.20. (Note that this example is situated in the Atlantic)

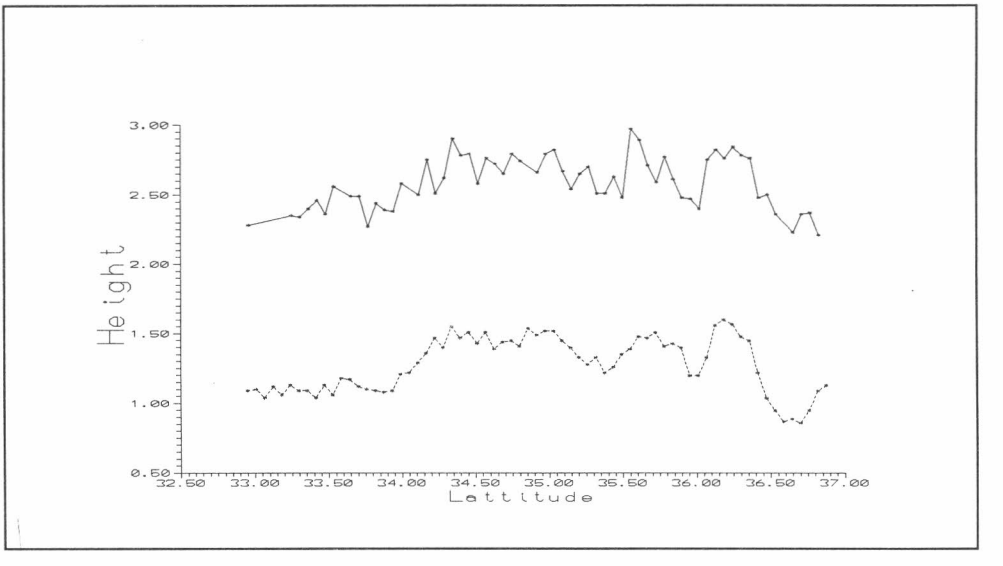

Figure 5. Shown here are the tracks 103 & 604 (full & dotted lines)
It's the same track but for two different 35 day periods.
It is seen that track 103 differs from track 604 by being more ragged and spiky, looks like there's a lot of noise on the track. The track has not been included on the error list but maybe it should.

Evaluation of the Ocean Tides in the Mediterranean Sea in a Collinear Analysis of Satellite Altimetry.

Per Knudsen (National Survey and Cadastre (KMS), Geodetic Division, Rentemestervej 8, DK-2400 Copenhagen, Denmark. Fax: +45 3587 5052)

Abstract. *In this paper the ocean tides in the Mediterranean Sea have been evaluated. The tidal signal was expressed as* $H(t)=\Sigma(U_i\cos(\omega_i t+\chi_i)+V_i\sin(\omega_i t+\chi_i))$ *where* ω_i *and* χ_i *are the tidal frequencies and astronomical arguments respectively, associated with* M_2, S_2, *and* N_2. *The estimated tides (except* N_2*) look very coherent from track to track. The magnitudes of the* M_2, S_2, *and* N_2 *tides are 2.9 cm, 2.4 cm, and 1.9 cm respectively. Along each track the collinear analysis method leaves unknown trends in the tide components, which may explain these low values. However, amplitudes around 10 cm are quite common on long tracks covering 2-3 ocean basins. The results display the complexity of the tides and may valuable in a future utilization of tide gauge data.*

INTRODUCTION

Ocean tide corrections of altimeter data in the Mediterranean Sea have not been available on the standard altimetric data files. Compared with other region the tides in the Mediterranean are quite small. At Naples the amplitudes of the four major constituents: M_2, S_2, N_2, and K_1 are 11.6, 4.3, 2.4, and 2.6 cm respectively (PALUMBO & MAZZARELLA, 1982). With the high precision of altimetric products, however, such magnitudes may affect estimates of the mean sea surface and the sea surface height variability significantly (e.g. THOMAS & WOODWORTH, 1990). In this paper the ocean tide signals are analyzed in the Mediterranean Sea using Geosat altimetry from ERM 1-22 (NOV 1986 - NOV 1987) in the form of 2 seconds averages.

COLLINEAR ANALYSIS

An altimeter derived observation of the sea surface height, h, may be described in terms of the mean sea surface height, h_0, the time varying sea surface topography, ζ_t, and an error, ϵ, by

$$h = h_0 + \zeta_t + \epsilon \qquad (1)$$

where the error, ϵ, accounts for the radial orbit errors and other altimetric errors. Along a set of collinear track segments (denoted as the j'th set) height observations $h_{jk\ell}$ are found at a distance along the tracks of μ_k at a time t_ℓ. The distance μ_k is related to time relative to the time ~~of e.g. the equator crossing~~ (~ 7 ~~km/s~~), while the times t_ℓ depend on the repeat period

of the satellite ($\sim$ 17 days) - e.g. the times of equator crossings.

The major differences between the heights of different tracks are caused by radial orbit errors. In order to reduce the effects of the radial orbit errors the tracks may be merged. This was done by removing a trend from each of the tracks, so that the differences between the tracks, are minimized. In this case the trends were modelled using 1 cycle per revolution cosine and sine terms. Such a procedure leaves a common trend in the j'th set of collinear tracks, $\bar{\epsilon}_j(\mu)$, unsolved. Therefore the adjusted heights are expressed as

$$h^a = h_0 + \delta\zeta_t + \delta\epsilon + \bar{\epsilon}_j(\mu) \tag{2}$$

where $\delta\zeta_t$ and $\delta\epsilon$ are those parts of ζ_t and ϵ respectively, that have not been removed together with the trends. If the mean values of the heights, eq.(2), in each point along the tracks are subtracted both the mean sea surface and the unsolved trend cancel out. If, furthermore, the residual errors are ignored (except for the noise of the measurements, n) then *sea surface height anomalies,* $\Delta h(t)$, are obtained. That is

$$\Delta h(t) = \delta\zeta_t + n \tag{3}$$

Analysis of these height anomalies are usually carried out in a single points, where the height anomalies form a time series, or along a single track, where the height anomalies form a profile (FU & ZLOTNICKI, 1989). Furthermore, the height anomalies may be analyzed in both dimensions simultaneously. **Note (!)** that the spectral contents of the data strongly depend on the lengths of the track segments, i.e. values of $\delta\zeta_t$ and not ζ_t are available.

EXTRACTION OF OCEAN TIDE SIGNALS

The variations of the sea surface heights due to ocean tide may be expressed as (e.g. CARTWRIGHT, 1992, MAZZEGA, 1985, and WOODWORTH & THOMAS, 1990)

$$H(t) = \sum_{i=1}^{N} \left[U_i \cos(\omega_i t + \chi_i) + V_i \sin(\omega_i t + \chi_i)\right] \tag{4}$$

or

$$\begin{aligned} H(t) &= \sum_{i=1}^{N} A_i\left[\cos(P_i)\cos(\omega_i t + \chi_i) + \sin(P_i)\sin(\omega_i t + \chi_i)\right] \\ &= \sum_{i=1}^{N} A_i \cos(\omega_i t + \chi_i - P_i) \end{aligned} \tag{5}$$

where

$$A_i = \sqrt{\left(U_i^2 + V_i^2\right)}, \quad P_i = \mathrm{tg}^{-1}\left(\frac{V_i}{U_i}\right) \tag{6}$$

are amplitudes and Greenwich phase lags respectively, and ω_i and χ_i are the tidal frequencies and astronomical arguments associated with the tidal constituents. In an estimation of the ocean tide two surfaces, $U_i(\phi,\lambda)$ and $V_i(\phi,\lambda)$ in eq.(4), are estimated for each constituent.

Then amplitudes and phase lags can be computed using eq.(6), so that the ocean tide can be expressed using eq.(5) in terms of amplitudes and phases.

In this type of analysis it is assumed that the height anomalies are due to ocean tide. Note (again), the trends cannot be estimated, since they were removed, when the tracks were merged. That is using eq.(3) and eq.(4)

$$\begin{aligned} \Delta h(t) &= \Delta h_0 + \delta H(t) \\ &= \Delta h_0 + \sum_{i=1}^{N} \left[\delta U_i \cos(\omega_i t + \chi_i) + \delta V_i \sin(\omega_i t + \chi_i) \right] \end{aligned} \tag{7}$$

where

$$\delta U_i = U_i - \bar{U}_{ij}(\mu), \quad \delta V_i = V_i - \bar{V}_{ij}(\mu) \tag{8}$$

are the tidal components relative to their trends along the j'th set of collinear tracks. In eq.(7) an additional parameter has been introduced. That is a correction term, Δh_0, which in this case reveals a possible aliasing of the mean sea surface height.

Before the tidal residuals are estimated from the Geosat ERM data it is important to consider the aliased periods of the tidal constituents due to the sampling of the altimetry. In Table I such periods are listed. The tidal constituents treated in this paper (M_2, S_2, N_2, and K_1) have aliased periods of 317 days, 169 days, 52 days, and 175 days respectively due to the repeat period of Geosat. Therefore, a separation of the S_2 and the K_1 is impossible (ZLOTNICKI, 1992). Here the K_1 tide is omitted, but together with a semi-annual variation it may affect the estimation of the S_2 tide. Furthermore an annual variation may affect an estimation of the M_2 tide, when altimeter data covering one year only are used.

Table I. Aliased periods of ocean tides due to the repeat period of the Geosat ground track (from WOODWORTH & THOMAS, 1990).

Constituent	Aliased Period
K_1	175 days
O_1	113 days
Q_1	74 days
P_1	12.2 years
M_2	317 days
S_2	169 days
N_2	52 days
K_2	88 days

RESULTS

The coverage of the observations were analyzed in order to determine selection criteria, so that tracks with a too poor sampling (too few repeats) and short tracks can be eliminated. Figure 1 showing a histogram of the sampling shows that in average about one half only of the 22 repeats are available. Most locations are sampled between 9 and 15 times. This makes an estimation of the M_2 tide, which has an aliased period of 317 days, uncertain. A histogram of the lengths of each set of collinear tracks is shown in Figure 2. The average length is about 1000 km. In this study sea surface height anomalies are computed at location, where at least 9 of the 22 repeat data are available and tracks shorter than 500 km were deleted.

The results show that the estimated M_2, S_2, and N_2 ocean tides have RMS amplitudes

of 2.9, 2.4, and 1.9 cm respectively. The individual (U, V) parameters estimated in each point along ascending and descending tracks are shown in Figure 4-9.

When these (U, V) vectors are evaluated it is important to have in mind that most of the tidal signal may have been removed together with the orbit errors. The problem is sketched in Figure 3. Here one track segment crosses one ocean basin with one tidal (amphidrome) system. On the northern hemisphere the tidal wave (a Kelvin wave) moves with the coast (or equator) on its right hand side. Hence, it moves out of the paper in the left side of the profile shown in Figure 3. Since only one ocean basin is covered most of the tidal signal will appear as a linear trend of the track and, subsequently, most of the signal will be removed when the collinear tracks are merged. Therefore the remaining signal are much reduced and, furthermore, the characteristics have changed, so that both the amplitudes and the phases of the tide may change rapidly along the profile (3 times instead of 1).

The above considerations may explain why the RMS values of the estimated tides are so small. A value around 10 cm for the M_2 would be more suitable. Actually, on the long tracks covering 2-3 ocean basins several values around 10 cm are found. This is also the case for the S_2 tide. The lack of signal is clearly seen on the short tracks in the eastern part of the Mediterranean.

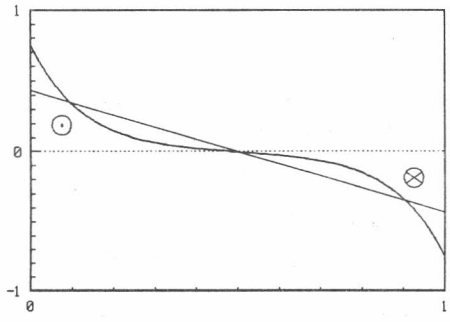

Figure 3. Sketch showing the tide across a basin and the linear trend that is removed.

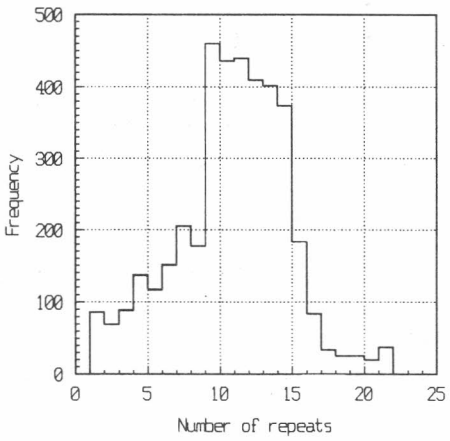

Figure 1. Histogram of the sampling in each point.

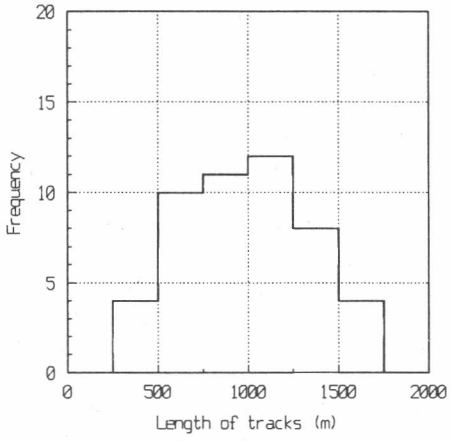

Figure 2. Histogram of the lengths of the track segments.

From track to track the M_2 vectors (Figure 4-5) and the S_2 vectors (Figure 6-7) are coherent. However, some tracks do not correlate at all with its neighboring tracks. This may be due to different data coverage, but annual and semi-annual height variations may play a role too. (In fact only seasonal signals may have been interpreted as tidal signals, see Table I). The N_2 tides appear to be quite small everywhere in the Mediterranean Sea.

The spectrum of the temporal variations is shown in Figure 10. Also the spectrum of

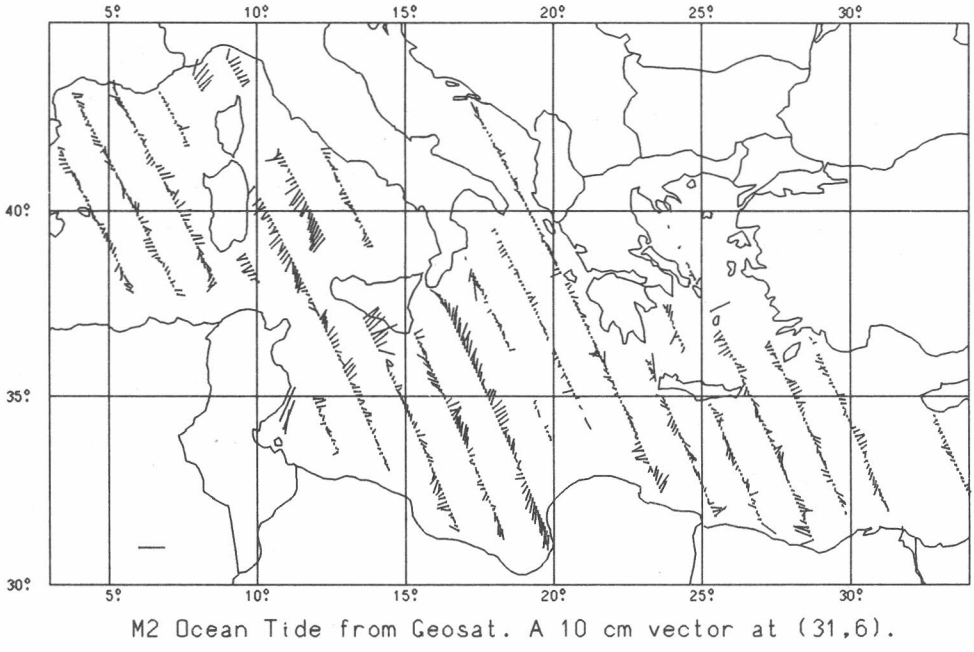

Figure 4. M_2 ocean tide along ascending tracks: *(U, V)* vectors.

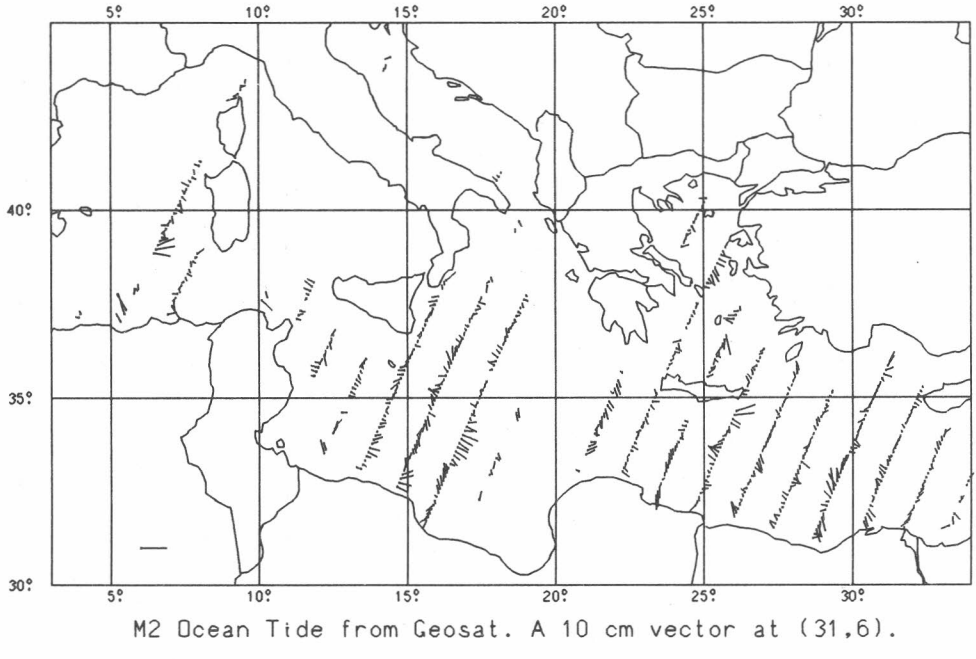

Figure 5. M_2 ocean tide along descending tracks: *(U, V)* vectors.

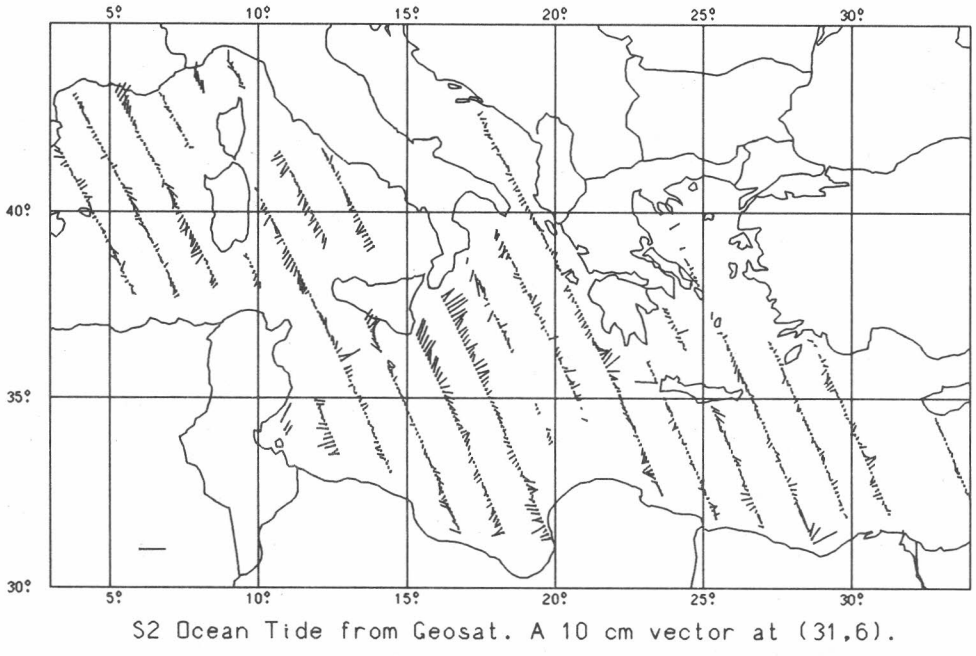

Figure 6. S_2 ocean tide along ascending tracks: *(U, V)* vectors.

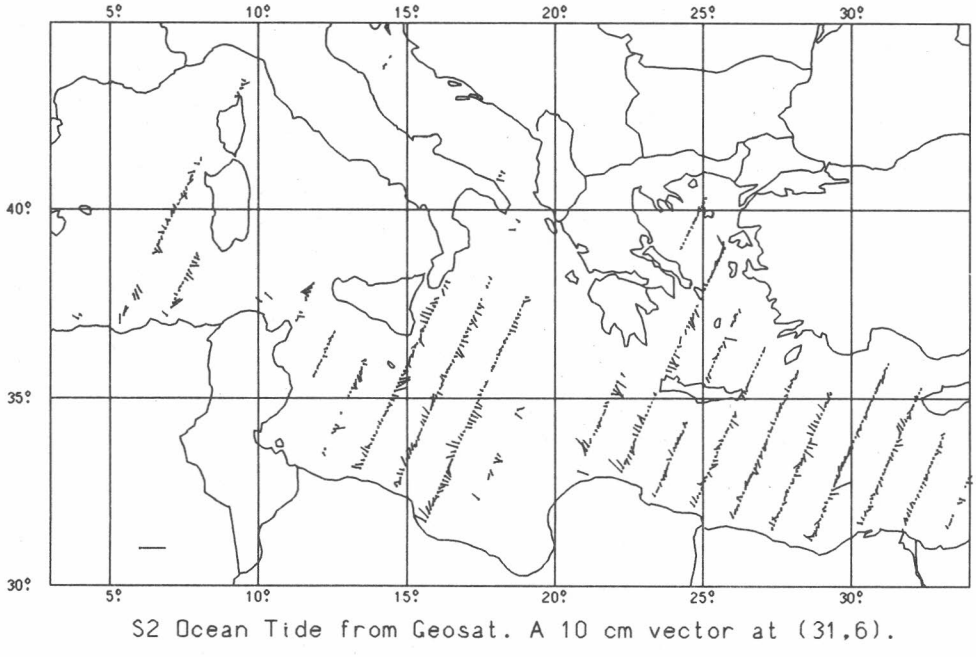

Figure 7. S_2 ocean tide along descending tracks: *(U, V)* vectors.

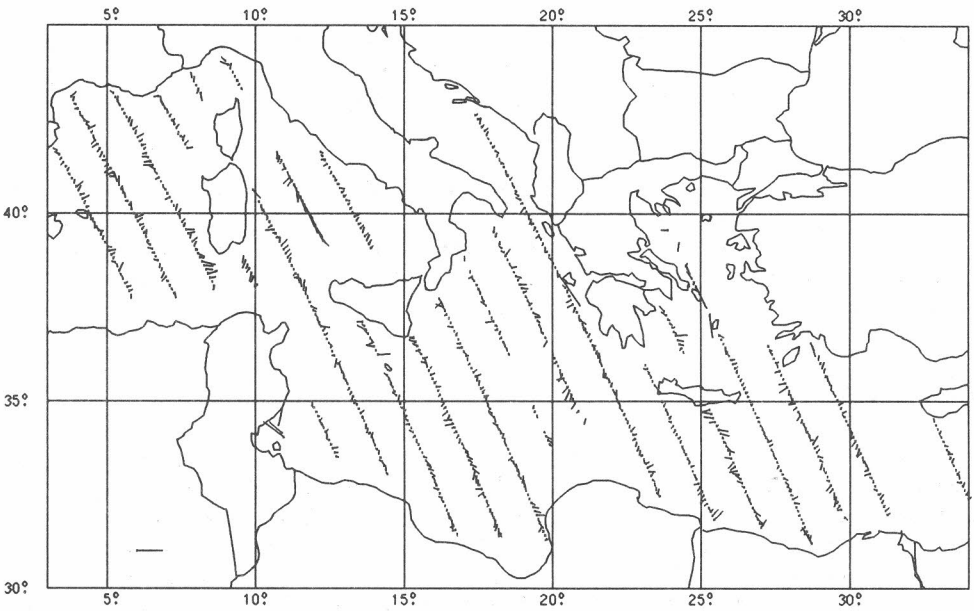

Figure 8. N_2 ocean tide along ascending tracks: *(U, V)* vectors.

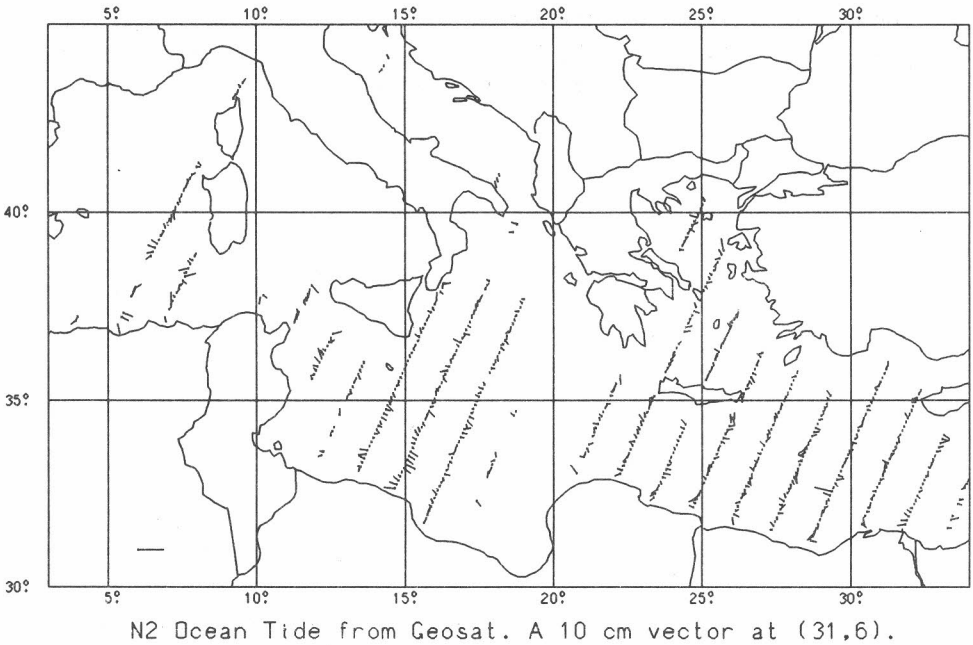

Figure 9. N_2 ocean tide along descending tracks: *(U, V)* vectors.

the variations after the estimated tides have been removed from the height anomalies is shown. The frequencies associated with the aliased periods of M_2, S_2, and N_2 are 1.15, 2.16, and 7.02 cycles/year respectively. The temporal covariance functions are shown in Figure 11. The RMS value of the height anomalies drops from 4.2 cm to 2.6 cm and the temporal correlations vanish. The spectra show that signals associated with 1 and 2 cycles/year approximately efficiently have been removed.

Finally, preliminary ERS-1 altimeter data were used in an estimation of the M_2, which has an aliased period due to the 35 days sampling of about 94 days. The result is shown in Figure 12. This (preliminary) result shown many details that fully agree with the pattern obtained using the Geosat data (Figure 4-5), so the influence of the annual changes on the Geosat M_2 estimate appears to be quite limited.

DISCUSSION

In this paper ocean tide signals have been evaluated in a collinear analysis of altimetry. The magnitudes of the M_2, S_2, and N_2 tides are 2.9 cm, 2.4 cm, and 1.9 cm respectively. The estimated tides (except N_2) look very coherent from track to track. However, along each track this analysis method leaves unknown trends in the tide components (eq.(8)). Furthermore, annual and semi-annual changes may have aliased the M_2, and S_2 tides respectively. These problems, however, may in future be solved by integrating ERS-1 data. Improved results may be obtained, if parametrizations of the surfaces U_i and V_i are found, so that the tidal signal can be estimated taking spatial correlations into account, so that ERS-1 and tide gauge data can be integrated properly.

Acknowledgement. This study is a contribution to the GEOMED project supported by EEC. The Geosat data were obtained from the Ohio State University and the ERS-1 data merged with orbits from DUT/SOM, were obtained from NOAA.

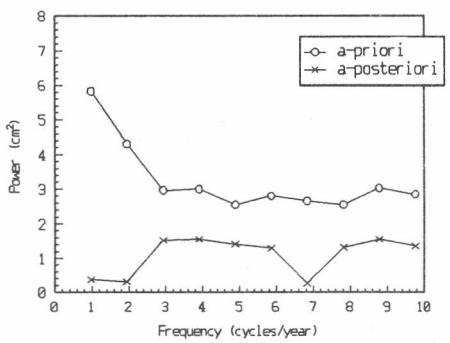

Figure 10. Spectra of temporal variations before and after the tidal components have been removed.

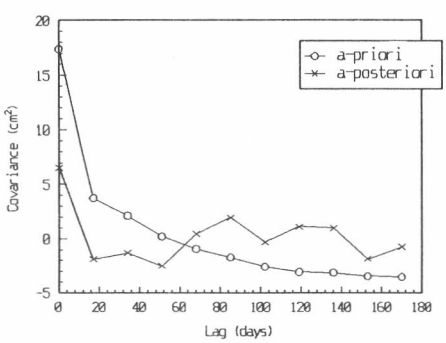

Figure 11. Covariance functions of temporal variations before and after the tidal components have been removed.

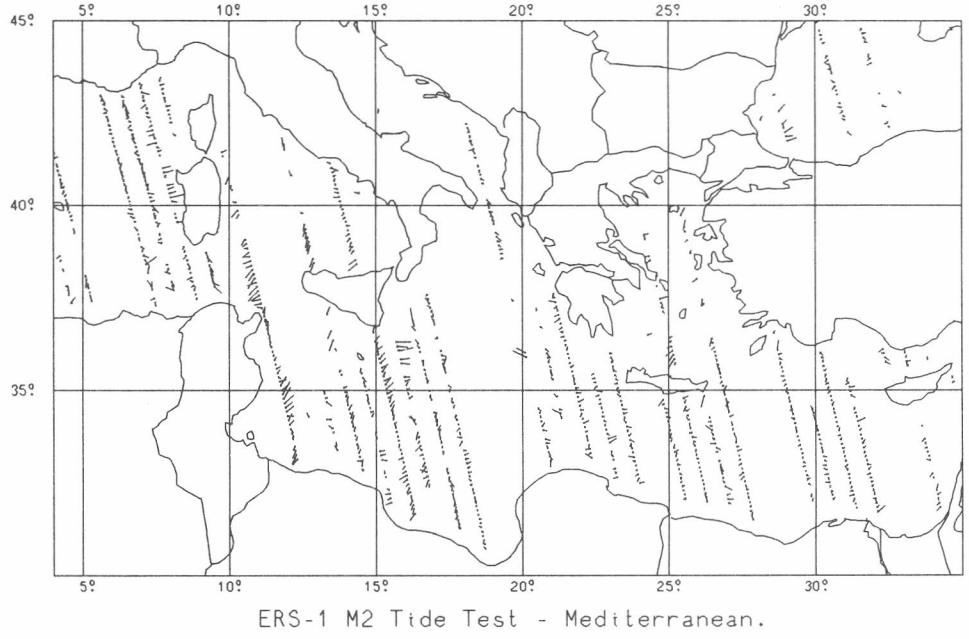

Figure 12. Test: M_2 estimation from 7 repeats of preliminary 35 days ERS-1 data.

REFERENCES

CARTWRIGHT, D.E.: *Theory of Ocean Tides with Application to Altimetry.* Lecture notes, IAG International Summer School on Altimetry for Geodesy and Oceanography, Trieste, June, 1992.

FU, L.-L., AND V. ZLOTNICKI: *Observing Oceanic Mesoscale Eddies from Geosat Altimetry: Preliminary Results.* Geophys. Res. Lett., Vol. 16, No. 5, 457-460, 1989.

KNUDSEN, P., AND M. BROVELLI: *Collinear and Cross-over Adjustment of Geosat ERM and Seasat Altimeter Data in the Mediterranean Sea.* Surveys in Geophysics, in press, 1992.

MAZZEGA, P.: *M2 Model of the Global Ocean Tide Derived from SEASAT Altimetry.* Marine Geodesy, Vol. 9, No. 3, 335-363, 1985.

PALUMBO, A., AND A. MAZZARELLA: *Mean Sea Level Variations and Their Practical Applications.* J. Geophys. Res., Vol. 87, No. C6, 4249-4256, 1982.

THOMAS, J.P., AND P.L. WOODWORTH: *The Influence of Ocean Tide Model Corrections on Geosat Mesoscale Variability Maps of the North East Atlantic.* Geophys. Res. Lett., Vol. 17, No. 13, 2389-2392, 1990.

WOODWORTH, P.L., AND J.P. THOMAS: *Determination of the Major Semidiurnal Tides of the Northwest European Continental Shelf From Geosat Altimetry.* J. Geophys. Res., Vol. 95, No. C3, 3061-3068, 1990.

ZLOTNICKI, V.: *Measuring Oceanographic Phenomena with Altimetric Data.* Lecture notes, IAG International Summer School on Altimetry for Geodesy and Oceanography, Trieste, June, 1992.

GEOID DETERMINATION WITH MASS POINT FREQUENCY DOMAIN INVERSION IN THE MEDITERRANEAN

Martin Vermeer

Finnish Geodetic Institute

Helsinki, December 14, 1992

ABSTRACT

We describe some tentative work done to show the possibility of geoid recovery in the Mediterranean using a frequency domain technique based on the representation of the geopotential by buried masses.

The technique, which has been described in many earlier publications, is flexible in allowing data input of many types, e.g. gravity anomalies, disturbances or satellite radar altimetry.

In the present study, we use as input gravity anomaly data compiled for us by Prof. Miguel SEVILLA, of the Complutense University in Madrid. As the global reference model to be subtracted we used OSU86F produced by Prof. Richard H. RAPP of Ohio State University.

1. INTRODUCTION

In the framework of the European Community financed international project GEOMED we undertook to do some computations on the geoid in the Mediterranean, using as input a 5' × 5' gravity anomaly grid, mostly based on shipboard gravimetry, generated by the group of Prof. SEVILLA (personal communication at the GEOMED meeting in Madrid in October 1992).

MARE NOSTRUM 2, (1992), pp 109-119

Due to severe time constraints and some difficulty in shifting the software to a different computer system in Helsinki, Finland, the results presented here are rather modest. We used the reference model OSU86F rather than the superior OSU91A, because only the former was readily available in the form needed here in Helsinki.

We decided to do the full computation on the FGI's VAX/VMS cluster, even though this meant a rather slow progression, as we knew this system and its quirks and had experience running part of our software on it. Still, we had to limit the resolution of our solution to 15' × 30' (while we chose to keep the whole Mediterranean area) in order to limit the CPU time requirement of the job.

We chose to re-grid the data given to us directly to this coarser resolution, using software that is actually intended to be used with point data only. As gravity is a very "rough" quantity on the Earth's surface, this resulted in block average values that were also pretty rough, also because no terrain effects of any kind were used. Even subtracting the global reference field OSU86F cannot be expected to improve this much, as it is, by its nature, global and cannot remove localized, high frequency, variations.

2. THE AREA OF STUDY AND THE DATA AREA

The area of study was the Mediterranean without the Black Sea. A set of gravity data has been compiled by M. SEVILLA (personal comm.) and was made available to us.

We prepared a control file for the FFT runs called `grid.dsc` which is depicted in Table 1. Interesting here are only the quantities MaxLat, MaxLon and Lat and Lon spacing (the latter in minutes of arc) which together define the "frame of

Table 1. Contents of the control file `grid.dsc`. This sample file actually is for satellite altimetry.

```
          0          Surface type
      0.000          Surface height
 4 1 1 1 1           Obs.type, "UseParts", Attitude laws
5.0E-02 2.0E+00 1.0E+00 0.0E+00 0.0E+00   Obs. std. devs
  6.0    1.0 0   Months, Secs / Pts. / Diff.quant.
     90.000         0.000      Inclination, Alpha
          1          Regional solution
   5000.000          Delta-H of grid sandwich
     55.250       -14.750      MaxLat, MinLon
     15.000        30.000      Lat, lon spacing
        128          Dimension of grid
      8.000          Trunc. wavelength (degs)
        128           Auxiliary grid dimension
          1           No. of topographic models
```

computation", as follows:

Latitude:	55.25 — 23.50
Longitude:	-14.75 — 48.75

The spacing is in the latitude direction 15', in the longitude direction 30'.

It can be seen from these figures that the model we are working with has *128 node points* in both latitude and longitude directions. In our software we have chosen to always use the power-of-two FFT transform, as this offers the greatest effectiveness. Inevitably there is a price to be paid for this: The choice of area bounds is constrained. We have however software to construct an area grid coverage meeting our requirements from arbitrarily distributed point data.

3. GENERATING THE GLOBAL REFERENCE FIELD

We generated a reference field for the area of study using the spherical harmonic expansion OSU86F, produced by the group of Prof. R.H. RAPP of Ohio State University. In the mean time a better model, OSU91A, has become available, but within the time constraint of this study, we could only get OSU86F into a useable form quickly.

For generating values of nine independent functionals of the geopotential, we used the program `leg05`. For a more detailed description of this software, cf. BALMINO *et al.* (1991), or VERMEER (1989).

The `leg05` software produced a grid at a resolution in both directions of 0°.5. From this, a denser grid was produced at the working resolution of 15' × 30', implying a 2 × densification of the grid in the latitude dimension. For this purpose the software `frefgrid` was used, which densifies a grid by any power of two using a forward/backward FFT technique.

More general software of this kind could certainly be written or adapted using cubic spline interpolation; this is one of those projects still in store for the future.

The global reference field OSU86F, in the Mediterranean area, is depicted in Fig.1.

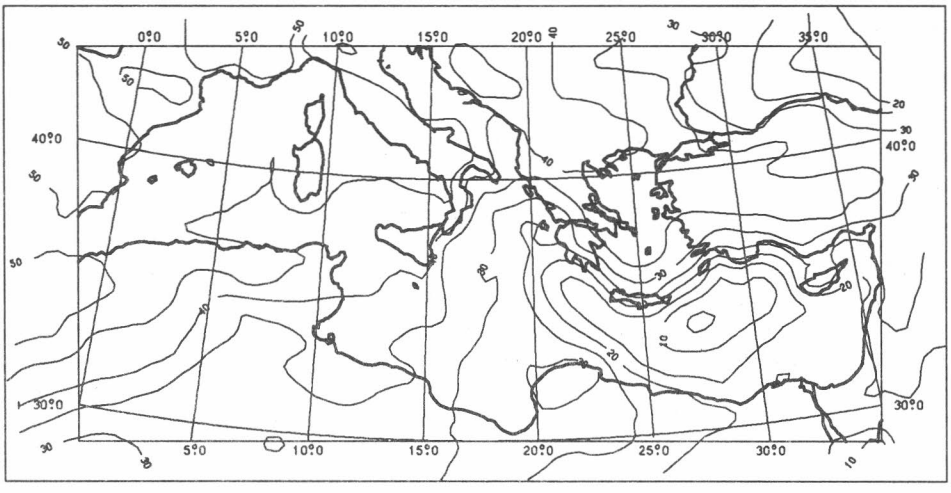

Fig.1: The Mediterranean geoid generated by OSU86F. Unit: m. Contour interval: 5 m.

4. GENERATING THE DATA WORK GRID

We used a crude technique, which nevertheless produced reasonable results quickly. The set of 5' × 5' values given by us was simply considered primary point data, measured at sea level. As the data was given only at sea, this fiction seems fairly realistic. We fed this data as a stream of point records through our gridding software `fgridder`, which not only binned the values into our 15' × 30' cells, but at the same time subtracted out the OSU86F gravity contribution, which was interpolated from the grid generated as discussed earlier.

In the first working grid thus obtained, only part of the cells had received a value, all of them at sea. This grid was then completed using simple inversion-free prediction by the program `ffillin`. Of the eight neighbours of every empty cell, those already containing values were averaged, giving the "diagonal" neighbours half weight. At the same time, these values were "depreciated" by multiplying with the value 0.8, or its square for diagonal neighbours. The value thus obtained was filled into the cell.

Table 2: Statistics of the residual gravity anomalies calculated.

Minimum:	-97.514 mGal
Maximum:	+84.882 mGal
RMS:	±12.115 mGal

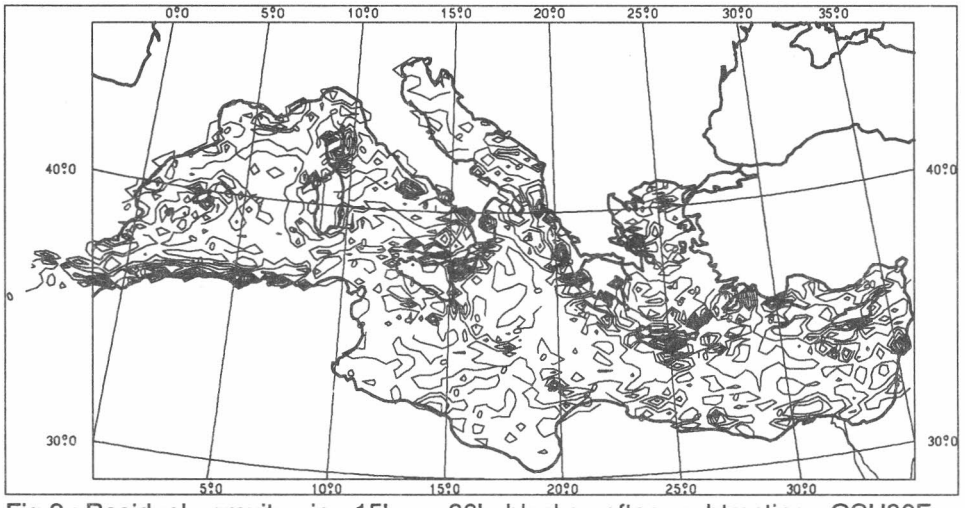

Fig.2 : Residual gravity in 15' × 30' blocks after subtracting OSU86F contribution. Unit: mGal, contour interval: 5 mGal.

This procedure was repeated a number of times, until the "edge values" started approaching zero. After that, the remaining missing values were simply zeroed.

We give the residual gravity values thus obtained with respect to OSU86F in Fig. 2. The statistics of these residuals, for the central quadrant of the area of study, are given in Table 2.

5. THE BURIED MASSES REPRESENTATION

In our method, the external geopotential is represented by a grid of *buried masses*, one mass being located in the *centre* of every 15' × 30' grid cell. Note that the grid cell centres are always in "even" locations with respect to the 0°.5 resolution grid nodes, which again are in latitudes and longitudes like 0°.25, 0°.75, etc.; this means that the grid cell boundaries are in *odd* locations. This is again one of those things that will improve once we have a more flexible way of interpolating reference model values to data grid node locations.

The depth of the mass points was kept constant at 60 km. This depth is proportional to the grid cell linear size, a principle that makes physical sense, cf. HEIKKINEN (1981).

The coefficients between each mass point and each observation type at the Earth's surface can be derived by the application of Newton's law of gravitation,

considering the nature of the observation type. The general coefficient is a function of the *difference* in longitude and (approximately) the *difference* in latitude only between mass point and data location, i.e. it describes a (discrete) *convolution.*

6. GENERATING THE COEFFICIENTS

6.1. The transfer coefficients

Our system is built in such a way, that first coefficient sets are generated for a set of nine *standard observables*: The disturbing potential, three components of the gravity disturbance vector, and five independent disturbing gravity gradient tensor components.

For the true observables then, which are linear combinations of these nine, a set of *transfer coefficients* is then derived and stored on ASCII file for future reference. Matrix multiplication then yields the final set of coefficients for the actual observables used.

This approach has the elegance of generality. It makes it also easy, using the same transfer coefficients, to derive simulated *true* observables, or (as was employed by us) the contribution to the observable used by the OSU86F global reference model, which is used in both the remove (gravity anomaly) and restore (geoid undulation) step.

More about the transfer coefficients, and a listing of those for gravity anomalies and for geoid undulations, is given in VERMEER (1992a).

6.2. Generating the observation equation coefficients

The observation coefficient matrix is generated using the program `fsyncoef`, as discussed using transfer coefficients from `synth`. The standard observable coefficient matrix was generated by `fcoef`, in five different locations (height, latitude combinations) to allow iterative interpolation taking both the topography and the Earth's curvature into account ("Spherical FFT", cf. VERMEER, FORSBERG (1992)).

The possibility to perform such an iteration was not used, however, in order to save time; the error made in doing so is small. In this case `fsyncoef` can be made to extract only the coefficients for reference latitude (mean latitude of area of computation) and height level 0.

7. APPLYING THE FAST FOURIER TRANSFORM

We inverted the system of equations by, for every frequency domain constituent, dividing the data value by the coefficient value. In case there are several data values for every grid cell, this division takes the form of the solution of a small system of normal equations; here, with only one observable, it degenerates to a simple division.

There are $128^2 = 16384$ such divisions to be made, i.e. one for every point in the area. Note that this makes the operation cheaper than the FFT transform itself, which always requires $n^2\ ^2\ln n$ operations, $n = 128$ being the linear size of the area.

The simplicity of the technique is a direct consequence of the convolution theorem of Fourier theory, cf. Vermeer.

8. INVERSION WITH REGULARIZATION

It is generally necessary to *regularize* the problem before a reasonable solution can be obtained. This is obvious in case of downward continuation, such as airborne gravimetry: The high frequency constituents of the geopotential cannot be recovered from measurements at altitude, and thus must be fixed more or less arbitrarily to find a solution and prevent the system of equations from going singular. Typically one uses *a priori* information on the allowed range of values of some functionals of the solution.

However, also in inversions of our kind it is necessary to apply constraints of this kind, mainly because of the differing spectral behaviour of gravity and geoid undulations. Some parts of the spectrum of the geopotential are poorly estimable because of this.

In our case we constrain both the mass point surface density and its horizontal gradient to geophysically "reasonable" values. We chose a value of ±1000 mGal for the *a priori* standard deviation of the mass surface density of our mass point "blanket" (remember, we work with values GM, which, divided by surface area $\sigma = I\ b$, have the same dimension as Newton's acceleration GMr^{-2}, and can thus be expressed in mGal!). For the horizontal gradient we chose $\pm 10^8$ E, i.e. in practice infinite, so this constraint was not applied at all.

We found for these parameters a "gain factor" (i.e. the amount of original gravity signal propagating into the solution) of 56%, a little on the low side.

9. TAPERING AND FILTERING

One other technique which must be used to produce acceptable results is *tapering*. With this is meant the smooth transition to zero of the residual input data by multiplying with a function window going smoothly to zero at its edges. We used a cubic taper with this behaviour for an edge width of 8°. At the same time, a frequency filter was applied to the residual solution, clipping off all frequency content below a limit corresponding to this 8°. Cf. VERMEER (1992a) for technicalities.

This is not necessarily the best way to handle the problem of low frequency content: Others prefer to simply remove a bias term from the residual solution. The choice depends on a judgement on the quality of the high-frequency part of the global model before proceeding to apply Fourier techniques.

10. PREDICTING GEOID UNDULATIONS

We predict geoid undulations from the mass point solution found by multiplying with the coefficient matrix for satellite radar altimetry, with the program `fpredict`. In this way we obtain accurate geoid undulations expressed in m.

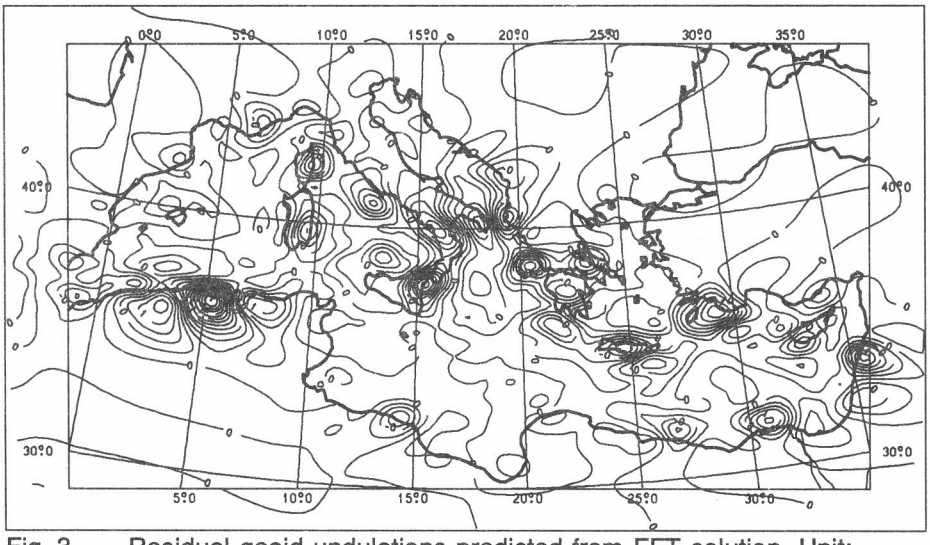

Fig. 3. Residual geoid undulations predicted from FFT solution. Unit: m, contour interval 0.25 m.

We refer to Fig. 3 for our results.

The statistics found for these residual geoid undulations are summarized in Table 3, again for the central quadrant of the area of study.

Table 3: Statistics of the residual geoid undulations predicted.

Minimum:	-2.961 m
Maximum:	+1.301 m
RMS	±0.357 m

11. RESTORING THE TOTAL GEOID

After computing the residual geoid, it should be added again to the geoid implied by the OSU86F global reference model. First we have to generate from the OSU86F standard observables grid file generated above, a grid file containing geoid undulations. We do this by multiplying with the satellite altimetry coefficient matrix in the program `fsynobs`. After that, the global and local contributions are added together by `faddrhs`. The result is shown in Fig. 4.

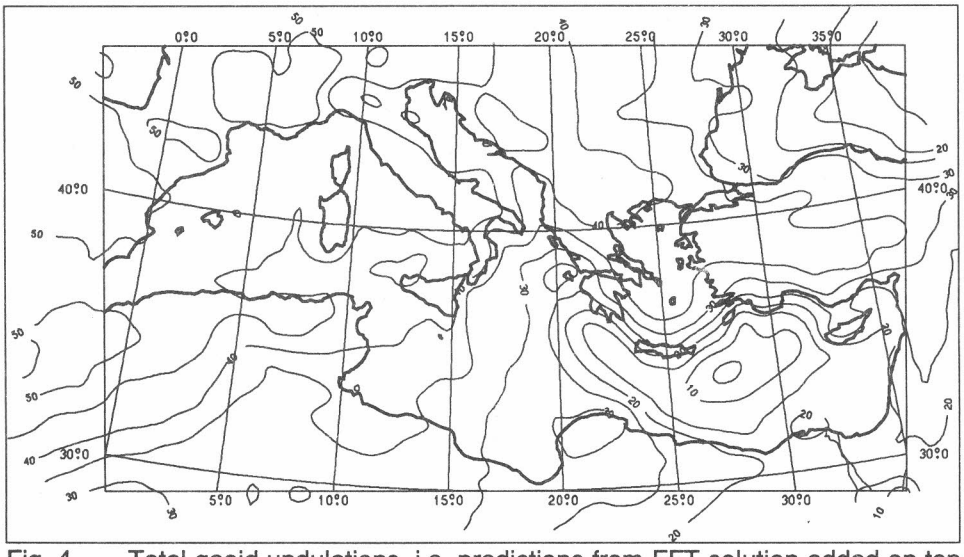

Fig. 4. Total geoid undulations, i.e. predictions from FFT solution added on top of the OSU86F contribution. Unit: m, contour interval 5 m.

12. RESULTS AND DISCUSSION

It can be seen from Fig. 3 that the residual geoid undulations found are large in some places, e.g. in the neighbourhood of Crete. They are expected to be large around Crete, where there is a very strong gravity signature with sharp edges having a strong high-frequency content.

Then we see a number of extrema in the residual geoid located along the coast (Algeria) and the coasts of islands. This could also be the result of strong "edges" in the gravity field occurring preferentially in such places. It is also possible that, in extrapolating the sea-only gravity data into land, applied a too strong "depreciation factor" leading to too sharp edges.

It is also seen that the effect of adding the local FFT solution to the OSU86F geoid is only barely visible in the figures.

It will be necessary to experiment further, both using better global reference models (OSU91A), and using more refined data processing (gridding) techniques. At the very least we should be able to use the 5' × 5' data at its original resolution. Also proper regularization parameters for that resolution should be established by numerical experimentation.

ACKNOWLEDGEMENTS

We gratefully acknowledge the use of the gravity data compiled by M. SEVILLA of the Institute for Astronomy and Geodesy, Complutense University, Madrid, covering the Mediterranean at a resolution of 5'. We also gratefully acknowledge the use of OSU86F, a spherical harmonic expansion produced by R.H. RAPP of Ohio State University.

The present work was done in the framework of European Community contract no. SC1*CT92-0808 ("GEOMED") and constitutes a first, preliminary demonstration of abilities. Financial support by the EC is gratefully acknowledged.

Finally we are happy to acknowledge the support by the Danish National Survey and Cadastre, where the author developed part of the software used in this study and who also supported in part his travels in connection with GEOMED.

REFERENCES

BALMINO, G. , J. BARRIOT, R. KOOP, B. MIDDEL, N.C. THONG, M. VERMEER (1991): Simulation of gravity gradients: a comparison study. Bulletin Géodésique 65:218-229.

HEIKKINEN, M. (1981): Solving the shape of the Earth by using digital density models. Finnish Geodetic Institute, Report 81:2, Helsinki.

VERMEER, M. (1989): FGI Studies on Satellite Gravity Gradiometry. 1. Experiments with a 5-degree buried masses grid representation. Finnish Geodetic Institute, Report 89:3, Helsinki.

VERMEER, M. (1992a): FGI Studies on Satellite Gravity Gradiometry. 3. Regional high resolution geopotential recovery in geographical coordinates using a Taylor expansion FFT technique. Finnish Geodetic Institute, Report 92:1, Helsinki.

VERMEER, M. (1992b): Exploiting Symmetry for Fast Inversion — The case of geophysical gravity inversion. Proc. Interdisciplinary Inversion Workshop I, Aarhus, ed. B.H. Jakobsen, GeoSkrifter 41, 93-98.

VERMEER, M., R. FORSBERG (1992): A generalised Strang van Hees approach to fast geopotential inversion. Manuscripta geodaetica 17: 302-314.

CATALAN GEOID 91: SUMMARY OF RESULTS

M.A. Andreu, C. Simó
Dept. Matemàtica Aplicada i Anàlisi
Universitat de Barcelona
Avda. Gran via de les Corts Catalanes, 585
E – 08007 Barcelona, Spain

In this paper we summarize some results of the computation of a gravimetric geoid in Catalonia [Andreu, Simó, 1992]. We have used the well known method of Least Squares Collocation (LSC) [Moritz, 1980] [Tscherning, 1984] and the remove-restore technique [Forsberg, Tscherning, 1981].

1 Data used for the geoid computation

1) Spherical harmonic coefficients: as a first approximation of the gravity field, we took the spherical harmonic expansion corresponding to the coefficients set OSU89B up to degree 360 [Rapp, 1990]. This is a good approximation of the gravity field in Catalonia. The figure 1 shows a geoid computed using this expansion and Bruns formula.

2) Topographic data: presently, two digital terrain models (DTM) are availables:

   - A detailed grid of $15'' \times 15''$ from *Institut Cartogràfic de Catalunya* (ICC). This model originally comes from the Defence Map Agency and it covers the area shown in the figure 2.
   - A coarse grid of $5' \times 5'$ mean heights from NGDC. This grid is part of the ETOPO5 model and it was provided by R.Forsberg. We found that this model needs to be shifted $7'.5$ in longitude and $-2'.5$ in latitude. After this shift, both models have a good agreement.

3) Gravity anomaly data: in Catalonia there are a lot of gravity measurements covering all the land. We have used the data from *Servei Geològic de Catalunya* (SGC) as the main set and we have completed this set with data from *Bureau Gravimétrique International.* We have selected 1718 gravity anomalies (85 % from SGC) close to a $2'.5 \times 2'.5$ grid. The figure 3 shows the distribution of the selected gravity anomalies.

2 Terrain corrections and residual gravity anomalies

In order to compute the terrain corrections we have used a residual terrain model (RTM). The reference surface was computed averaging blocks of $35' \times 35'$ of the ETOPO5 terrain model. In the computation of the effect of the RTM on the gravity anomaly it is only necessary to take into account the topography up to a distance of 40 Km from each station. The table 1 shows the statistics of the gravity anomaly when we subtract the contribution of the spherical harmonic expansion and the effect of the RTM.

MARE NOSTRUM 2, (1992), pp 121-131

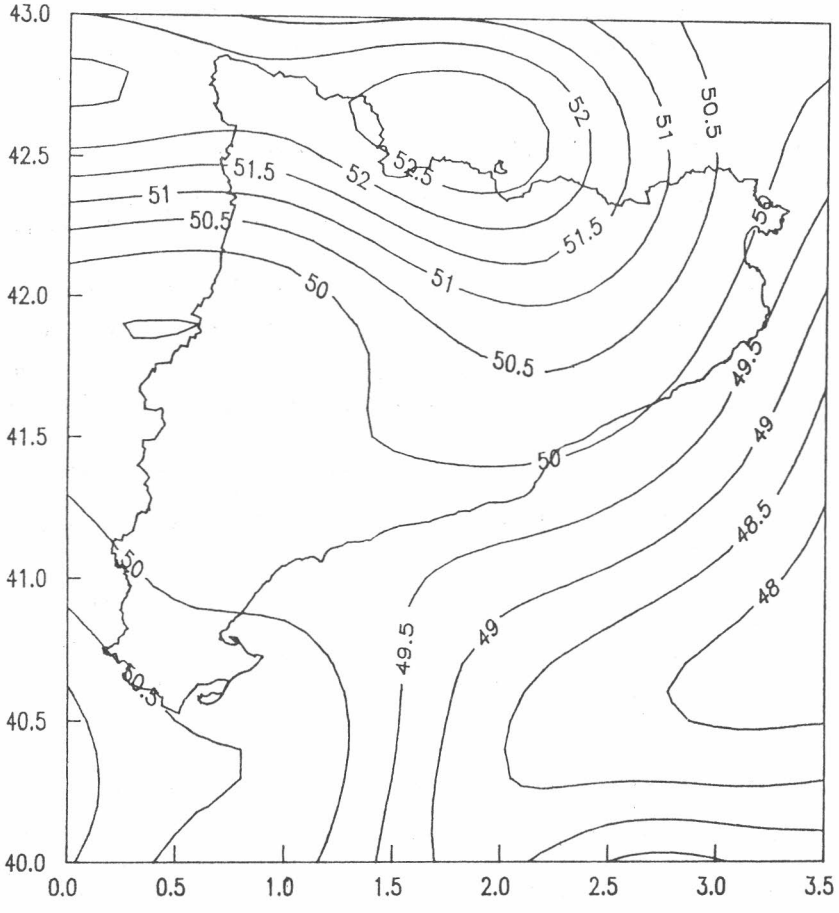

Figure 1: Geoid (m) using only spherical harmonic expansion OSU89B up to degree 360.

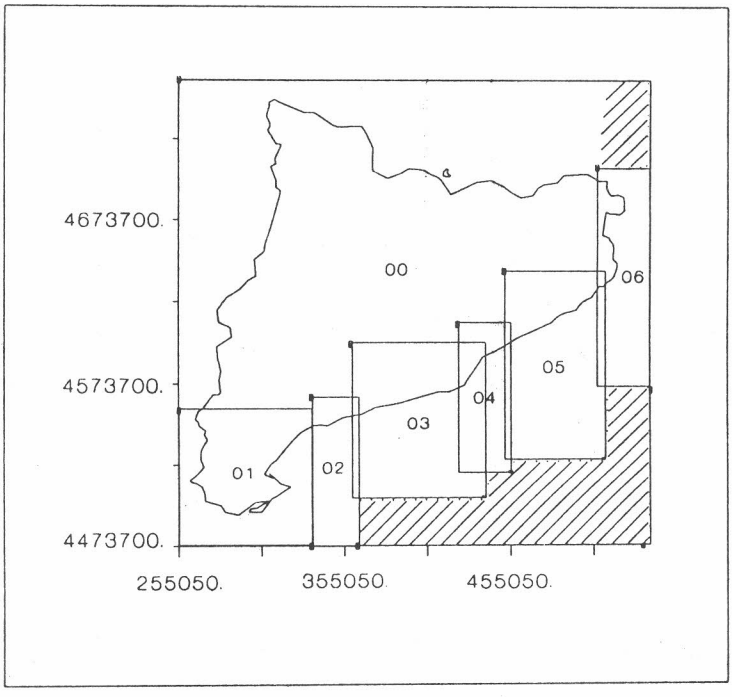

Figure 2: The detailed terrain model covers the area not marked. Latitude and longitude in UTM coordenates.

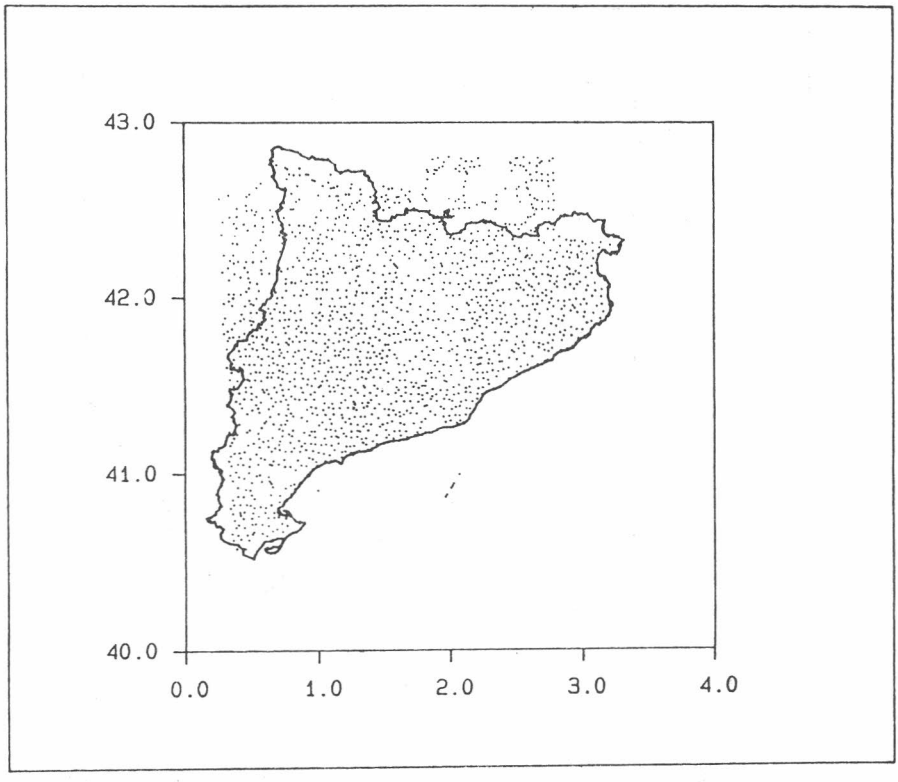

Figure 3: 1718 gravity anomaly selected close to a 2′.5 × 2′.5 grid.

	Mean $mgal$	Var. $mgal^2$	Min. $mgal$	Max. $mgal$
Δg_{obs}	10.39	980.63	−70.53	210.70
$\Delta g_{obs} - \Delta g_0$	−7.83	864.86	−122.34	143.55
$\Delta g_{obs} - \Delta g_0 - \Delta g_m$	4.50	133.52	−27.85	43.01

Table 1: Statistics of the residual gravity anomaly. Δg_{obs}: observed gravity anomaly. Δg_0: gravity anomaly using spherical harmonic expansion. Δg_m: contribution of RTM using detailed DTM up to 20 km and coarse DTM up to 40 km.

But, we have observed that residual gravity anomaly and topographic height are correlated. The regression line (figure 4) is the following:

$$\Delta g = 0.60 + 8.39 \cdot 10^{-3} H \quad (\Delta g \text{ in mgal and } H \text{ in m}).$$

In order to avoid this trend, we modified the reference surface multiplying each height by α:

$$\alpha = 1 - \frac{m}{0.1119},$$

where m is the slope of the regression line. The statistics of the new residual gravity anomalies are shown in the table 2.

	Mean $mgal$	Var. $mgal^2$	Min. $mgal$	Max. $mgal$
$\Delta g_{obs} - \Delta g_0 - \Delta g_{mm}$	−0.62	103.82	−37.91	30.99

Table 2: Statistics of the last residual gravity anomaly. Δg_{mm}: contribution of RTM using the modified surface.

3 Covariance model

After removing the contribution of spherical harmonic coefficients and the effect of RTM, we have the residual gravity anomalies. We can compute the empirical covariance function in the usual way [Knudsen, 1987] averaging products of these gravity anomalies.

The following step in our computation was to fit the covariance model to the empirical covariance function using the method exposed in [Knudsen, 1987]. The covariance model used was the following:

$$K(P,Q) = a \sum_{n=2}^{360} \sigma_n^{(e)} \left(\frac{R^2}{r\,r'}\right)^{n+1} P_n(\cos\psi) + \sum_{n=361}^{\infty} \frac{A}{(n-1)(n-2)(n+4)} \left(\frac{R_B^2}{r\,r'}\right)^{n+1} P_n(\cos\psi),$$

where $\sigma_n^{(e)}$ are the error degree-variances related to the potential coefficients set, a is a factor which represents the quality of the approximation of the potential coefficients set, R is the mean

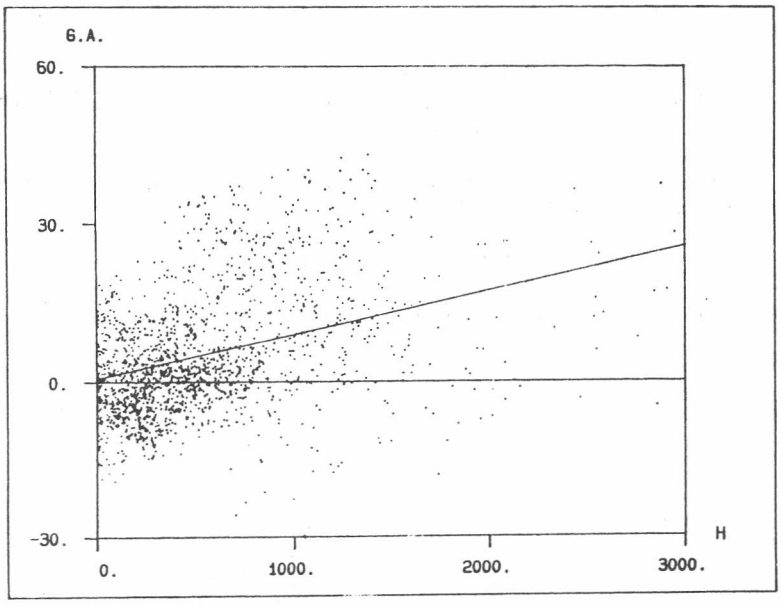

Figure 4: Relationship between residual gravity anomaly and height. Gravity anomaly in mgal and topographic height (H) in m.

earth radius, r and r' are the radial distances of P and Q, R_B is the radius of a Bjerhammar sphere, P_n are the Legendre polynomials and ψ is the spherical distance between P and Q.

The result of the estimation of the three parameters was the following:

$$a = 0.3751,$$
$$R_B - R = -459 \text{ m},$$
$$Var. = 103.90 \text{ mgal}^2.$$

4 Predictions

After fitting the covariance model, we were able to make predictions of several quantities related with gravity potential as gravity anomalies, geoid undulations and deflections of the vertical. For this purpose, we used the Least Squares Collocation method (GEOCOL program, C.C.Tscherning). The input data were the selected gravity anomalies, and the covariance model was the one estimated in the preceding section.

1) Gravity anomaly: we compared gravity anomaly observed and predicted in 33 stations (not used as input data). The results of this comparison are shown in the table 3.

	Obs.	Pred.	Dif.
Mean	10.93	10.65	0.28
St.Dv.	17.86	17.81	2.39

Table 3: Comparison of observed and predicted gravity anomalies (mgal) in 33 stations.

2) Geoid undulations: we computed geoid heights on a grid in the zone of latitude between 40° and 43°, and longitude between 0° and 3°.5. The geoid undulations were computed adding the contribution of:

   - Spherical harmonic expansion OSU89B up to degree 360.
   - LSC (min.: −0.66 m, max.: 0.69 m).
   - RTM (min.: −1.56 m, max.: 2.32 m). This effect was computed using a fixed area: longitude $[-2°, 5°.5]$ and latitude $[38°, 45°]$.

   The figure 5 shows the level curves of the geoid using the ellipsoid of reference WGS84. The figure 6 shows the absolute error of the geoid estimated by LSC. But we were interested in the relative error, this means the error in the difference of the geoid undulations between two points. For this reason, we estimated the error using a fix point (see figure 7) and we found that the relative error is about 10 cm per 100 km.

3) Deflections of the vertical: we also compared the computed value of 8 deflections of the vertical with a preliminary determination of this deflections. The differences between both values show:

$$\text{Mean} = 0''.2,$$
$$\text{St.Dv.} = 0''.8.$$

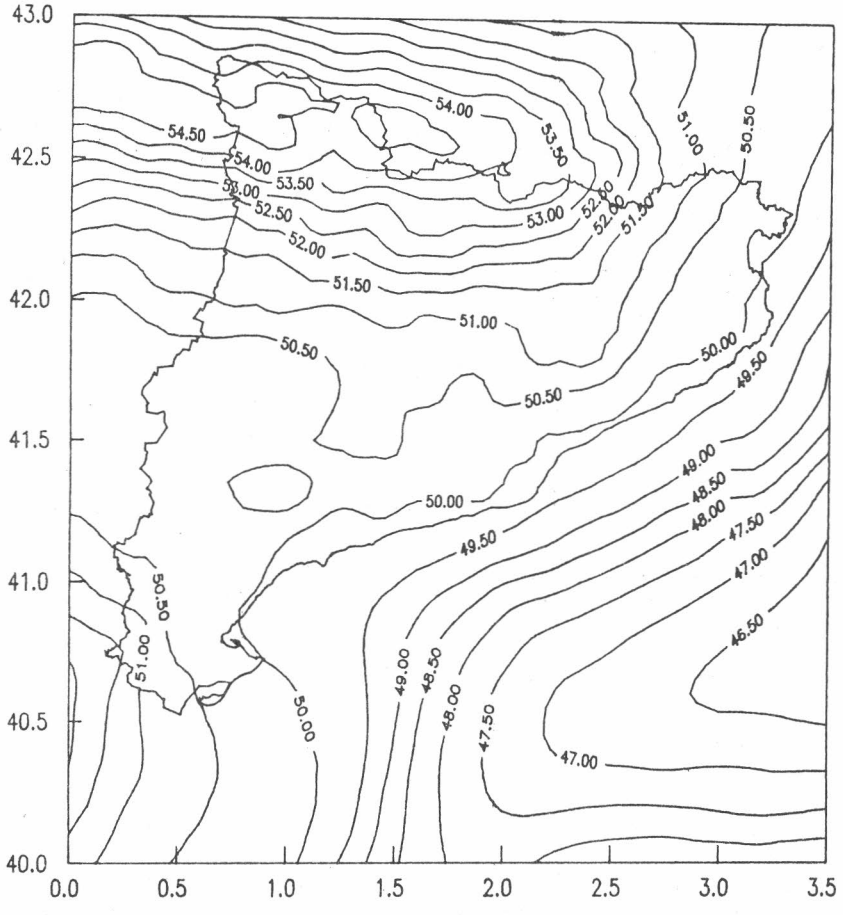

Figure 5: Catalan Geoid UB91 (m). Ellipsoid of reference WGS84. Min.: 46.12 m. Max.: 54.98 m.

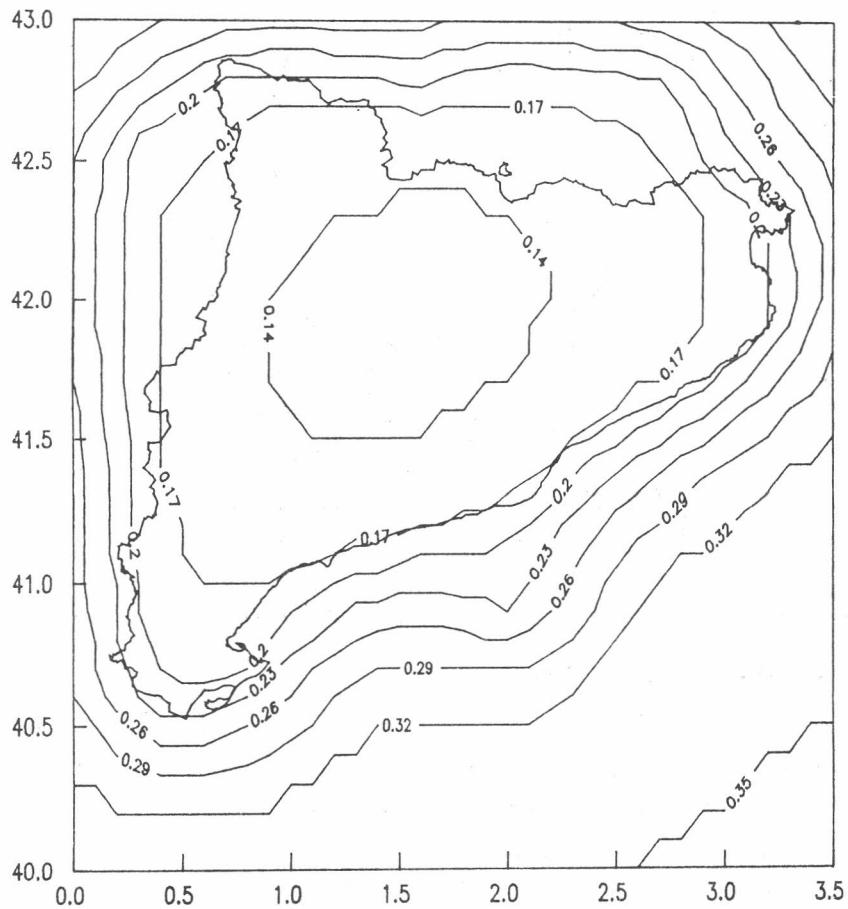

Figure 6: Error estimates of geoid heights computed by LSC. Min.: 0.13 m. Max.: 0.35 m.

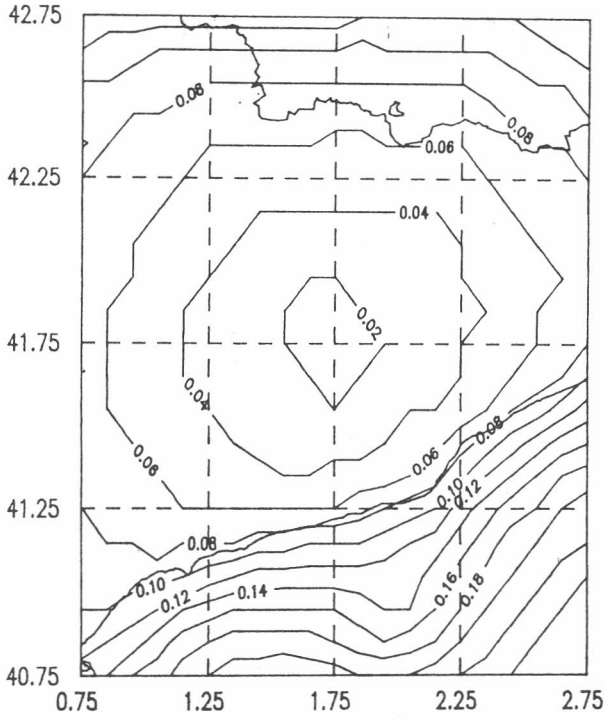

Figure 7: Error estimates of geoid heights using a fix point. Relative error: 10 cm per 100 km.

5 Conclusions and outlook

We are able to make predictions of:

- Gravity anomaly with an error of 2 mgal.
- Geoid height with an absolut error of 13-20 cm and a relative error of 10 cm/100 km.
- Deflections of the vertical with and error of 0″.8.

Improvements:

The next step in our computations will probably include:

- DTM with higher resolution (perhaps $3'' \simeq 100$ m).
- Density data of the crust.
- Gravimetric data at the sea near the coast.
- Deflections of vertical.
- GPS data.

Acknowledgements

The authors are grateful to several institutions and persons which make this work possible: ICC, C.C.Tscherning, R.Forsberg, A.Casas and G.Balmino.

References

[1] Andreu, M.A., Simó, C.: Determinació del geoide UB91 a Catalunya, Monografies tècniques n. 1, Institut Cartogràfic de Catalunya (1992).

[2] Forsberg, R., Tscherning, C.C.: The use of Height Data in Gravity Field Approximation by Collocation, Journal of Geophysical Research, vol. 86, n. B9, pp. 7843-7854 (1981).

[3] Knudsen, P.: Estimation and Modelling of the local empirical covariance function using gravity and satellite altimeter data, Bulletin Geodésique, vol. 61, pp. 145-160 (1987).

[4] Moritz, H.: Advanced Physical Geodesy, 2^{on} ed., Wichmann (1989).

[5] Rapp, R.H., Paulis, N.K.: The developement and analysis of geopotential coefficient models to spherical harmonic degree 360, Journal of Geophysical Research (1990).

[6] Tscherning, C.C.: Local approximation of the gravity potential by least squares collocation. Summer School on Local Gravity Field Approximation, Beijing, China, ed. by K.P. Schwarz, University of Calgary (1984).

PUBLICACIONES DEL INSTITUTO DE ASTRONOMIA Y GEODESIA DE LA UNIVERSIDAD COMPLUTENSE — MADRID

(Antes Seminario de Astronomía y Geodesia)

1.—Efemérides de 63 Asteroides para la oposición de 1950 (1949).
2.—E. PAJARES: Sobre el cálculo gráfico de valores medios (1949).
3.—J. PENSADO: Orbita del sistema visual σ^2 U Maj (1950).
4.—Efemérides de 79 Asteroides para la oposición de 1951 (1950).
5.—J. M. TORROJA: Corrección de la órbita del Asteroïde 1395 "Aribeda" (1950).
6.—R. CARRASCO y J. M. TORROJA: Rectificación de la órbita del Asteroide 1371 "Resi" (1971).
7.—J. M. TORROJA y R. CARRASCO: Rectificación de la órbita del Asteroide 1560 (1942 XB) y efemérides para la oposición de 1951 (1951).
8.—M. L. SIEGRIST: Orbita provisional del sistema visual Σ 728-32 Orionis (1951).
9.—Efemérides de 79 Asteroides para la oposición de 1952 (1951).
10.—J. PENSADO: Orbita provisional de Σ 1883 (1951).
11.—M. L. SIEGRIST: Orbita provisional del sistema visual Σ 2052 (1952).
12.—Efemérides de 88 Asteroides para la oposición de 1953 (1952).
13.—J. PENSADO: Orbita de ADS 9380 = Σ 1879 (1952).
14.—F. ALCÁZAR: Aplicaciones del Radar a la Geodesia (1952).
15.—J. PENSADO: Orbita de ADS 11897 = Σ 2438 (1952).
16.—B. RODRÍGUEZ-SALINAS: Sobre varias formas de proceder en la determinación de períodos de las marcas y predicción de las mismas en un cierto lugar (1952).
17.—R. CARRASCO y M. PASCUAL: Rectificación de la órbita del Asteroide 1528 "Conrada" (1953).
18.—J. M. GONZÁLEZ-ABOIN: Orbita de ADS 1709 = Σ 228 (1953).
19.—J. BALTÁ: Recientes progresos en Radioastronomía. Radiación solar hiperfrecuente (1953).
20.—J. M. TORROJA y A. VÉLEZ: Corrección de la órbita del Asteroide 1452 (1938 DZ_1) (1953).
21.—J. M. TORROJA: Cálculo con Cracovianos (1953).
22.—S. AREND: Los polinomios ortogonales y su aplicación en la representación matemática de fenómenos experimentales (1953).
23.—J. M. TORROJA y V. BONGERA: Determinación de los instantes de los contactos en el eclipse total de Sol de 25 de febrero de 1952 en Cogo (Guinea Española) (1954).
24.—J. PENSADO: Orbita de la estrella doble Σ 2 (1954).
25.—J. M. TORROJA: Nueva órbita del Asteroide 1420 "Radcliffe" (1954).
26.—J. M. TORROJA: Nueva órbita del Asteroide 1557 (1942 AD) (1954).
27.—R. CARRASCO y M. L. SIEGRIST: Rectificación de la órbita del Asteroide 1290 "Albertine" (1954).
28.—J. PENSADO: Distribución de los períodos y excentricidades y relación período-excentricidad en las binarias visuales (1955).
29.—J. M. GONZÁLEZ-ABOIN: Nueva órbita del Asteroide 1372 "Haremari" (1955).
30.—M. DE PASCUAL: Rectificación de la órbita del Asteroide 1547 (1929 CZ) (1955).
31.—J. M. TORROJA: Orbita del Asteroide 1554 "Yugoslavia" (1955).
32.—J. PENSADO: Nueva órbita del Asteroide 1401 "Lavonne" (1956).
33.—J. M. TORROJA: Nuevos métodos astronómicos en el estudio de la figura de la Tierra (1956).
34.—D. CALVO: Rectificación de la órbita del Asteroide 1466 "Mündleira" (1956).
35.—M. L. SIEGRIST: Rectificación de la órbita del Asteroide 1238 "Predappia" (1956).

36.—J. PENSADO: Distribución de las inclinaciones y de los polos de las órbitas de las estrellas dobles visuales (1956).

37.—J. M. TORROJA y V. BONGERA: Resultados de la observación del eclipse total de Sol de 30 de junio de 1954 en Sydkoster (Suecia) (1957).

38.—ST. WIERZBINSKI: Solution des équations normales par l'algorithme des cracoviens (1958).

39.—J. M. GONZÁLEZ-ABOIN: Rectificación de la órbita del Asteroide 1192 "Prisma" (1958).

40.—M. LÓPEZ ARROYO: Sobre la distribución en longitud heliográfica de las manchas solares (1958).

41.—F. MÚGICA: Sobre la ecuación de Laplace (1958).

42.—F. MARTÍN ASÍN: Un estudio estadístico sobre las coordenadas de los vértices de la triangulación de primer orden española (1958).

43.—ST. WIERZBINSKI: Orbite améliorée de h 4530 = γ Cen = Cpd —48°, 4965 (1958).

44.—D. CALVO BARRENA: Rectificación de la órbita del Asteroide 1164 "Kobolda" (1958).

45.—M. LÓPEZ ARROYO: El ciclo largo de la actividad solar (1959).

46.—F. MÚGICA: Un nuevo método para la determinación de la latitud (1959).

47.—J. M. TORROJA: La observación del eclipse de 2 de octubre de 1959 desde El Aaiun (Sahara) (1960).

48.—J. M. TORROJA, P. JIMÉNEZ-LANDI y M. SOLÍS: Estudio de la polarización de la luz de la corona solar durante el eclipse total de Sol del día 2 de octubre de 1959 (1960).

49.—E. PAJARES: Sobre el mecanismo diferencial de un celóstato (1960).

50.—J. M. GONZÁLEZ-ABOIN: Sobre la diferencia entre los radios vectores del elipsoide internacional y el esferoide de nivel (1960).

51.—J. M. TORROJA: Resultado de las observaciones del paso de Mercurio por delante del disco solar del 7 de noviembre de 1960 efectuadas en los observatorios españoles (1961).

52.—F. MÚGICA: Determinación de la latitud por el método de los verticales simétricos (1961).

53.—M. LÓPEZ ARROYO: La evolución del área de las manchas solares (1962).

54.—F. MÚGICA: Determinación simultánea e independiente de la latitud y longitud mediante verticales simétricos (1962).

55.—P. DÍEZ-PICAZO: Elementos de la órbita de la variable eclipsante V 499 Scorpionis (1964).

56.—J. M. TORROJA: Los Observatorios Astronómicos en la era espacial (1965).

57.—F. MARTÍN ASÍN: Nueva aportación al estudio de la red geodésica de primer orden española y su comparación con la red compensada del sistema europeo (1966).

58.—F. SÁNCHEZ MARTÍNEZ: La Luz Zodiacal. Luz del espacio interplanetario (1966).

59.—J. M. GONZÁLEZ-ABOÍN: Variaciones de las coordenadas geodésicas de los vértices de una red, por cambio de elipsoide de referencia (1966).

60.—F. SÁNCHEZ MARTÍNEZ y R. DUMONT: Fotometría absoluta de la raya verde y del continuo atmosférico en el Observatorio Astronómico del Teide (Tenerife), de enero de 1964 a julio de 1965 (1967).

61.—M. REGO: Estudio del espectro de la estrella 31 Aql. en la región $\lambda\lambda$ 4000-6600 Å (1969).

62.—C. MACHÍN: Mareas terrestres (1969).

63.—J. M. TORROJA: La estación para la observación de satélites geodésicos de la Facultad de Ciencias de la Universidad de Madrid (1969).

64.—M. J. SEVILLA: Reducción automática de posiciones de estrellas (1970).

65.—J. M. TORROJA: Memoria de las actividades del Seminario de Astronomía y Geodesia de la Facultad de Ciencias de la Universidad de Madrid en 1969 (1970).

66.—M. J. SEVILLA: Los cálculos de estación en triangulación espacial (1970).

67.—MANUEL E. REGO: Determinación de las abundancias de los elementos en la atmósfera de la estrella de alta velocidad 31 Aql. (1970).

68.—M. J. FERNÁNDEZ-FIGUEROA: Análisis cualitativo del espectro de la estrella peculiar HD 18474 (1971).

69.—J. M. TORROJA: Memoria de las actividades del Seminario de Astronomía y Geodesia de la Universidad Complutense de Madrid en 1970 (1971).

70.—R. VIEIRA y R. ORTIZ: Descripción de un aparato para medida de coordenadas (1971).

71.—J. M. TORROJA: Memoria de las actividades del Seminario de Astronomía y Geodesia de la Universidad Complutense de Madrid en 1971 (1972).

72.—M. J. FERNÁNDEZ-FIGUEROA: Observación y estudio teórico del espectro de la estrella peculiar HD 18474 (1972).

73.—M. J. SEVILLA: Cálculo de las constantes de distorsión y parámetros del disco obturador para cámaras balísticas (1973).

74.—R. PARRA y M. J. SEVILLA: Cálculo de efemérides y previsiones de pasos de satélites geodésicos (1973).

75.—M. REGO y M. J. FERNÁNDEZ-FIGUEROA: Resultado de las observaciones de α Peg efectuadas desde el satélite europeo TDI (1973).

76.—E. SIMONNEAU: Problemas en la determinación de abundancias de elementos en las estrellas en condiciones de equilibrio termodinámico local y alejadas del equilibrio termodinámico local (1974).

77.—J. ARANDA: Construcción de modelos de estructura interna para estrellas en la secuencia principal inicial (1974).

78.—R. ORTIZ, M. J. SEVILLA y R. VIEIRA: Estudio de la calibración, técnica de medida y automatización de datos en un comparador para medidas de placas estelares (1974).

79.—M. J. SEVILLA: Método autocorrector para el cálculo de direcciones de satélites geodésicos y análisis de los errores en la restitución de un arco de órbita (1974).

80.—M. A. ACOSTA, R. ORTIZ y R. VIEIRA: Diseño y construcción de un fotómetro fotoeléctrico para la observación de ocultaciones de estrellas por la Luna (1974).

81.—T. J. VIVES, C. MORALES, J. GARCÍA-PELAYO y J. BARBERO: Fotometría fotográfica UBV del cúmulo galáctico King 19 (1974).

82.—R. ORTIZ y R. VIEIRA: Control automático en posición y tiempo de los sistemas de obturación de las cámaras de observación de satélites geodésicos (1974).

83.—J. M. TORROJA: Memoria de las actividades del Seminario de Astronomía y Geodesia de la Universidad Complutense de Madrid en 1972 y 1973 (1974).

84.—M. J. FERNÁNDEZ-FIGUEROA y M. REGO: α CrB en el ultravioleta lejano (1975).

85.—J. M. TORROJA, R. VIEIRA, R. ORTIZ y M. J. SEVILLA: Estudio de mareas terrestres en España (1975).

86.—M. J. SEVILLA y R. PARRA: Levantamiento gravimétrico de Lanzarote (1975).

87.—P. KUNDANMAL SUKHWANI: Modelos teóricos de curvas de luz. Su aplicación al sistema β Lyrae (1975).

88.—M. J. SEVILLA: Coordenadas astronómicas y geodésicas. Desviación relativa de la vertical (1975).

89.—C. TEJEDOR: Fotometría fotoeléctrica R. G. U. del cúmulo galáctico IC 2581 (1976).

90.—M. J. SEVILLA: Nuevos coeficientes para la reducción automática de posiciones de estrellas (1976).

91.—M. REGO: Técnicas observacionales en espectroscopía astrofísica (1976).

92.—M. J. SEVILLA: Determinación de la latitud por distancias cenitales de la polar, método de Littrow (1976).

93.—T. J. VIVES: Determinación fotométrica del tipo espectral de la componente desconocida de una estrella binaria eclipsante (1976).

94.—M. REGO y M. J. FERNÁNDEZ-FIGUEROA: Contraste y determinación por métodos astrofísicos de fuerzas de oscilador (1977).

95.—M. J. SEVILLA y R. CHUECA: Determinación de acimutes por observación de la Polar. Método micrométrico (1977).

96.—JOSÉ M. GARCÍA-PELAYO: Fotometría R G U en un campo del anticentro galáctico, cerca del NGC 581 (1977).

97.—JOSÉ M. GARCÍA-PELAYO: Datos fotométricos de 2.445 estrellas estudiadas en la región de Casiopea, entre los cúmulos abiertos Trumpler 1 y NGC 581 (1977).

98.—PREM K. SUKHWANI y RICARDO VIEIRA: Spectral Analysis of Earth Tides (1977).

99.—JOSÉ M. TORROJA y RICARDO VIEIRA: Earth Tides in Spain. Preliminary results (1977).

100.—PREM K. SUKHWANI y RICARDO VIEIRA: Three different methods for taking in account the gaps in spectral analysis of Earth Tides records (1978).

101.—R. VIEIRA: Mareas terrestres (1978).

102.—M. J. SEVILLA y A. NÚÑEZ: Determinación de la longitud por el método de Mayer. Programas de cálculo automático (1979).

103.—M. J. SEVILLA y A. NÚÑEZ: Determinación de la latitud por el método de Sterneck. Programas de cálculo automático (1979).

104.—M. J. SEVILLA: Determinación de la latitud y la longitud por el método de alturas iguales. Programas de cálculo automático (1979).

105.—P. K. SUKHWANI y A. GIMÉNEZ: Corrección de efectos atmosféricos para imágenes tomadas desde satélites Landsat (1979).

106.—M. J. SEVILLA: Inversión de Matrices Simétricas en el método de mínimos cuadrados (1979).

107.—A. GIMÉNEZ: Análisis de la curva de luz del sistema binario eclipsante S Velorum (1979).

108.—M. J. SEVILLA: Determinación del acimut de una referencia por observación de la estrella polar. Programa de cálculo automático (1979).

109.—M. J. SEVILLA: El sistema IAU (1976) de constantes astronómicas y su repercusión en la reducción de posiciones de estrellas (Primera parte) (1980).

110.—M. J. SEVILLA y R. PARRA: Determinación de la latitud por el método de Horrebow-Talcott. Programas de Cálculo Automático (1980).

111.—M. J. SEVILLA: Determinación de la latitud y la longitud por fotografías cenitales de estrellas (1980).

112.—R. VIEIRA y M. OREJANA: Comunicaciones presentadas en las XLI y XLII Jornadas del Grupo de Trabajo de Geodinámica del Consejo de Europa. Luxemburgo (1979-80).

113.—M. J. SEVILLA: Sobre un método de cálculo para la resolución de los problemas geodésicos directo e inverso (1981).

114.—R. VIEIRA, J. M. TORROJA, C. TORO, F. LAMBAS, M. OREJANA y P. K. SUKHWANI: Comunicaciones presentadas en el IX Symposium Internacional de Mareas Terrestres. Nueva York (1981).

115.—M. A. MONTULL, M. J. SEVILLA y A. GONZÁLEZ-CAMACHO: Aplicación de la V. L. B. I. al estudio del movimiento del Polo (1981).

116.—A. GONZÁLEZ-CAMACHO y M. J. SEVILLA: Algunas relaciones entre diferentes ejes que se consideran en la rotación de la Tierra (1981).

117.—R. VIEIRA, F. LAMBAS y E. GIMÉNEZ: Modificaciones realizadas en un gravímetro LaCoste Romberg mod. G para su utilización en registro continuo de la gravedad (1981).

118.—R. VIEIRA: La microrred de mareas gravimétricas del Sistema Central (1981).

119.—J. M. TORROJA y R. VIEIRA: Informe sobre el desarrollo del programa de investigación sobre mareas terrestres en el último bienio (1981).

120.—F. LAMBAS y R. VIEIRA: Descripción, estudio de la precisión y aplicaciones geodésicas y geofísicas de los nuevos niveles de lectura electrónica (1981).

121.—M. J. SEVILLA: Programación del método de la cuerda (1981).

122.—J. M. TORROJA: Historia de la Ciencia Arabe. Los Sistemas Astronómicos (1981).

123.—M. J. SEVILLA y R. VIEIRA: Comunicaciones presentadas en la Sesión Científica de la Real Academia de Ciencias Exactas, Físicas y Naturales, celebrada el día 13 de enero de 1982 (1982).

124.—M. J. SEVILLA y P. ROMERO: Aplicación del método de colocación a la reducción de placas fotográficas de estrellas (1982).

125.—M. J. SEVILLA y A. G. CAMACHO: Deformación rotacional de una tierra elástica (1982).

126.—M. J. SEVILLA y P. ROMERO: Obtención de las medidas de la precisión en la determinación de la latitud y la longitud por fotografías cenitales de estrellas (1982).

127.—M. J. SEVILLA, A. G. CAMACHO y P. ROMERO: Comunicaciones presentadas en la IV Asamblea Nacional de Astronomía y Astrofísica. Santiago de Compostela (1983).

128.—M. J. SEVILLA: El sistema IAU (1976) de constantes astronómicas y su repercusión en la reducción de posiciones de estrellas (Segunda parte) (1983).

129.—M. J. SEVILLA: Geodesia por satélites y navegación (1983).

130.—L. GARCÍA ASENSIO, A. G. CAMACHO, P. ROMERO y M. J. SEVILLA: Comunicaciones presentadas en la V Asamblea Nacional de Geodesia y Geofísica (1983).

131.—M. J. SEVILLA: Anomalías de la gravedad basadas en el sistema geodésico de referencia 1980 (1983).

132.—J. M. TORROJA: Historia de la Física hasta el siglo XIX. La Mecánica Celeste (1983).

133.—A. G. CAMACHO y M. J. SEVILLA: The Molodensky Problem for an homogeneous liquid core (1984).

134.—J. M. TORROJA: La obra astronómica de Alfonso X El Sabio (1984).

135.—H. MORITZ: Sistemas de referencia en Geodesia (1984).

136.—H. MORITZ: Rotación de la Tierra (1984).

137.—A. G. CAMACHO y M. J. SEVILLA: Autofrecuencias del movimiento del Polo para un modelo de Tierra de tipo Jeffreys Molodensky (1984).

138.—J. M. TORROJA: Nuevas definiciones en el problema de la medida del tiempo (1984).

139.—M. J. SEVILLA: Astronomía Geodésica (1984).

140.—M. J. SEVILLA y M. D. MARTÍN: Diseño de una Microrred en la Caldera del Teide para el estudio de deformaciones de la corteza en la zona (1986).

141.—R. VIEIRA, C. DE TORO y V. ARAÑA: Estudio Microgravimétrico en la Caldera del Teide (1986).

142.—M. J. SEVILLA, M. D. MARTÍN y A. G. CAMACHO: Análisis de Datos y Compensación de la primera campaña de observaciones en la Caldera del Teide (1986).

143.—M. J. SEVILLA y P. ROMERO: Hamiltonian Formulation of the polar motion for an elastic earth's model (1986).

144.—P. ROMERO y M. J. SEVILLA: The Sasao-Okubo-Saito equations by Hamilton Theory. First Results (1986).

145.—R. VIEIRA, M. J. SEVILLA, A. G. CAMACHO y M. D. MARTÍN: Geodesia de precisión aplicada al control de movimientos y deformaciones en la Caldera del Teide (1986).

146.—R. VIEIRA, J. M. TORROJA, C. DE TORO, B. DUCARME, J. KAARIAINEN, E. MEGÍAS y J. FERNÁNDEZ: Comunicaciones presentadas en el X Symposium Internacional de Mareas Terrestres. Madrid, 1985 (1986).

147.—M. J. SEVILLA, A. G. CAMACHO y P. ROMERO: Comunicaciones presentadas en el X Symposium Internacional de Mareas Terrestres. Madrid, 1985 (1986).

148.—M. J. SEVILLA: Formulación de modelos matemáticos en la compensación de redes Geodésicas: III Curso de Geodesia Superior (1986).

149.—H. LINKWITZ: Compensación de grandes redes geodésicas: III Curso de Geodesia Superior (1986).

150.—H. HENNEBERG: Redes geodésicas de alta precisión: III Curso de Geodesia Superior (1986).

151.—M. J. SEVILLA: Cartografía Matemática (1986).

152.—P. ROMERO y M. J. SEVILLA: Tratamiento Canónico del problema de Poincare. Movimiento del Polo. (1986)

153.—A. G. CAMACHO y M. D. MARTÍN: Constreñimientos internos en la compensación de Estaciones. (1986)

154.—J. OTERO: An Approach to the Scalar Boundary Value Problem of Physical Geodesy by Means of Nash-Hörmander Theorem. (1987)

155.—M. J. SEVILLA: Introducción al Problema Clásico de Molodensky. (1987)

156.—F. SANSÓ: Problemas de Contorno de la Geodesía Física. (1987)

157.—M. J. SEVILLA: Colocación mínimos cuadrados. (1987)

158.—L. MUSSIO: Estrategias del Método de colocación. Ejemplos de aplicación. (1987)

159.—M. J. SEVILLA, P. MUÑOZ, J. VELASCO y P. ROMERO: Calibración de un Distanciómetro de infrarrojos en una Base Interferométrica (1987).

160.—A. RIUS, J. RODRÍGUEZ, M. J. SEVILLA, R. VIEIRA, J. FERNÁNDEZ, C. DE TORO, A. G. CAMACHO y V. ARAÑA: Comunicaciones presentadas en la Sesión Científica de la Real Academia de Ciencias Exactas, Físicas y Naturales, celebrada el día 4 de mayo de 1988 (1988).

161.—R. VIEIRA, A. G. CAMACHO y C. DE TORO: Cálculo de la Corrección de Marea en la Península Ibérica (1988).

(continúa en la cuarta de cubierta)

162.—A. G. CAMACHO, R. VIEIRA, C. DE TORO y J. FERNÁNDEZ: Estudio Gravimétrico de la Caldera del Teide (1988).

163.—A. J. GIL, M. J. SEVILLA, G. RODRÍGUEZ y J. OTERO: Aplicaciones de la colocación y Estudios del Geoide (1988).

164.—R. VIEIRA, J. FERNÁNDEZ, C. DE TORO, A. G. CAMACHO y M. V. RUYMBEKE: Investigaciones Geodinámicas en la Isla de Lanzarote (1988).

165.—M. J. SEVILLA, P. ROMERO, A. NÚÑEZ y B. BADA: Compensaciones y resultados (1988).

166.—R. VIEIRA, C. DE TORO y A. G. CAMACHO: Investigaciones en mareas (1988).

167.—A. NÚÑEZ, M. J. SEVILLA y J. M. AGRIA: Determinación Astrogeodésica del Geoide en Portugal (1988).

168.—M. J. SEVILLA y P. ROMERO: Pre-Processing Geodetic Data of the Volcanic area of Teide to monitoring deformations (1988).

169.—M. J. SEVILLA y A. J. GIL: Fórmulas diferenciales para los problemas Geodésicos directo e inverso en el método de la cuerda (1988).

170.—Zd. SIMÓN, V. STANCHEV, C. DE TORO, A. P. VENEDIKOV y R. VIEIRA: Relation between earth tide observations and some other data (1988).

171.—J. OTERO: On the Global Solvability of the fixed gravimetric boundary value problem (1989).

172.—R. VIEIRA, J. FERNÁNDEZ, C. DE TORO y A. G. CAMACHO: Comunicaciones presentadas en el XI International Symposium on earth tides. Helsinki (1989).

173.—A. RIUS y C. JACOBS: Precise V.L.B.I. surveying at the Madrid DSCC (1989).

174. J. OTERO y M. J. SEVILLA: Modelo matemático para el ajuste simultáneo mínimos cuadrados de un bloque fotogramétrico (1989).

175.—F. SACERDOTE: I Problemi sopradeterminati in Geodesia Fisica e Il Problema dell'Altimetria-Gravimetria (1989).

176.—M. J. SEVILLA: Soluciones progresivas en el método de Mínimos Cuadrados (1989).

177.—M. J. SEVILLA y P. ROMERO: Compensación de Redes de Nivelación Trigonométrica (1989).

178.—J. OTERO y M. J. SEVILLA: On the optimal choice of the standard parallels for a conformal conical projection (1990).

179.—R. VIEIRA, J. FERNÁNDEZ, M. VAN RUYMBEKE, A. G. CAMACHO, J. ARNOSO y C. TORO: Geodynamic Research in Lanzarote (Canary Islands) (1990).

180.—M. J. SEVILLA, A. GIL y P. ROMERO: Adjustment of the first order gravity net in the Iberian Peninsula (1990).

181.—R. VIEIRA, J. MAKINEN, A. G. CAMACHO y M. J. SEVILLA: Observaciones absolutas de la gravedad en España (1991).

182.—M. J. SEVILLA: Criterios de precisión cartográfica (1991).

183.—A. P. VENEDIKOV, R. VIEIRA y C. DE TORO: A new method for earth tide analysis (1992).

Depósito Legal: M. Sep. 894 - 1958
ISSN: 0213 - 6198
Realigraf, S. A. - Burgos, 12 - 28039 Madrid